Struct Bond (2020) 183: 251–320
https://doi.org/10.1007/430_2020_53

Published online: 2 August 2020

Photofunctions of Dye-Clay Hybrids: Recent Developments

Tetsuo Yamaguchi, Jae-Min Oh, and Makoto Ogawa

Contents

Abstract Precise design of hybrid nanostructures based on dyes in hybrid materials toward controlled photochemical reactions and novel photoinduced phenomena is overviewed with the emphasis on the recent developments. Various clays and clay minerals with different origins and characteristics have been used as hosts to control the location, orientation, and aggregation as well as the dynamic states (rotation and diffusion) of the dyes. The designed nanostructures affect photochemical properties such as efficiency, selectivity, and the rate of some photochemical reactions. Using the photochemical reactions in nanospaces, unique photoinduced phenomena such

T. Yamaguchi and M. Ogawa (✉)
School of Energy Science and Engineering, Vidyasirimedhi Institute of Science and Technology, Rayong, Thailand
e-mail: makoto.ogawa@vistec.ac.th

J.-M. Oh
Department of Energy and Materials Engineering, Dongguk University-Seoul, Seoul, South Korea
e-mail: jaemin.oh@dongguk.edu

as nanostructural/morphological change and adsorption/desorption triggered by irradiation have been found.

Keywords Clays and clay minerals · Host-guest · Photochemistry · Photoinduced phenomena · Photophysics

Abbreviations

$[Ru(bpy)_3]^{2+}$	Tris(2,2-bipyridine)ruthenium(II)
AFM	Atomic force microscopy
ATR	Attenuated total reflection
AZ	Azobenzene
$C_{12}TMA$	Dodecyltrimethylammonium ion
$C_{16}TMA$	Hexadecyltrimethylammonium ion
CEC	Cation exchange capacity
CT	Charge transfer
DMSO	Dimethylsulfoxide
HE	A synthetic hectorite (Sumecton SWF)
KF	A natural montmorillonite (Kunipia F)
LB	Langmuir-Blodgett
LbL	Layer-by-layer deposition
LDH	Layered double hydroxide
LP-RD	A synthetic hectorite (Laponite RD)
LP-XLG	A synthetic hectorite (Laponite XLG)
MC	Merocyanine
MV^{2+}	Methyl viologen
PEMA	Poly(ethyl methacrylate)
PIC	*Pseudo*isocyanine
PMMA	Poly(methyl methacrylate)
PSS	Poly(styrene sulfonate)
PVP	Poly(vinyl pyrrolidone)
R6G	Rhodamine 6G
SA	A synthetic saponite (Sumecton SA)
SP	Spiropyran
STN^+	Stilbazolium ion
SWy-1	A Na-montmorillonite from Wyoming, USA
SYn-1	A synthetic mica-montmorillonite
TEOS	Tetraethoxysilane
TMA	Tetramethylammonium ion
TPP	Tetraphenylporphine
TSM	Fluoro-tetrasilicic mica

1 Introduction

Photochemical reactions in heterogeneous systems may differ significantly from analogous reactions in homogeneous liquids/solutions or gas phases [1–6]. Important roles of the media/supports to control such parameters as the reaction rates/yields and product selectivity have been recognized so far, so that various photofunctional hybrids have been designed by organizing molecular species in/on solid surfaces. The location (proximity), orientation, association/aggregation, as well as the freedom (rotation and diffusion) of molecules on the surfaces or in the solids vary depending on the host-guest interactions at the interface to affect the characteristics and functions. The molecular and supramolecular designs (by the selection of host and guest and their composition and the additives) have been done using nanospace materials such as zeolites, mesoporous silicas, MOFs, COFs, and layered materials for organizing molecular and polymeric photofunctional species, and unique/useful photofunctions of the resulting hybrids have been reported [7–11]. Materials with defined (ordered) nanospaces have advantages as supports to accommodate guest species because their structure-property relationships will provide indispensable information on designing materials with controlled properties [12]. Spectroscopic properties, which are very sensitive to the environment, of the immobilized species, have given insights to the nanoscopic structures of the host-guest systems where conventional instrumental analysis does not have access [11–16]. By utilizing photoprocesses, one can obtain such information as distribution [17–20], orientation [21, 22], and mobility [23] of the guest species on/in nanospaces.

In this chapter, among possible host-guest systems, the studies on the organization of photofunctional species on/in clays (more accurately clay minerals and their synthetic analogs) will be summarized with the emphasis on the developments in the last two decades. The attention will mainly be focused on the role of the nanostructures, which directly and indirectly correlate the photofunctions of the guest species and the host-guest systems (Fig. 1).

2 Characteristics of Dye-Clay Hybrids for Photochemical Studies and Photofunctional Materials

Smectites have been used most extensively for a wide range of application including environmental and biomedical ones [24–28]. Smectites are a type of swellable 2:1 type layered clay minerals and consist of negatively charged silicate layer and charge compensating interlayer cations which are exchangeable [29–31]. The negative charge in the layers is generated by isomorphous substitution of framework metal cations with similar size and lower valency, and to compensate this negative charge, metal cations such as sodium and calcium occupy the interlayer space. The terms of bentonite and montmorillonite have often confused, bentonite is a term of a natural resource, and montmorillonite is the name of a clay mineral. The amount as well as

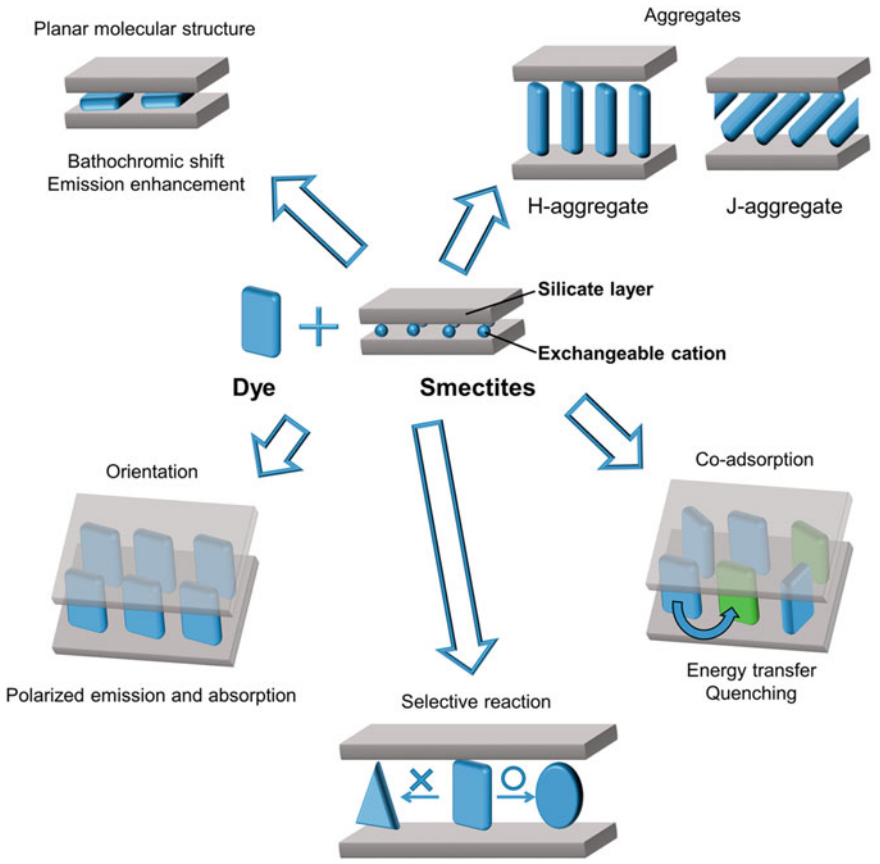

Fig. 1 Possible effects of dye-smectite hybridization

the site of the isomorphous substitution influences the surface and colloidal properties of smectites. Impurities present both within the structure and on the particle surface, and elements and their amounts vary depending on the source of the clay minerals. Synthetic analogs of smectites, i.e., hectorite (Laponite, Rockwood Ind. Co. and Sumecton SWF, Kunimine Ind. Co.) [32], saponite (Sumecton SA, Kunimine Ind. Co.) [33], and swelling mica (sodium-fluor-tetrasilicic mica, TSM, Topy Ind. Co. and others) [33], do not contain colored impurities so that they are advantages for the photochemical studies. In addition to the commercially available ones, synthetic analogs of smectite have been prepared in the laboratory and used for the adsorption of dyes [25, 34]. The interlayer cation, which compensates the negative charge of the silicate layer, is exchangeable by the reactions in suspension and in solid state [35–37].

Cation exchange with interlayer exchangeable cations and the adsorption of polar molecules by ion-dipole interactions with interlayer cations and/or hydrogen bonding with the surface oxygen atom of the silicate sheets are known driving forces for

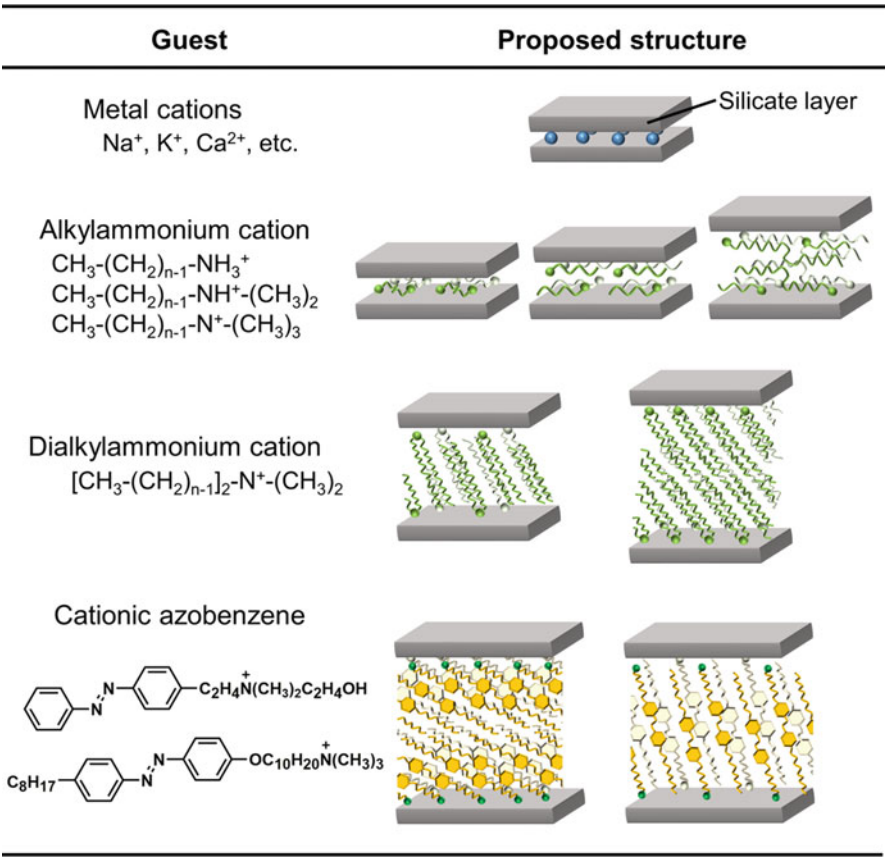

Fig. 2 Examples of organic cationic dyes and schematic drawing for possible arrangements of alkylammonium cations [62, 63]

the intercalation [38–52]. One of the characteristic features of smectites is the possible surface modification. Nanoporous pillared smectites have been obtained using inorganic particles and small organic cations as pillars [53–55]. Organophilic modification has been conducted by the cation exchange with cationic surfactants of various structures (Fig. 2) [26, 33, 56–61]. Due to the variation of the layer charge density and the molecular structures of the surfactants, host-guest systems with controlled microstructures and properties have been obtained.

Layered alkali silicates, namely, magadiite ($Na_2Si_{14}O_{29}{\cdot}nH_2O$) and octosilicate ($Na_2Si_8O_{17}{\cdot}nH_2O$), which are characterized by the higher layer charge density than smectites, have also been used as hosts to construct photofunctional dye-silicate hybrids. The reactions of the layered alkali silicates involve covalent attachments through the reactions with the surface silanol groups [20, 64]. On the other hand, layered double hydroxides (LDHs) are composed of positively charged brucite-type layers of mixed-metal hydroxides and exchangeable anions located at the interlayer

spaces, which compensate for the positive charge of the brucite-type layers [65]. Due to the structural characteristics and compositional variation, the application of LDHs in such areas as adsorption/separation of ions [65–69], catalysis [66–68], polymer additives [66–68], and medical and biochemical uses [66, 68] has been proposed so far. The chemical composition of the LDHs is expressed as $[M(II)_{1-X}M(III)_X(OH)_2][A^{n-}_{X/n}]^{X-}$ where M(II) = Mg, Co, Ni, etc.; M(III) = Al, Cr, Fe, etc.; and A is an interlayer anion such as CO_3^{2-} and Cl^-.

In addition to the crystalline structures, the particle size and its distributions of layered solids are key issues in order to achieve optimum performance of layered solids and their intercalates; accordingly, attention has been paid for the powder morphology during the syntheses as well as classification [27, 70, 71]. Powders [36, 72], suspensions [73, 74], and thin films [55, 75–77] have been used for the evaluation of the photoprocesses, as well as for other application [78]. One of the unique and attractive properties of smectites is their spontaneous swelling in water. Platy particles pile up with their *ab* plane parallel to the substrate to form a film when the suspension is evaporated on a flat substrate [55, 75, 79]. The preparation of thin films by the Langmuir-Blodgett technique (LB technique) from exfoliated platelets of clays has also been reported [80, 81]. Inorganic-organic multilayered films have also been prepared via alternate adsorption of a cationic species and an anionic sheet of an exfoliated layered solid (layer-by-layer deposition technique, hereafter abbreviated as LbL technique) [82–86].

3 Surface Modification

In addition to the structural and compositional variation of smectites and other clay minerals (Table 1), the possible surface modification with organic/inorganic cations and polymers makes the variation of the material more versatile (Fig. 2) [87]. Long-chain alkylammonium ions have been studied most extensively in the chemistry of organophilic smectites, and the practical application of the organophilic smectites as adsorbents [25, 88] has been extensively reported. Phospholipids have been utilized for the construction of environmentally benign organoclay [89, 90]. Several non-ionic surfactants have also been used for the surface modification of smectites [75, 91–93]. Intercalation of alkylammonium ions with more complex structures into layered silicates to precisely design hydrophobic nanospace, and, recently, flexibility of the interlayer surfactant aggregates has been discussed based on quasi-elastic neutron scattering data [57].

Microporous and mesoporous solids have been obtained by crosslinking the nanosheets. The pioneering example is the pillaring with polyoxocations (e.g., $[AlO_4Al_{12}(OH)_{24}(H_2O)_{12}]^{7+}$) [94, 95]. Nanoporous solids composed of silicate layers and metal/metal oxide finite particles have been prepared [96–100]. The microporous solids composed of silicate nanosheet and small organoammonium cations (e.g., tetramethylammonium ion, TMA) have been prepared and used for the separation/sensing and other functional materials [101–107]. The adsorptive

Table 1 Abbreviation of specific clays discussed in this chapter

Abbreviation in this chapter	Product name	Type and origin	Producer/authorization company
KF	Kunipia F	Na-montmorillonite from Tsukinuno, Yamagawa, Japan	Kunimine Ind. Co., Reference Clay Sample of Clay Science Society of Japan
SWy-1		Na-montmorillonite from Wyoming, USA	Source Clays Repository of the Clay Minerals Society
SYn-1	Barasym SSM-100	Synthetic mica-montmorillonite	Source Clays Repository of the Clay Minerals Society
SA	Sumecton SA	Synthetic saponite	Kunimine Ind. Co., Reference Clay Sample of Clay Science Society of Japan
HE	Sumecton SWF	Synthetic hectorite	Kunimine Ind. Co.
LP-XLG	Laponite XLG	Synthetic hectorite	Laporte Industry
LP-RD	Laponite RD	Synthetic hectorite	Laporte Industry
TSM		Fluor-tetrasilicic mica	Topy Industry Co.

properties of smectites modified with aliphatic and aromatic ammonium ions have also been investigated [101, 108, 109]. Pore size and porosity are controlled by selecting pillaring agents.

Synthetic clays by hydrothermal method have been developed as summarized in Table 1 and become necessary products for clay research thanks to the high purities and regular chemical equations. The careful syntheses of the clay minerals have been done to control the size of the silicate layers and layer charge densities. The research about the ion exchange led to the development of organically modified clays, which enabled to intercalate non-polar organic compounds into the interlayer spaces [110, 111]. The LB and LbL techniques have been used to fabricate thin films, while the effective swelling and subsequent evaporation of organically modified clays [76] led the thick films with improved quality.

4 Photophysics of Dye-Clay Hybrid Systems

4.1 Changes in the Absorption Properties, Color Change, and Stability

4.1.1 Effects of Host-Guest Interactions

The interactions between lone pair of the oxygen atom of silicate layer of clays and π-electron of dyes were proposed to affect for relatively planar structured dyes such as crystal violet [38, 39, 45–47], rhodamine B [48], pyronin Y [49], thiazines [50–

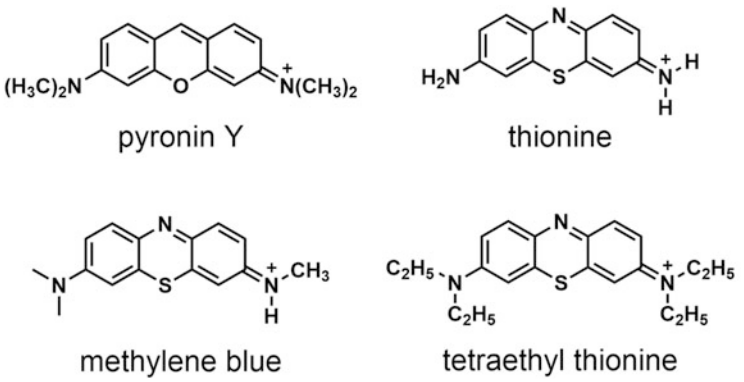

Scheme 1 Molecular structures of pyronin Y and thiazines

52], and methylene blue [40–44, 112, 113]. The adsorption of pyronin Y (Scheme 1) has been examined in aqueous suspensions of smectites (Wyoming bentonite from Wards Natural Establishment Inc., a natural bentonite from Ünye, Turkey and LP-XLG) [49, 114]. Depending on the concentration and the dye-clay ratios, the absorption shifted, which has been explained as a result of the interactions between pyronin Y and silicate layer as well as the dye aggregation, although this latter effect will be exhaustively explained in Sect. 4.1.2. Thiazine dyes such as thionine [51], methylene blue [41, 42, 51], and tetraethyl thionine [51] (Scheme 1) showed hypsochromic shifts in clay suspensions [41, 51]. Thionine had absorption at 595 and 560 nm in an aqueous solution, which were attributed to a π-π^* transition of monomer and the absorption of H-dimer (see further details on aggregation types in Sect. 4.2.1), respectively [51]. By the addition of a Na-montmorillonite, a new absorption appeared at 528 nm, which was proposed to be caused by the interactions between the π-electron of thionine and the oxygen of the silicate layers, and another new absorption at 690 nm appeared, which was ascribed to J-aggregate (consult Sect. 4.1.2). Methylene blue [40, 115] and tetraethyl thionine [51] also showed hypsochromic shifts of monomer and a new absorption appeared by the addition of a montmorillonite. In LP-XLG, the absorption of thionine and tetraethyl thionine did not shift compared to the solution [51]. It was thought that the thionines had weaker π-interactions with the silicate layer than those with the bentonites. In the presence of a vermiculite (obtained from Zonolite), the absorption of the dimer increased and that of the monomer decreased, while the absorption shift was not observed [51]. The authors thought that the limited interlayer expansion for the vermiculite restricted the molecular conformation of thiazines to interact with the vermiculate. Thus, the hypsochromic shifts of the absorption of the dimers of pyronin and thiazines in the clay suspensions were observed by the interactions between lone pair of oxygen atom of silicate layer and π-electron of dyes. It suggested that the pyronin formed dimer in an aqueous solution, while it was de-aggregated and adsorbed in the interlayer space of the clays. The polarized IR spectra of the film of pyronin Y in LP-XLG and the Wyoming montmorillonite [49] suggested that the

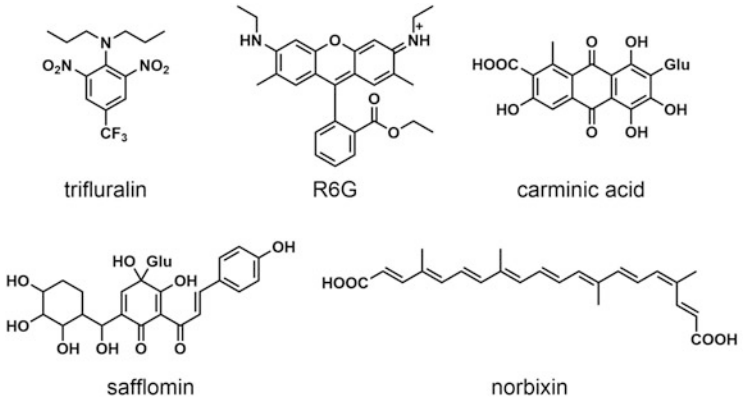

Scheme 2 Molecular structures of dyes, which were reported to be stabilized by the host-guest interactions with clays

interactions between the oxygen of the layered silicates and the π-electron of the dyes made the molecular orientation of the dyes parallel to the silicate layer.

Stability of dyes is one of the prerequisites for the practical application, and the dye-clay interactions have been expected to play a role in it [116–126]. The improvements of the stability of the dyes upon irradiation and heating have been seen in (1) cationic dyes with smectites, (2) anionic dyes with layered double hydroxides (LDHs), and (3) nonionic dyes with organically modified smectites and LDHs. The improvements of the stabilities of the dyes by the hybridization with the layered materials were explained as results of reducing the intensity of the incident light by the absorption and scattering with the host [127–129], electronic stabilization of the dye [130–132], and suppressed gas diffusion mainly oxygen in the hydrophobic environment [111, 133–139].

An example of the improved chemical stability of the anthocyanin by the interactions with SA was shown by the color change upon exposure to acidic and basic atmospheres repeatedly [102]. Such natural dyes as β-carotene, anthocyanin, carmine, annatto, and carthamus yellow were adsorbed on a hydrotalcite [111, 139] and organically modified montmorillonite [110, 111]. Carminic acid, safflomin, and norbixin (Scheme 2) are the main components of carmine, carthamus yellow, and annatto, respectively [132]. When interacted with the hydrotalcite, the absorption spectra of carmine showed bathochromic shift as shown in Fig. 3a. The absorption shift was explained by the electrostatic interactions between carmine and the hydrotalcite and the planar molecular conformation induced by the adsorption on the hydrotalcite. As a result, the photostability was improved. Carthamus yellow showed the same trend as carmine. On the other hand, the stability of annatto was not affected in the presence of the hydrotalcite, suggesting the adsorption of annatto at the external surface of the hydrotalcite. The planar conformation was induced by the intercalation and was thought to contribute to the photostability of the dyes through the decrease of the lifetime of the excited state by the effective internal conversion. It

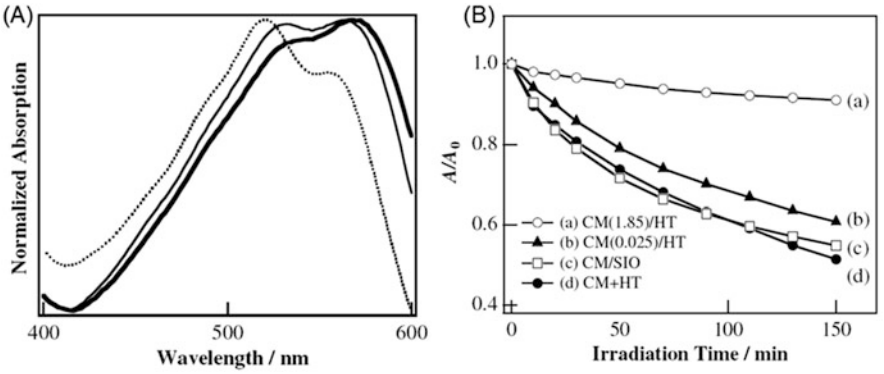

Fig. 3 (**a**) Diffuse reflectance UV-vis spectra of carmine intercalated in the hydrotalcite at the amount of 0.025 g/g (*dotted line*), 0.46 g/g (*thin line*), and 1.85 g/g (*thick line*). (**b**) Change of the absorbance during the irradiation for carmine intercalated in the hydrotalcite with the amount of (**a**) 1.85 g/g and (**b**) 0.025 g/g, (**c**) carmine mixed with SiO_2, and (**d**) carmine mixed with the hydrotalcite (Reproduced from the reference [132] with permission)

is known that a rate constant of internal conversion is limited by Franck-Condon factor which is the overlap integral of vibrational parts of wave functions in the states before and after the transition [140]. Carmine and carthamus yellow were reported to have planar molecular conformations in hydrotalcite, expecting similar molecular conformation in excited state to that of the ground state. The conformation similarity increased the Franck-Condon factor and increased an effective internal conversion from the excited states. The opposite phenomenon (the dyes adsorbed on the external surface of smectites exhibited a decreased internal conversion rate) was also reported as discussed in Sect. 4.2.1. The change of the molecular conformation of the adsorbed dyes in the excited states was allowed on the external surface, while the molecular vibration was suppressed if compared with those in solutions.

Photodecomposition of trifluralin (Scheme 2) was reported as a cyclization between an alkylamino group and one of two nitro groups to form an imidazole ring [141]. The adsorption of trifluralin onto SWy-1 suppressed the molecular motion to form the imidazole ring improving the photostability [142].

Rhodamine 6G (R6G in Scheme 2) was intercalated into smectites, KF, SA, and synthetic hectorites (HE and LP-RD) [143]. The stability of R6G against irradiation was remarkably improved on KF in both of a suspension and a film. As shown in Fig. 4, the emission intensity of R6G depended on the clays, and there is a linear correlation between the photoluminescence intensity and the dye stability, suggesting the quenching of the excited state of R6G was the key parameter to determine the stability. The stability of R6G was substantially modified upon the adsorption onto KF, where the energy transfer from R6G to KF led shorter lifetime of the excited state of R6G.

Improvement of the stability of R6G upon visible light irradiation was also reported for a polymer-smectite intercalation compound [143, 144]. R6G was intercalated in SA with poly(vinyl pyrrolidone) (PVP) to obtain a film, which the

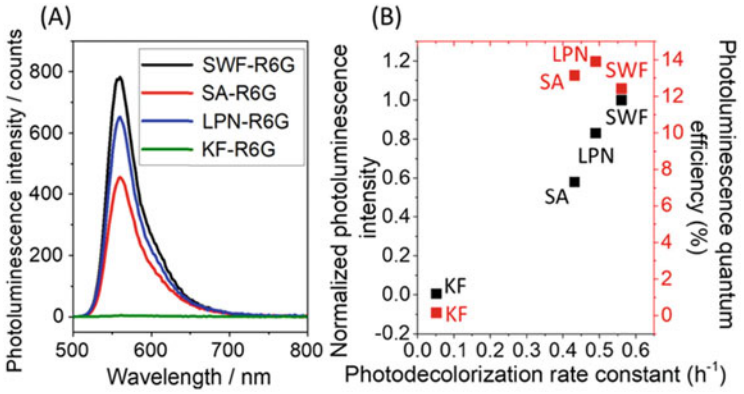

Fig. 4 (**a**) Photoluminescence spectra and (**b**) the relationship between the photodecolorization rate constant and the photoluminescence intensity (*black squares*) and the photoluminescence quantum efficiency (*red squares*) of R6G in HE, SA, LP-RD, and KF suspensions (Reproduced from the reference [143] with permission)

decoloration suppressed upon visible light irradiation over the R6G in SA or in PVP [144]. It was thought that the suppressed oxygen diffusion in the layered structure of SA-PVP contributed to the observed stability.

Another important process is charge transfer (CT) interactions from dyes to layered materials which induce bathochromic shift of absorption spectra [145, 146]. Hybridization of biphenyl with a synthetic hectorite (laponite)-induced absorption at 320 nm attributed to the CT transition, where the biphenyl acted as an electron donor and electron-deficient sites or Lewis acid sites of laponite were electron acceptors [147]. The CT interactions induced a triplet state of biphenyl by recombination from the CT state, and subsequent phosphorescence at 480 nm was observed at 130°C which was stronger than the fluorescence.

Anthraquinone-2-sulfonic acid was hybridized with MgAl-LDH ($Mg_{0.65}Al_{0.35}(OH)_2(CO_3)_{0.01}$), and the hybrid showed photoinduced reduction of the anthraquinone in formamide as shown by the color change from colorless to red [148]. The red color returned to the initial colorless in the dark. The mono-anionic and di-anionic anthraquinones with different lifetime were observed (13.9 and 16.9 min). The solvent was thought to act as the electron donor, and a surface of the MgAl-LDH provides a high pH environment to stabilize the anionic anthraquinone.

Another example is the diverse coloration of retinal Schiff base by the interactions with different smectites. Retinal in rhodopsin as a photoreceptive unit exists as a protonated Schiff base in a *cis*-isomeric state [149], and the rhodopsin provides three different environments for the retinal Schiff base to give blue ($\lambda_{max} = 425$ nm), green ($\lambda_{max} = 530$ nm), and red ($\lambda_{max} = 560$ nm) colors with broad absorption [150]. The similar absorption changes of the retinal Schiff base were observed by mixing the retinal Schiff base with three montmorillonites, Bengel Bright 11 obtained from Wyoming, USA (Hojun Ind. Co., Japan) (479 nm), a

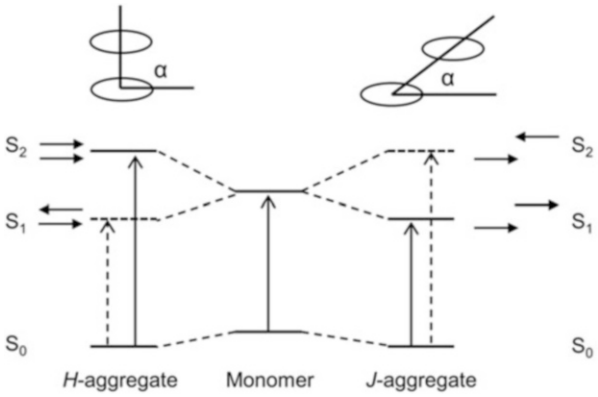

Fig. 5 Schematic representation of the relationship between the dye arrangement and energy level change by molecular aggregation

montmorillonite obtained from Mikawa, Japan (503 nm), and Bengel A obtained from China (Hojun Ind. Co., Japan) (532 nm) [151]. This is a rare example for the retinal Schiff base to show the color variation after the isolation from the protein.

4.1.2 Effect of the Dye Aggregation

Aggregation of such dyes [152–156] as acridine orange [157–159], methylene blue [23, 40, 160], azobenzenes [62, 161–169], merocyanines [170, 171], rhodamines [172–178], nile blue A [179], and porphyrins [180–182] has been reported to be induced by the interactions with layered materials [183, 184]. According to Kasha's molecular exciton theory [185], J- and H-aggregates are distinguished by an angle between the line connecting centers of the dyes and the long axis of the dye molecule (α in Fig. 5). When the angle α is larger than 54.7° as shown on the left side in Fig. 5, the transition from S_0 to S_2 is allowed, it is called H-aggregate, and it's characterized by a hypsochromic shift in the absorption band. When the angle α is smaller than 54.7° as shown on the right side in Fig. 5, the head-to-head aggregate is stabilized, and the transition from S_0 to S_1 is allowed. The aggregate shows a bathochromic shift (redshift) upon aggregation and is J-aggregate. Some dyes were intercalated into layered materials as monomolecular or bimolecular layers. The tilt angle between the silicate layer and dyes transition moment may cause shifts in the absorption spectra.

The effects of the length of the alkyl chain of the guest molecules were shown to affect the stability of aggregates in layered materials [159, 171]. Equilibrium constants K_b (M^{-1}) of the adsorption of *N*-alkylated acridine oranges [158], whose alkyl chains were methyl to tetradecyl (Scheme 3), onto KF were estimated [159]. The rate constant of disaggregation k_m (M^{-1} s^{-1}) was estimated by the change in the absorption change of the monomer. As shown in Fig. 6, the second-order rate constants k_m increased by increasing the length of the alkyl group for short alkyl chains (number of C atoms up to 4), and the opposite behavior was observed for large alkyl chains (C atoms $>$ 4). The variation of k_m was thought to be due to a

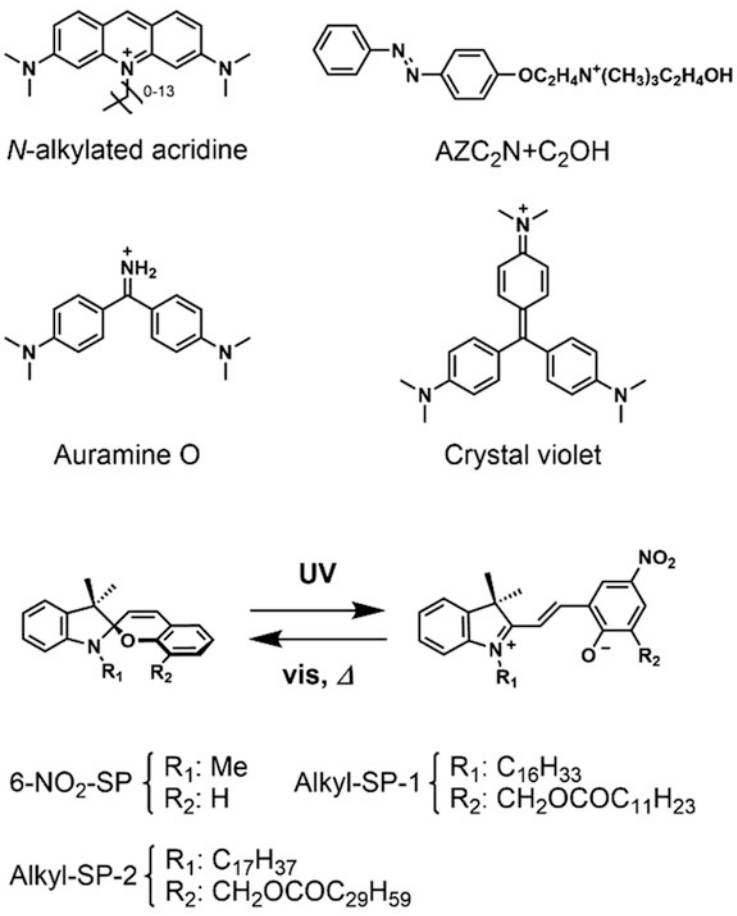

Scheme 3 Molecular structures of dyes which formed aggregates in layered materials

compromise between the steric repulsion and the hydrophobic attraction between the alkyl chains, respectively.

By freeze-drying the suspensions, auramine O (Scheme 3) was hybridized with three montmorillonites SYn-1, SAz-1, and SWy-1 obtained from Source Clays Repository of the Clay Minerals Society [63]. The basal spacings of SYn-1 and SAz-1 did not change by the hybridization, while the absorption due to H-aggregate was observed. The authors proposed that auramine O was adsorbed on the external surface of SYn-1 and SAz-1 as H-aggregates. The absorption and the emission of J- and the H-aggregates of auramine O were observed for SWy-1 depending on the dye loading.

Structure of the intercalation compounds of an amphiphilic cationic azobenzene ($AZC_2N^+C_2OH$, in Scheme 3) KF was proposed from the basal spacing (1.86 nm, corresponding to the gallery height of 0.9 nm) and the bathochromic shift of the

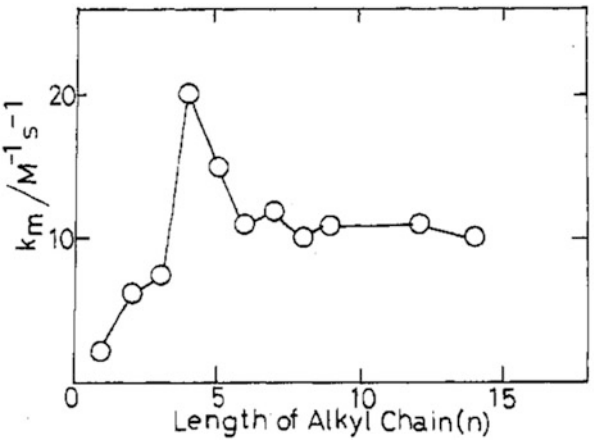

Fig. 6 Dependence of the second-order rate constant, k_m, on the alkyl chain length of 1–14 (Reproduced from the reference [159] with permission)

visible absorption spectra, which was thought to be due to the head-to-tail orientation [62]. Considering the molecular size of $AZC_2N^+C_2OH$ and the observed bathochromic shifts of the visible absorption spectrum, it was proposed that $AZC_2N^+C_2OH$ formed J-aggregate as monolayer or bilayer as shown in Fig. 2. The absorption spectrum of $AZC_2N^+C_2OH$ intercalated in magadiite showed a hypsochromic shift, indicating the formation of H-aggregate, which has a gallery height of 1.57 nm [165, 186]. It was considered that the larger layer charge density of magadiite led the $AZC_2N^+C_2OH$ with the higher tilt angle to the silicate layer than that in KF to lead the H-aggregate (head-to-tail dimer).

The absorption spectra of methylene blue (Scheme 1) in the aqueous dispersions of smectites, whose layer charge densities were reduced by Hofmann-Klemen effect, was investigated [23, 115]. The phenomenon called Hofmann-Klemen effect is attributed to the migration of interlayer lithium ions to the vacancies in the octahedral sheet of smectites by heating. The absorption of J-aggregate decreased, and the dimer increased by reducing the layer charge density of the montmorillonite (obtained from Apache Country, Arizona) [115]. The same trend was seen in montmorillonites obtained from San Diego Country, California, and Horní Dunajovice, Czech Republic; a beidellite obtained from Stebno, Czech Republic; and a smectite obtained from Grand Country, Washington.

Dialkylated spiropyrans (Alkyl-SP-1 and Alkyl-SP-2 in Scheme 3) were intercalated into a film of a didodecyldimethylammonium exchanged montmorillonite, and the aggregation of photochemically formed merocyanines was investigated [171]. A photomerocyanine formed from 6-NO_2-SP has a characteristic absorption at 552 nm, while those of Alkyl-SP-1 and Alkyl-SP-2 absorbed at 493 and 617 nm, which were attributed to H- and J-aggregates, respectively.

Aggregation of dyes in the interlayer space has been reported. The emission of dyes is weaker for H-aggregate due to that the transition dipoles weaken each other [187, 188], while the emission of J-aggregate is intense, and the Stokes shift is smaller than those of the monomer [189–191]. Aggregates of pseudoisocyanine (PIC

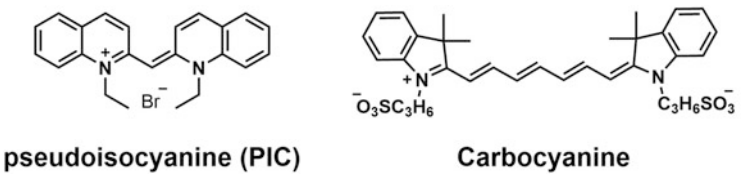

Scheme 4 Molecular structures of cyanines adsorbed on clays

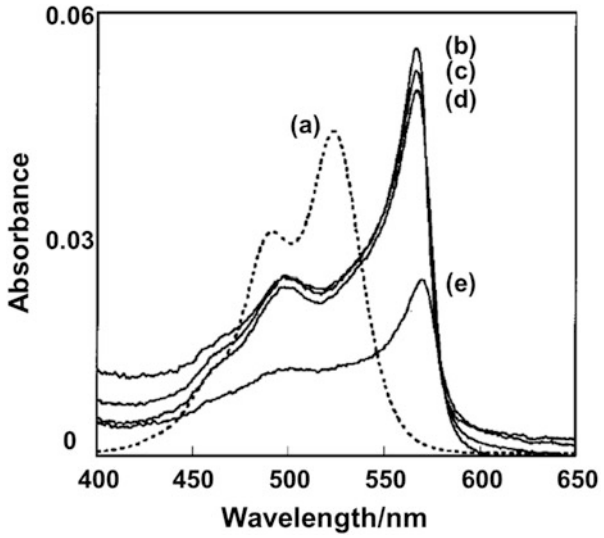

Fig. 7 Absorption spectra of the (**a**) 5×10^{-6} M PIC aqueous solution and aqueous mixtures containing (**b**) 20, (**c**) 10, (**d**) 5, and (**e**) 1 mg of KF and 100 mL of 5×10^{-6} M PIC aqueous solution (Reproduced from the reference [193] with permission)

in Scheme 4) have been studied from 1935 [192] and those in layered materials have been reported from 1996 [193]. PIC has absorption at 490 and 520 nm in an aqueous solution, and the absorption of J-aggregate at 577 nm is seen only at high concentration [194]. An aqueous suspension of KF (10 mg/L) with PIC (5×10^{-6} M) showed absorption at 570 nm, which was attributed to the J-aggregate as shown in Fig. 7. The absorption of J-aggregates increased with increasing the concentration of KF. The aggregation of PIC was investigated using montmorillonites (SWy-1, SAz-1, and SYn-1 supplied from Source Clays Repository of the Clay Minerals Society and KF), SA, synthetic hectorites (SWN supplied from Coop Chemical and LP-RD), TSM [195–200], and magadiite [201] to find H-aggregate in SWy-1, SWN, LP-RD, and SA [197, 199, 202, 203]. For TSM, KF, SAz-1, and SYn-1, the absorption of J-aggregate was observed, and the absorption of the H-aggregate increased with the increase of the loading amount of PIC. There was no clear correlation between the cation exchange capacity (CEC) and the types of aggregates. It was proposed that the particle size of the clays can be a factor to determine the aggregation. The broadening of the absorption spectra of PIC due to the aggregation

was observed for magadiite and dodecyltrimethylammonium (C_{12}TMA)-exchanged magadiite [201]. Because, in magadiite, the absorption shift was smaller and the Stokes shift was larger than those of J-aggregate observed in other clays, PIC formed aggregates in magadiite, while they were not the H- and the J-aggregates.

The H- and the J-aggregates of PIC were switched by swelling of host SA [204]. A SA film with 46.4 meq/100 g (70%CEC) of PIC had absorption of the monomer and a shoulder of the H-aggregate. By adding DMSO, the absorption of the J-aggregate increased, and the monomer and the H-aggregate decreased. The absorption spectrum returned to the initial shape by removing DMSO by washing with ethanol and subsequently drying.

Aggregation of rhodamine 6G (R6G, Scheme 2) in the films of Wyoming montmorillonites [176, 205] and laponites [172, 174–176] was investigated. R6G had absorption at 527 nm in an aqueous solution, [172] and, by adding the montmorillonite, absorption at 534 nm due to J-aggregate and two shoulders at around 500 and 470 nm appeared [205]. The absorption at 500 nm increased, and the shift of the monomer absorption from 527 to 538 nm was observed in a laponite film, which corresponded to the formation of the H- and the J-aggregates [172]. H- and J-aggregates were observed in the absorption and emission spectra of the film of a hexadecyltrimethylammonium (C_{16}TMA) exchanged KF [206]. Effective quenching of the emission from the H-aggregate [207] was observed for auramine O in SYn-1 powder [63], PIC in LP-RD powder [196], and merocyanine 540 in a bentonite (obtained from Ordu/Ünye in Turkey) and the bentonite exchanged with C_{16}TMA [208].

4.2 Changes in the Photoluminescence Properties

4.2.1 Effects of the Host-Guest Interactions

Adsorption on the external surface and in the interlayer space of layered materials suppresses molecular motion of dyes and induces a planar conformation [183, 209–217]. Three different effects of electrostatic interactions and the suppression of the molecular motion on the emission spectra have been proposed: (1) the bathochromic shift of emission by electrostatic interactions, (2) smaller Stokes shift than that in solutions owing to the similar molecular conformation of the excited and ground states inducing hypsochromic shift and increase intensity of the hypsochromic emission, or (3) decrease of the internal conversion rate due to the fixation of the molecular conformation in the excited state on the external surface. These effects were reported for porphyrins [17, 218–222], auramine O [223], and triphenylbenzene derivatives [224].

Porphyrins have two π-π^* transitions known as Soret band at around 400–500 nm and Q-band at around 500–700 nm. The Soret band and the Q-band of tetraphenylporphine (TPP, Scheme 5) and Fe(III)-TPP shifted by the adsorption on a purified Wyoming bentonite from 416 to 445 nm and 620 to 664 nm, respectively [218]. The shift of the absorption was explained by the coplanar structure of the

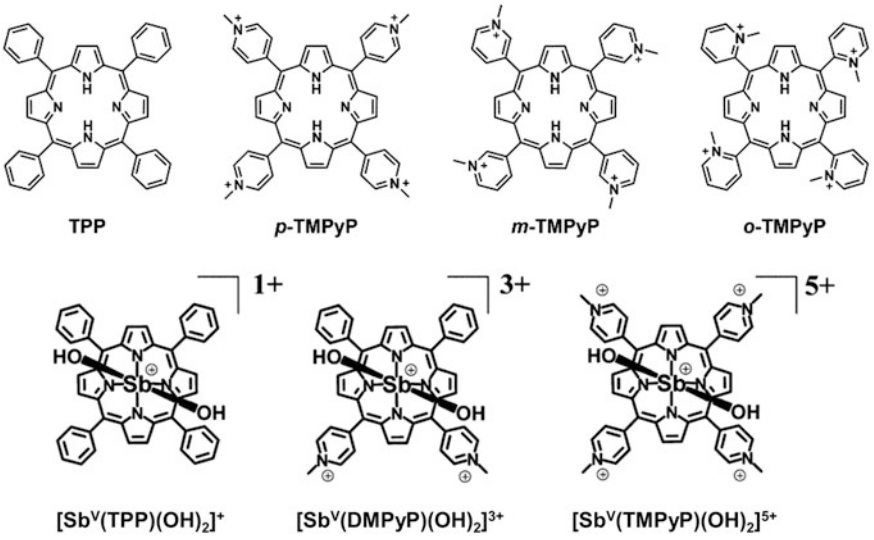

Scheme 5 Molecular structures of porphyrin derivatives and Sb-porphyrin complexes adsorbed on clays (Reproduced from the reference [225] with permission)

porphyrin moieties and the phenyl substituents on the silicate layer. The relationship between the shift of the Soret band and the molecular structure of porphyrins has been studied to find that the matching of the intercharge distance of the porphyrins and the distance of the adjacent negative charge of the silicate layer was important [17, 219–221]. The shifts of the Soret bands of *p*-TMPyP, *m*-TMPyP, and *o*-TMPyP (Scheme 5) on SA were 30, 12, and 6 nm compared to their aqueous solutions [221]. The shifts were larger when the intercharge distance of the porphyrins (*p*-TMPyP, 1.05; *m*-TMPyP, 0.99; and *o*-TMPyP, 0.88 nm) was closer to the distance of the adjacent negative surface charge (1.19 nm). The planar structure of the three porphyrin derivatives on SA was proposed to be a reason for the shift of the fluorescence to longer wavelength region as shown in Fig. 8 [225, 226]. Fluorescence quantum yields and rate constants of the internal conversion of $[Sb^{V}(TPP)(OH)_2]^{+}$ and $[Sb^{V}(DMPyP)(OH)_2]^{3+}$ (Scheme 4) increased by the adsorption because the excited states of the two derivatives had more similar structures to the ground states than those in solutions. Among the three tested porphyrins, $[Sb^{V}(TMPyP)(OH)_2]^{5+}$ adsorbed on SA had the fluorescence quantum yield same as that in an aqueous solution, while the internal conversion rate was lower than those of the others, suggesting the suppression of the molecular motion to keep the molecular structure in the excited state by the stronger electrostatic interactions with SA if compared with $[Sb^{V}(TPP)(OH)_2]^{+}$ and $[Sb^{V}(DMPyP)(OH)_2]^{3+}$.

The fluorescence of methyl viologen (MV^{2+}) shown in Scheme 6 in hectorite and montmorillonite was observed as a result of the photoinduced charge transfer from the silicate layers to MV^{2+} [227]. Change of the emission spectra of MV^{2+} by the adsorption on layered materials has been studied [227]. MV^{2+} and viologen derivatives have been intercalated into montmorillonites [227–231], saponite [232, 233],

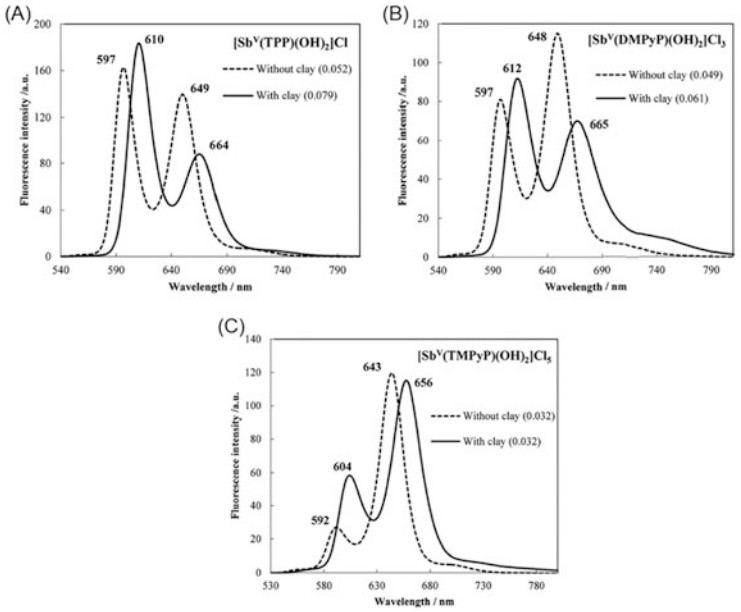

Fig. 8 Fluorescence spectra of *p*-TMPyP (A), *m*-TMPyP (B), and *o*-TMPyP (C) with clay (*solid line*) and without clay (*dashed line*) (Reproduced from the reference [226] with permission)

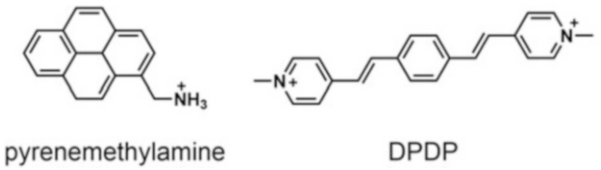

Scheme 6 Molecular structures of dyes which form excimer in the interlayer space

hectorite [227, 231], nontronite [227, 231], vermiculite [229], titanates [234], niobates [235–238], and layered zirconium phosphate [239, 240]. The absorption spectra of MV^{2+} showed bathochromic a shift by the intercalation into smectites (KF, SA, and LP-XLG) [233], the layered zirconium phosphate/phosphonates [239, 240], and niobate [235–238]. The intercalated hybrid showed reversible color change to blue by the photoinduced charge transfer from the host. Non-emissive MV^{2+} showed fluorescence in an aqueous suspension of a hectorite (San Bernardino) and a montmorillonite (Clay Spur, Wyoming), and this phenomenon was explained by the planar structure of MV^{2+} on the silicate layer [231]. This phenomenon can be explained as "adsorption-induced emission." The emission intensity of MV^{2+} increased by the decrease of the loading amount (by the increase of the concentration of the clays). The self-quenching of fluorescence of MV^{2+} on

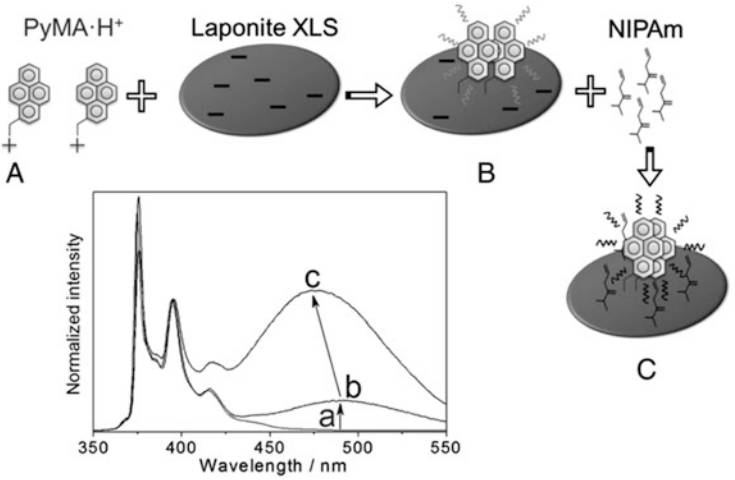

Fig. 9 Schematic illustration of the adsorption of pyrenemethylamine and *N*-isopropylacrylamide on LP-XLS and the corresponding normalized emission spectra. (**a**) Pyrenemethylamine in the aqueous solution; (**b**) pyrenemethylamine adsorption on LP-XLS; (**c**) co-adsorption of *N*-isopropylacrylamide on LP-XLS. The spectra a, b, and c correspond to the conditions A, B, and C (Reproduced from the reference [253] with permission)

the clays was proposed as a reason of the weaker emission at the high loading amount.

Absorption at 410 and 450 nm appeared in powder of pyrene hybridized with LP-RD by UV irradiation. Electron spin resonance experiment with and without O_2 (triplet quencher) indicated that the absorption was from a triplet state of radical cation of pyrene [241]. The radical cation of pyrene was thought to be generated by the photoinduced charge transfer from pyrene to LP-RD. The color of the hybrid was different depending on the pre-activation temperature of LP-RD. The intensity of the ESR signal was higher when the pre-activation temperature was lower, suggesting the interactions of the surface water/OH groups with the adsorbed pyrene.

4.2.2 Excimer Formation

Pyrene has been used as a probe to investigate the surface chemistry [242–247] and refractive index [248] of clays as well as the surface modification with alkylammonium surfactants [249–252]. Excimer emission of pyrenemethylamine (Scheme 6) was enhanced by adding LP-XLS to an aqueous solution of pyrenemethylamine, suggesting change in the intermolecular distance between the adjacent pyrenemethylamine molecules [253]. As shown in Fig. 9, co-adsorption of *N*-isopropylacrylamide further enhanced the excimer emission, suggesting that *N*-isopropylacrylamide reduced the intermolecular distance of pyrenemethylamines to induce effective intermolecular interactions.

Packing of DPDP [254] (Scheme 6) changed by the swelling of SA with DMSO [255]. DPDP was intercalated into SA film with various loading amounts from 0.033 to 49.7 meq/100 g (from 0.05 to 75%CEC). At the loading from 0.033 to 26.5 meq/100 g, the emission of the monomer at 482 nm decreased, while new emission at 588 nm of excimer appeared by the increase of the concentration. The gallery height of the hybrid increased from 0.48 to 0.93 nm by the swelling of SA with DMSO and the excimer emission enhanced, suggesting that the swollen SA provides the interlayer expansion large enough for the π-π stacking of DPDP.

4.2.3 Energy and Electron Transfer Between Molecules Adsorbed on Clays

The construction of photocatalyst by energy transfer in the interlayer space is a topic of interest [256–262]. Adsorption on layered materials is a way to concentrate dyes and to control the proximity, which resulted in efficient energy [19, 263–269] and electron transfer [18, 31, 270, 271]. Expected effects of hybridization of dyes and layered materials are (1) efficient quenching of the excited state of the dyes for photostabilization, (2) separation of the photosensitizer from photocatalyst to avoid the photocatalytic decomposition of sensitizer, and (3) directional energy and electron transfer by locational and orientational design.

A possible way to improve the photostability is quenching the photoexcited state by energy transfer as discussed in Sect. 4.1. The stability of herbicides [272–274], bioresmethrin [275], and norflurazon [276] was improved by energy or electron transfers to methyl green co-adsorbed on montmorillonite and to thioflavin T on SWy-1. The separation of the photosensitizer from the photocatalyst (anatase particle) by smectite nanosheet induced durability of the photosensitizer. The photocatalytic oxidation of benzene to phenol was done in an aqueous suspension of anatase with the tris(2,2-bipyridine)ruthenium(II) (designated as $[Ru(bpy)_3]^{2+}$)-synthetic saponite, resulting in a high yield of benzene decomposition and selectivity of phenol. The hybrid was processed as a film to be used as the photocatalyst layer to obtain a photocatalytic flow reactor [277, 278].

The fluorescence of $[Ru(bpy)_3]^{2+}$ was quenched by SO_2 gas [107] suggesting a possible gas sensor application. The fluorescence of $[Ru(bpy)_3]^{2+}$ was quenched by the MV^{2+} co-adsorbed on smectites, and the quenching efficiency was higher when smectites with larger particle sizes (e.g., TSM) was used if compared with those on clays with smaller particle sizes (e.g., SA and LP-XLG) [279]. Such quenchers as cyanine, MV^{2+}, and anthraquinone derivatives were co-adsorbed with cyanine dyes on laponite RDS (Southern Clay Products, Inc.) to quench the fluorescence of the J-aggregate of the cyanine [280].

MV^{2+} (Scheme 7) in the interlayer space of smectites acted as an electron acceptor [232, 233, 281–284]. It was reported the photoinduced electron transfer from TPP (Scheme 5) to MV^{2+} under visible light irradiation to form the TPP radical cation and MV^{+} radical cation [281]. The color of MV^{2+} intercalated in a hectorite-like layered silicate changed by the adsorption of *N*,*N*-dimethylaniline and

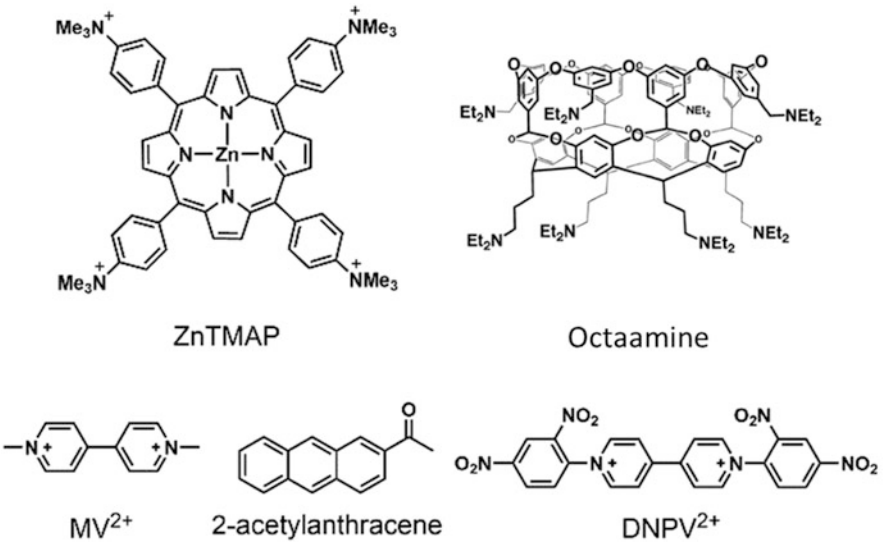

Scheme 7 Molecular structures of dyes exhibited energy and electron transfer on layered materials

2,4-dichlorophenol [285], and the color depended on the layer charge density and the concentration of the adsorbents. The hectorite-like layered silicate was synthesized from LiF, Mg(OH), and SiO_2 sol with various ratios to vary the layer charge density [286]. The color of the hybrids of the hectorite and MV^{2+} changed from yellow to purple green and purple by the adsorption of *N*,*N*-dimethylaniline depending on the layer charge density and the increase of the concentration of *N*,*N*-dimethylaniline. Color changed from yellow to orange was seen by the adsorption of 2,4-dichlorophenol. The color of the hybrids with *N*,*N*-dimethylaniline was explained to the formation of methyl violet, and that with 2,4-dichlorophenol was attributed to the charge-transfer complexes.

Effects of the molecular location and orientation on the energy transfer between adjacent molecules have been investigated in porphyrin-smectites systems [19, 211, 260, 264, 266, 284]. Energy transfer from Zn complexed aniline-substituted porphyrin (ZnTMAP, Scheme 7) to pyridine-substituted porphyrin (*p*-TMPyP, Scheme 5) was investigated in SA suspension by monitoring the contribution of the fluorescence from ZnTMAP excited at 428 nm, which matched the absorption of Soret band of ZnTMAP [287]. When the two porphyrins adsorbed on SA individually and subsequently mixed, the contribution of the fluorescence intensity of ZnTMAP was the same in the concentration region of the porphyrins to 6.6 meq/100 g (10%CEC, for each), while the contribution decreased in the higher concentration region (Fig. 10). When the two porphyrins were co-adsorbed on SA, the contribution of the fluorescence intensity of ZnTMAP was decreased from 0.6 to 0.1 with increase of the concentration of the two porphyrins to 0.066 meq/100 g (0.1%/CEC for each), and then, the contribution of ZnTMAP gradually decreased and become negligibly small at 29.8 meq/100 g (45%CEC for each) as shown in Fig. 10. These results

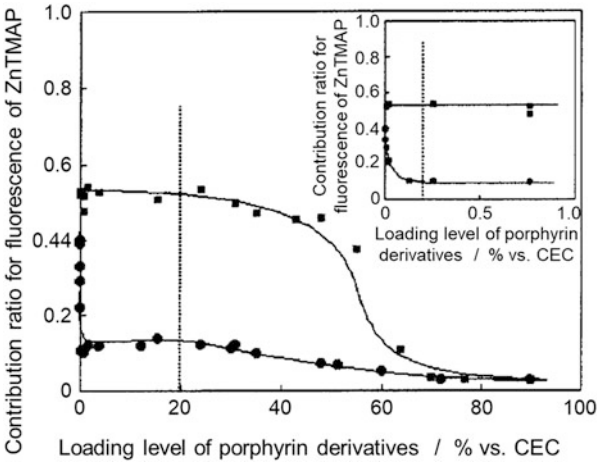

Fig. 10 Contribution of ZnTMAP for fluorescence at various porphyrin loading levels for independent adsorption (*squares*) and co-adsorption (*circles*) (Reproduced from the reference [287] with permission)

suggested that the energy transfer between SA layers was major in the suspension prepared with SAs that adsorbed porphyrins individually, while the intralayer energy transfer was major in the suspension prepared with SA with porphyrins by the co-adsorption.

The sequential energy and electron transfers from 2-acetylanthracene to Zn-*p*-TMPyP to $DNPV^{2+}$ (Scheme 6) on SA were reported [288]. 2-Acetylanthracene was encapsulated in octaamine to be adsorbed on SA with 1:1 ratio of Zn-*p*-TMPyP. In a suspension of SA with 2-acetylanthracene in octaamine and Zn-*p*-TMPyP, the decrease of fluorescence of 2-acetylanthracene and the increase of that of Zn-*p*-TMPyP compared to suspensions were seen, suggesting the energy transfer from 2-acetylanthracene in octaamine to Zn-*p*-TMPyP. The shorter lifetime of Zn-*p*-TMPyP in a suspension of SA with $DNPV^{2+}$ than that in a suspension without $DNPV^{2+}$ suggested the electron transfer from Zn-*p*-TMPyP to $DNPV^{2+}$.

4.3 Alignment of Dyes by Host-Guest Interactions: Study by Linear Polarized Light

Film of propylammonium-exchanged titanate ($Na_2Ti_3O_7$) was prepared by casting an aqueous suspension and used as a host of cationic dyes. Pseudoisocyanine (PIC in Scheme 7) intercalated in the titanate film showed absorption anisotropy [289] as shown in Fig. 11. The absorbance in the visible region with 5° of the angle between the film plane and the incident light was decreased by the rotation of the incident polarized light from 0° to 90°, while the small absorption change was observed with 90° of the angle between the substrate plane and the incident light. It suggests that a transition moment of PIC, which corresponds to the long molecular axis, was parallel to the substrate.

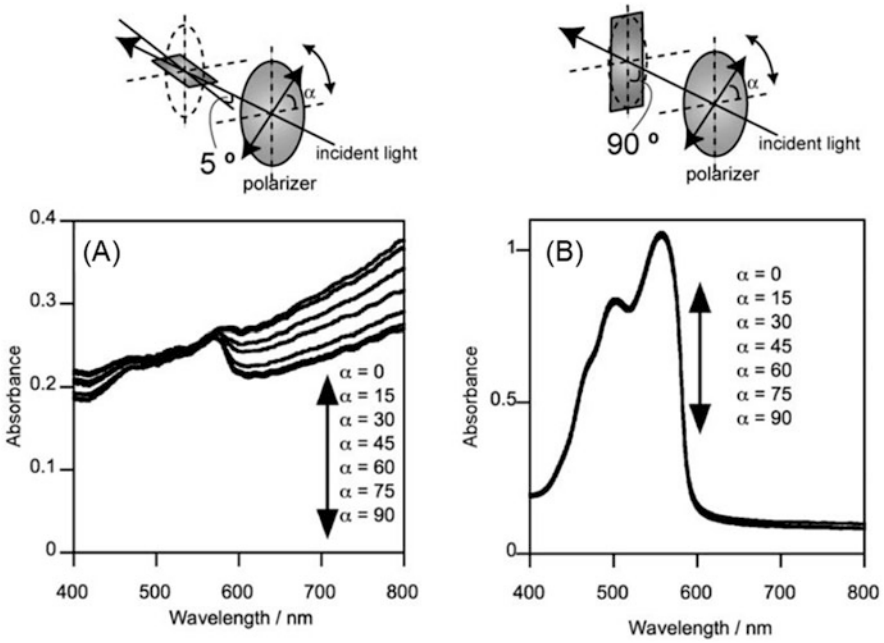

Fig. 11 Polarized visible spectra of a film of PIC-Ti_3O_7. The angle between the substrate plane and the incident light was set to (**a**) 5° and (**b**) 90° by rotating the film; a represents the angle between the polarization direction of the incident light and the rotation axis of the film (Reproduced from the reference [289] with permission)

The angles between molecular axes of the following porphyrin derivatives, *p*-TMPyP, *trans*-DMPyP, and *cis*-DMPyP (Scheme 4), and the silicate layer of SA were estimated by polarized visible light attenuated total reflection (polarized vis-ATR) spectra [290]. Figure 12 shows that the absorbance of *p*-TMPyP of s-polarized light was larger than that of the p-polarized light. A similar difference in the polarized absorption spectra was observed in *trans*-DMPyP and *cis*-DMPyP. The angles between the molecular axes of the three porphyrins and the surface of the silicate layer were estimated to be less than 5°.

Fluorescent dyes adsorbed in layered materials showed linearly polarized emission, suggesting the alignment of the dye dipole in the interlayer space [291–293]. A laponite film was prepared by spin-coating an aqueous suspension and was used to accommodate rhodamine 6G (R6G, in Scheme 2) by cation exchange by immersing the film in an R6G solution [206, 294, 295]. Fluorescence intensity excited by horizontally polarized light depended on the direction of the polarizer. The angle between the long axis of R6G and the silicate layer was estimated to be 28° from the difference of the fluorescence intensities observed with horizontal or vertical axes of the film.

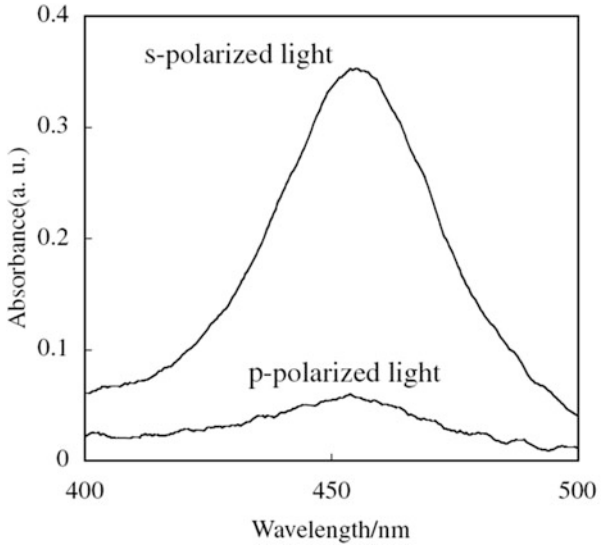

Fig. 12 Polarized vis-ATR spectra of *p*-TMPyP with s- and p-polarized light (Reproduced from the reference [290] with permission)

Polarized fluorescence of rhodamine B [296], fluorescein [297], pyrene [298], cyanine [299], niflumic acid [300], bis(*N*-methylacridinium) [301], tris (8-hydroxyquinolate-5-sulfonate)aluminum(III) [302], polyphenylene [303], and polythiophene [304] in LDH films prepared by LbL technique was reported. The anisotropic value *r* as defined by Eq. (1) was derived to discuss the dye orientation from emission anisotropy.

$$r = \frac{I_{VV} - I_{VH}}{I_{VV} + 2I_{VH}} \tag{1}$$

In (1), I_{VV} and I_{VH} are emission intensities with vertical and horizontal directions excited by vertical light [305]. The fluorescence spectra of a carbocyanine (Scheme 4) intercalated in a MgAl-LDH [303] showed anisotropy (Fig. 13) with the *r* value as high as 0.8, where the value was higher than that in a solution (0.2) and nearly twice of the theoretical highest value in the case without macroscopic alignment (0.4) [299]. The *r* value of the carbocyanine was larger than pyrene (0.26) [298], fluorescein (0.3) [297], and fluorenone derivatives (0.25) [306], which have planar molecular structures. The orientation of the intercalated dye in MgAl-LDH was thought to induce the anisotropy.

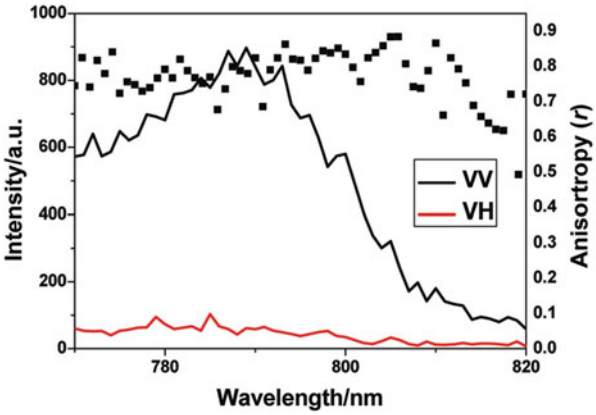

Fig. 13 Polarized fluorescence with the intensities of I_{VV} and I_{VH} and the r value for the hybrid of the carbocyanine in MgAl-LDH (Reproduced from the reference [303] with permission)

5 Photochemical Reactions

5.1 Intramolecular Reactions Affected by Host-Guest Interactions

Molecular reactions of organic compounds interacted in clays are different from those in solutions. The molecular reactions of the organic molecules were affected by the polarity of interlayer space and/or by the suppression of molecular vibration in the interlayer space [8, 10, 307].

5.1.1 Azobenzene

Azobenzene (AZ) shows photoisomerization from *trans*- to *cis*-isomer by UV irradiation, and the *cis*-isomer returns to the initial *trans*-isomer by heat or visible light irradiation as shown in Scheme 8. The half-lives of the thermal isomerization of the *cis*-isomer to the *trans*-isomer of AZ in a benzene solution at room temperature and 60°C were 119 [308] and 1.5 h [309], respectively, in the dark following first-order kinetics. The polarity and the viscosity of the solvent affect the photoisomerization of AZ [310, 311], and the photoisomerization was suppressed in packed states [312]. Accordingly, the host-guest interactions are expected to affect the photoisomerization.

Here, a fraction of the *cis*-isomer of AZ is used as a measure of photoisomerization. The fractions of the *cis*-isomer of AZ at the photostationary state in cyclohexane [313] and in toluene [314] solutions were 80 and 90%, respectively. Although the fraction of the *cis*-isomer is different depending on the substituents of the azobenzene and the wavelength of the incident light [315], the fraction of the *cis*-isomer in polymethyl methacrylate (PMMA) was as high as that in the toluene solution [316]. The fraction of the *cis*-isomer became smaller in poly (styrenesulfonate) (PSS) [317], azobenzene polymer [318], SiO_2 [316], and zeolite

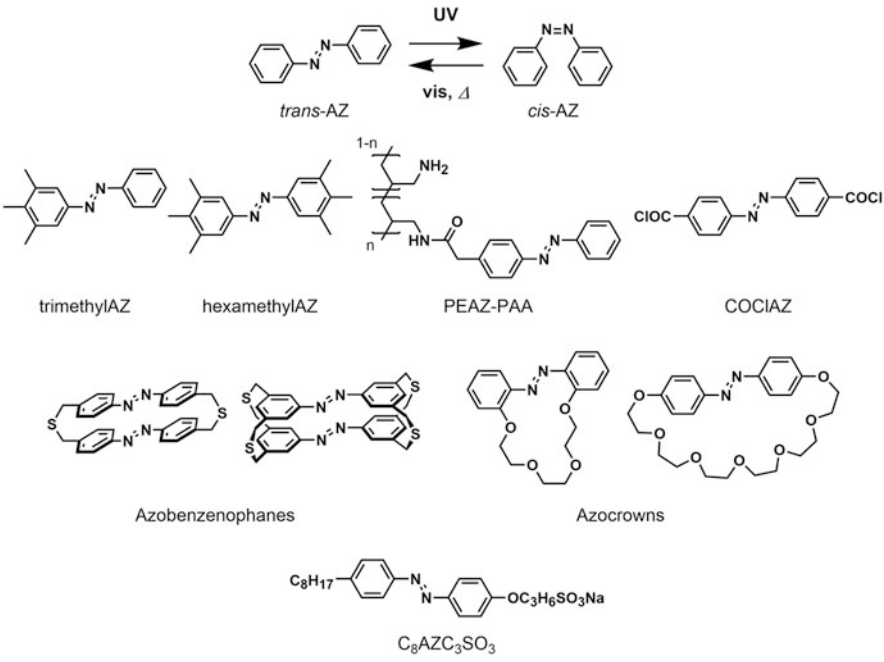

Scheme 8 Molecular structures of azobenzenes introduced in this chapter

[313] as summarized in Table 2. The fraction (83%) of the *cis*-isomer of trimethylAZ was larger than that (60%) of hexamethylAZ in the methylcyclohexane-isohexane 2:1 solution [319] and that (64%) of C_1AZC_2OH (in Table 2) in a SiO_2 film prepared by a sol-gel reaction with tetraethoxysilane (TEOS), but it was smaller than that (93%) in the ethanol solution [316] (Table 2). It was explained that the steric repulsion between the azobenzene derivatives and the media is an important factor to change the molecular fraction of the *cis*-isomer. The azobenzene derivatives, which were introduced as building blocks of co-polymers (PEAZ and COClAZ in Scheme 8), showed a smaller fraction (65–70% for PEAZ and 50% in a swelled film for COClAZ) of the *cis*-isomer than that in the AZ solution of cyclohexane. The steric repulsion between the azobenzene part and the other part of the polymer suppressed the isomerization. LB films with amphiphilic azobenzene derivatives (as summarized in Table 2) have been studied [320–332]. The fraction of the *cis*-isomer was as high as 90% in the LB films of $C_8AZC_3SO_3$ (Scheme 8) with poly (diallyldimethylammonium chloride) [332].

AZ was adsorbed on a sodium montmorillonite by solid-solid reactions [334] and from vapor [335]. Adsorption of AZ on a kaolinite from aqueous solution was also reported [217]. Photochemical studies of AZ in layered materials were initiated by Ogawa et al., and the first one was that on the AZ intercalated in an organically modified montmorillonite [334]. Then, amphiphilic cationic azobenzenes were intercalated into a montmorillonite [161], followed by the intercalation of various

Table 2 Fraction of *cis*-isomer of azobenzene derivatives

Derivative	State	*cis*-isomer fraction	Excitation wavelength (nm)	Reference
AZ	Cyclohexane	80%	254	Kojima et al. [313]
	Toluene	91%	365	Fischer et al. [314]
	Zeolite NaY (pore size: 0.74 nm)	80%	313	Kojima et al. [313]
	Sodium mordenite (pore size: 0.7 × 0.65 nm)	50%	313	Kojima et al. [313]
TrimethylAZ	Methylcyclohexane-isohexane 2:1	83%	313	Gegiou et al. [319]
HexamethylAZ	Methylcyclohexane-isohexane 2:1	60%	313	Gegiou et al. [319]
C_1AZC_2OH	Ethanol	93%	365	Ueda et al. [316]
	PMMA ($M_n = 1.0 \times 10^5$, $T_g = 105°C$)	93%	365	Ueda et al. [316]
	SiO_2 (sol-gel film)	64%	365	Ueda et al. [316]
PEAZ-PAA	Multilayer film with polystyrenesulfonate (PSS)	Dry film: 31% Swollen film: 50%	320–380	Suzuki et al. [317]
COClAZ	Introduced as a part of polymers in *N*,*N*-dimethylacetamide	65–70%	370–400	Beattie et al. [318]
$AZC_2N^+C_2OH$	MCM-41 with 3.2 nm pore size	70%	350	Ogawa et al. [333]
$C_8AZC_{20}Py^+$	LB film with dimyristoylphosphatidic acid (DMPA)	Ca. 90%	365	Maak et al. [332]

ionic azobenzenes (summarized in Table 3) into layered clay minerals [62, 163–165, 167, 186, 336–340], layered double hydroxide (LDH) [341], potassium hexaniobate ($K_4Nb_6O_{17}$) [342], and a titanoniobate [343] by ion exchange reactions.

The photochromism of AZ was observed in organically modified KF [334] and TSM [162, 349]. The fraction of the *cis*-isomer of AZ in didodecyldimethylammonium ($2C_{18}2C_1N^+$)-TSM was about 80% at the

Table 3 Molecular structures of cationic azobenzenes intercalated in smectites

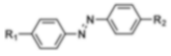	Derivatives	R_1	R_2	References
	C_1AZC_2OH	OCH_3	OC_2H_4OH	Okada et al. [344]
	AminoAZ	H	NH_2	Ogawa et al. [345]
	AZN^+	H	$N^+(CH_3)_3$	Ogawa et al. [345]
	AZC1N+	H	$CH_2N^+(CH_3)_3$	Bujdák et al. [337]
	$AZC_2N^+C_2OH$	H	$C_2H_4N^+(CH_3)_2C_2H_4OH$	Ogawa et al. [167, 186, 344, 346]
	$C_2AZC_2N^+$	C_2H_5	$OC_2H_4N^+(CH_3)_3$	Okada et al. [344]
	$C_8AZC_{10}N^+$	C_8H_{17}	$OC_{10}H_{20}N^+(CH_3)_3$	Ogawa et al. [161, 165]
	$C_8AZC_{10}N^+C_2OH$	OC_8H_{17}	$OC_{10}H_{20}N^+(CH_3)_2C_2H_4OH$	Takagi et al. [347]
	$C_{12}AZC_5N^+$	$OC_{12}H_{25}$	$OC_5H_{10}N^+(CH_3)_3$	Ogawa et al. [62, 161, 163–165]
	N^+AZN^+	$N^+(CH_3)_3$	$N^+(CH_3)_3$	Umemoto et al. [348]
	$N^+C_1AZC_1N^+$	$CH_2N^+(CH_3)_3$	$CH_2N^+(CH_3)_3$	Bujdák et al. [337]

photostationary state under a 500 W super high-pressure Hg lamp [162], while that in octadecyltrimethylammonium cation ($C_{18}3C_1N^+$)-TSM was about 35% under a 100 W high-pressure Hg lamp [349]. The difference of the fraction of the *cis*-isomer is thought to be due to the molecular packing of the surfactants in the interlayer space. The thermal *cis*- to *trans*-isomerization of AZ in $C_{18}3C_1N^+$-TSM took 2 days [349] which was faster than the half-life of *cis*-AZ in a benzene solution (5 days) [308]. The thermal isomerization of *cis*-AZ in the solution followed a first-order kinetics while in such polymers as poly(methyl methacrylate) (PMMA) [350] and poly(ethyl methacrylate) (PEMA) [351] and a silica gel synthesized by sol-gel method did not follow the first-order kinetics [350], indicating that the azobenzene molecules were in several environments in these solid-state materials.

The photochromism of cationic azobenzenes in montmorillonites [62, 161, 344], saponites [163, 337, 352], a fluorohectrite [337], taeniolite [163], and magadiite [164, 165, 186, 346] was reported [167]. Organically modified fluoro-tetrasilicic mica [345], montmorillonite [353], and beidellite [353] were also used. As summarized in Table 2, the fraction of the *cis*-isomer of $AZC_2N^+C_2OH$ in mesoporous silica (MCM-41) with the pore size of 3.2 nm was 70% [333], and those of AZ in a zeolite NaY (pore size: 0.74 nm) and a sodium mordenite (pore size: 0.7 × 0.65 nm) were 80 and 50%, respectively [313]. The fraction of *cis*-isomer of the cationic azobenzene ($AZC_2N^+C_2OH$, Table 3) in magadiite at room temperature was 80%, similar to AZ in a cyclohexane solution [165]. It was thought that the structural change of azobenzenes was accommodated by the change of the basal spacing to achieve the relatively high yield of *cis*-isomer. The thermal isomerization of *cis*-isomer of $AZC_2N^+C_2OH$ in magadiite followed the first-order kinetics, indicating that $AZC_2N^+C_2OH$ was homogeneously distributed in magadiite. The fraction of *cis*-isomer at the photostationary state decreased in KF [161] and magadiite [165] at low temperatures. The fraction of *cis*-isomer of the cationic azobenzenes ($C_8AZC_{10}N^+$ and $C_{12}AZC_5N^+$, in Table 3) in KF at room temperature was about 50%, while *cis*-isomer was practically not detected at the temperature lower than 200 K, suggesting that the molecular motion was suppressed in the interlayer space of KF.

There are several examples of the suppression of the *trans*- to *cis*-isomerization. In a fluorohectorite (obtained from Corning Inc.) in both suspensions and films, photoisomerization of $N^+C_1AZC_1N^+$ (Table 3) was suppressed, while AZC_1N^+ isomerized as shown by the change in the absorption spectrum (Fig. 14) [337]. It was explained that attractive electrostatic forces between the silicate layers and the dicationic $N^+C_1AZC_1N^+$ hindered the isomerization. Photoisomerization of N^+AZN^+ (Table 3) was suppressed by the adsorption on SA [348]. Both *trans*- and *cis*-isomers of N^+AZN^+ were exchanged on SA. The *cis*-isomer showed photoisomerization to the *trans*-isomer on SA by 420 nm light irradiation with a higher quantum yield than that in an aqueous solution (without clay), while *trans*-isomer on SA did not show photoisomerization. The suppression of the *trans*- to *cis*-isomerization was thought to be due to the matching of the intercharge distance of the *trans*-isomer and that of the adjacent negative surface charge of the silicate layer. The *trans*-isomer interacted with the silicate layer with both of two cationic moieties

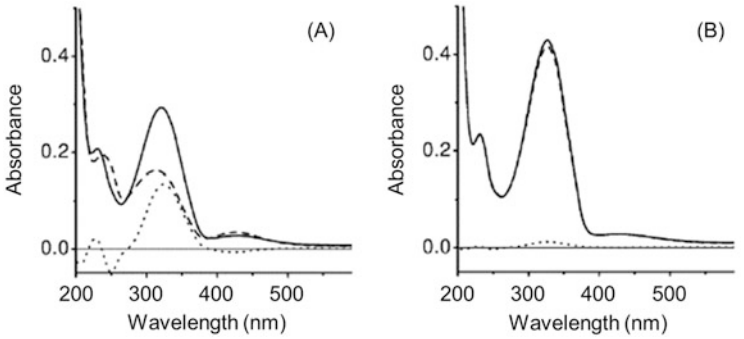

Fig. 14 UV-vis absorption spectra of (**a**) AZC_1N^+ and (**b**) $N^+C_1AZC_1N^+$ in a fluorohectorite dispersion. The spectra were recorded before (*solid line*) and after the UV irradiation (*dashed line*). Difference spectra were derived by subtracting the spectrum before the irradiation from that of the irradiated solution (*dotted line*) (Reproduced from the reference [337] with permission)

and the molecular motion was suppressed. In the case of the *cis*-isomer, one of the two cationic moieties interacted with the surface charge, leading that the *cis*-form isomerized to the *trans*-isomer.

Nonionic azobenzenes intercalated in organically modified clays and cationic azobenzenes exchanged on clays showed photochromism with the relatively high fraction of the *cis*-isomer at the photostationary state. When a dicationic azobenzene was adsorbed on SA, the isomerization of the *trans*-isomer was suppressed. By the design of the interlayer space of clays, the control of the photochromism of azobenzene such as the fraction of the *cis*-isomer, thermal fading speed to achieve quick response, and bistability is expected.

5.1.2 Diarylethene

Photochromism of diarylethenes is attributed to reversible photocyclization between two aryl rings [354]. Open-ring isomer of diarylethenes shows photocyclization under UV irradiation and closed-ring isomer with a planar π-system forms. Both of the open-ring and the closed-ring isomers do not show the thermal isomerization to give P-type (thermally irreversible, but photochemically reversible) photochromism. The reversibility and the durability of the diarylethenes have been investigated by Irie through molecular design [354]. The points are (1) substitution with a ring structure to suppress the *cis-trans* isomerization of stilbene and (2) substitution with thiophene rings to stabilize the closed-ring isomer as shown in Scheme 9. The open-ring isomer of the diarylethenes has two molecular conformations,

Scheme 9 Molecular design of diarylethenes

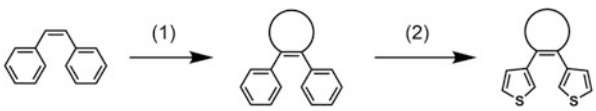

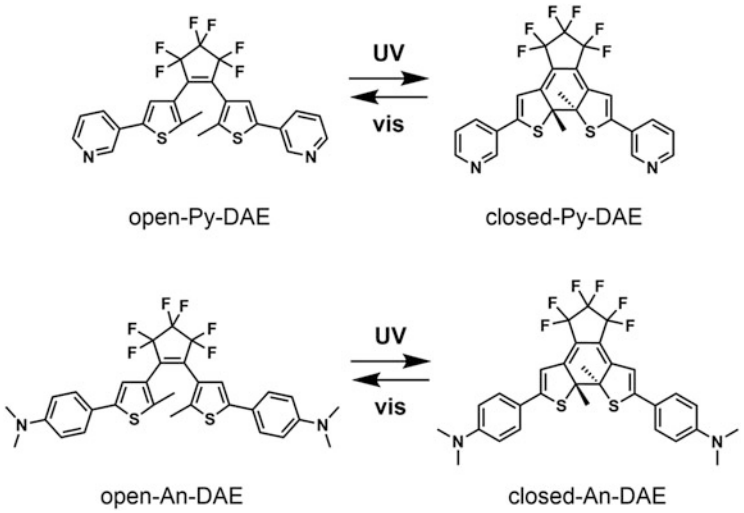

Scheme 10 Molecular structures of diarylethenes hybridized with clays

photoinactive parallel and photoactive antiparallel conformations, and the ratio of these conformations are almost equal in solution [354]. In addition to the photoinduced oxidation of thiophen rings [355], a photoinactive isomer, which formed by the condensation of two thiophen rings, was reported as a deactivation process of diarylethenes [356–359]. In order to improve the reversibility and the yield of photocyclization, control of the molecular conformation of the diarylethene has been examined by the molecular and supramolecular designs using such intramolecular interactions as hydrogen bonds [360, 361], intramolecular steric repulsion [362, 363], as well as the host-guest interactions in nanospaces [364, 365]. Almost unity quantum yield (98%) of a ring-closing reaction of a diarylethene derivative was achieved in a hexane solution by restricting the molecular motion with intramolecular hydrogen bonds, being smaller in polar solvents (in methanol solution: 54%) [360, 361].

Restricted molecular motion by host-guest interactions is expected to affect the ring-closing reaction. A pyridine- and aniline-substituted diarylethenes (Py-DAE and An-DAE, Scheme 10) were intercalated into KF and magadiite by cation exchange [366, 367] and covalent functionalization [368, 369], respectively. An intercharge distance in the parallel conformation of Py-DAE (0.9 nm), which was shorter than that of the antiparallel conformation (1.3 nm), matched with the distance between adjacent negative charge of KF (0.9 nm) so that the parallel conformation was preferred on KF. As a result, a change of absorption owing to the photocyclization of Py-DAE in KF suspension was smaller than that in a solution (without clay) [367]. The reversibility of Py-DAE photochromism was improved by co-intercalation of dodecylpyridinium ion [366]. The formation of the parallel conformation was suppressed by the co-intercalation of dodecylpyridinium.

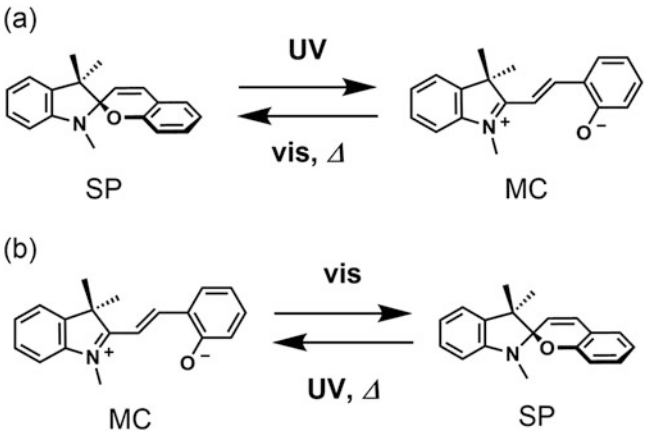

Scheme 11 The photochromism of spiropyran in (**a**) non-polar and (**b**) polar environment

An-DAE covalently bound on magadiite gave improved reversibility of the photocyclization compared with that in an ethanol solution [368, 369]. The molecular rotation from the antiparallel to the parallel conformation of An-DAE was suppressed by the covalent attachment to the silicate layer. Reversibility of photochromisms was also improved by restricting the molecular motion by the confinements. It was also claimed that the suppression of the parallel conformation improved the reversibility. The suppression of the generation of the photoinactive isomer was also concerned for the reversibility.

5.1.3 Spiropyran

Photochromism of spiropyran is dependent on the polarity of the molecular environment. In a non-polar environment, spiropyran (SP) is more stable than photomerocyanine (photoMC) (Scheme 11) as zwitter ionic structure [370]. 6-NO_2-MC is photochemically formed from 6-nitrospiropyran (6-NO_2-SP, in Scheme 12) in toluene showing blue color with a half-life of 5.6 s at room temperature, while 6-NO_2-MC in ethanol was red and the half-life is 17 min [371]. The phenoxyl moiety of merocyanine is protonated in acidic condition, and the protonated merocyanine shows yellow; thus, photochromism of spiropyran in the acidic condition is related to three isomers of spiropyran, merocyanine, and protonated merocyanine forms [370, 372, 373].

SP, the protonated MC, and 6-NO_2-SP were intercalated into KF by mixing in a mixed solvent of methanol and water and subsequent filtration [170]. The hybrids of KF were yellow, suggesting that SP and 6-NO_2-SP converted to the protonated MC, which was stabilized by the interactions with hydroxyl groups at the edge of the silicate layer. 6-NO_2-MC generated from 6-NO_2-SP is red in a toluene suspension of

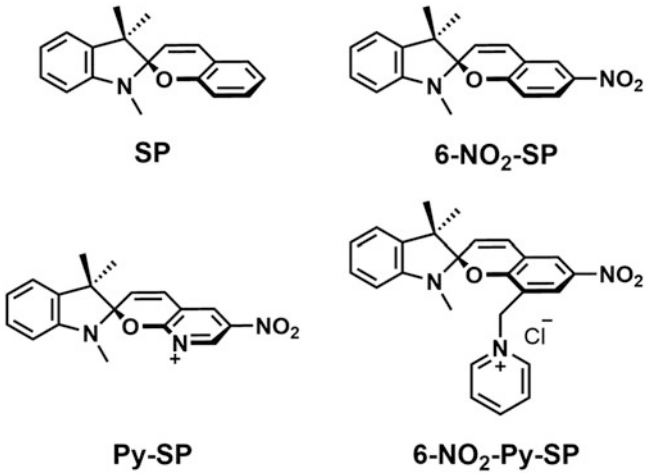

Scheme 12 Chemical structures of spiropyrans hybridized in clays

HE by the UV irradiation [374], indicating that 6-NO_2-MC adsorbed on HE by the host-guest interactions.

Dihydropyrenes [375], Stenhouse salts [376, 377], and binaphthyl-bridged imidazole dimers [378, 379] showed negative photochromism (opposite behavior to normal photochromism in non-polar environment; photodecoloration by visible light and thermal coloration) (Scheme 11b). High conversion of the photoisomerization of the negative photochromic compounds with respect to normal photochromism is possible because of the absence of the visible light absorption by the photochemically formed colorless isomer. In polar environments such as in mesoporous silicas [380–383], zeolites [383–385], and LDHs [386, 387], MC form is thermally more stable than SP form. These characteristics were utilized to control negative photochromism [380, 381, 388]. Both of Py-SP and 6-NO_2-Py-SP showed negative photochromism on KF [389, 390]. It was thought that the cationic parts of pyridine and aniline moieties electrostatically interacted with negative charges on the silicate layers and the merocyanine forms were stabilized.

Nonionic spiropyrans, SP and 6-NO_2-SP, and a cationic spiropyran, 6-NO_2-Py-SP, showed normal photochromism in a cetyltrimethylammonium (CTA^+) exchanged KF [170, 391, 392]. The CTAB provided the hydrophobic environment for the spiropyran derivatives to show normal photochromism [171]. The hydrophobicity of the clays is controlled by intercalating a wide variety of surfactants.

5.2 *Intermolecular Reactions*

The intermolecular reactions in/on nanospaces have been used for (1) stereoselective reaction and (2) trigger of photoinduced phenomena [393]. Intermolecular distance and orientation of guests in layered materials have been utilized to control the stereoselective reactions [394, 395].

5.2.1 Diels-Alder Reaction in Clay Interlayer

Diels-Alder reaction is known as a [4 + 2] cycloaddition between a π-conjugated diene and an alkene to form a six-membered ring. A major reaction product is predicted by Woodward-Hoffman rules, while some by-products are included in the products [394, 395]. Because the kinetically stable product is the major product of Diels-Alder reaction (endo rules), high temperatures are not recommended to accelerate Diels-Alder reaction with keeping the reaction selectivity. The addition of the catalyst, which does not affect the reaction selectivity, is proposed to increase the rate constant for Diels-Alder reaction. Acceleration of the dimerization of 1,3-cyclohexadiene [396] and the cycloaddition between 2,3-dimethyl-1,3-butadiene and acrolein [397] in the presence of a montmorillonite (K10) with Fe(III) was reported. A reaction yield of the dimerization of 1,3-cyclohexadiene increased to 49% even at 0°C for 10 h by adding K10 with Fe(III) with keeping the product selectivity the same compared to a reaction yield (30%) at 200°C for 20 h without K10 [398]. The yield (80% at 20°C for 3 h in water) of the cycloaddition increased to 95% at 20°C for 0.3 h by adding the K10 with Fe(III). The reaction condition was optimized to −24°C for 4 h in dichloromethane to achieve the yield of 96% with keeping the product isomer ratio. Though the role of the clay for the improved selectivity of Diels-Alder reaction was not explained clearly [396, 397], molecular packing of guests in clays are thought to contribute [176, 193].

5.2.2 [2 + 2] Photocycloaddition

According to Woodward-Hoffman rules, a [2 + 2] cycloaddition does not progress by heat and is photochemically allowed. Some of the stereoisomers are obtained by the [2 + 2] cycloaddition due to a biradical process [399]. Packing (orientation) at the

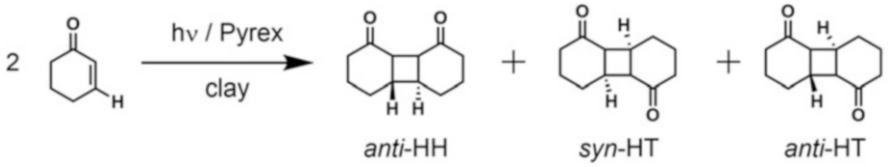

Scheme 13 Photocycloaddition of 2-cyclohexene-1-one

initial state and the molecular conformation of the intermediates affect the stereoselective [2 + 2] cycloaddition. Three products are possible by the cycloaddition of 2-cyclohexene-1-one in a solution as shown in Scheme 13. The reaction yield of photocycloaddition of 2-cyclohexene-1-one in the benzene solution under UV irradiation for 10 h (without clay) was 25%, and the ratio of the products of *anti*-HH, *syn*-HT, and *anti*-HT was 8:0.1:29 (Scheme 13) [400, 401]. By adding SA, the reaction yield remarkably increased to 72%, and the ratio of the products of *anti*-HH, *syn*-HT, and *anti*-HT was 82:0.1:5 [400, 401]. It was proposed that 2-cyclohexene-1-one aggregated in a parallel fashion, which led the effective photocycloaddition to *anti*-HT. The photoluminescence of the excimer of 2-cyclohexene-1-one was observed for the clay suspension.

Stilbene shows *cis-trans* isomerization and dimerization. Four possible photodimers of the stilbene are obtained as shown in Scheme 14. The photochemistry of stilbazolium ion (STN^+, Scheme 14) has been investigated to find stereoselective photodimerization [214, 402–410]. A higher reaction yield of photodimerization of STN^+ (the total yield, 98%, and the *cis*-isomer, 14%; *syn*-HT, 70%, and *syn*-HH, 5%, respectively) under UV irradiation for 30 min in an aqueous suspension of a saponite than that in a solution (the total yield, 69%, and the *cis*-isomer, 67%, *syn*-HT, 2%, and *anti*-HH, 2%, respectively) was reported [402]. Cyano- and methyl-substituted STN^+ were used to show that the hetero dimer was a major product thanks to the formation of the exciplex between the electron-donating methyl-substituted and the electron-accepting cyano-substituted stilbenes in the interlayer space of SA [404]. Recently, three stilbazolium derivatives, STN, $MeSTN^+$, and $C_{16}STN^+$ (in Scheme 14), were intercalated into a *N*-(2-(2,2,3,3,4,4,4-heptafluorobutanamido)ethyl)-*N,N*-dimethylhexadecan-1-ammonium bromide exchanged SA by mixing in HCl aqueous solution to examine the selectivity of the photochemical reactions [409]. Three factors, (1) electronic interactions between the negatively charges SA surface and the stilbazolium derivatives, (2) hydrophobic interactions among the long alkyl chains of the surfactants, and (3) both hydrophobic and lipophobic interactions of the perfluoropropyl moieties of the surfactant, affected the selectivity.

A [2 + 2] cycloaddition in the interlayer space of a hydrotalcite [411] led oligomer of phenylenediacrylate with a head-to-head structure [412]. *p*-Phenylenediacrylate was exchanged on a hydrotalcite (Alcamac Cl supplied by Kyowa Chemicals Ltd.) and was irradiated a 300 W medium pressure Hg lamp for 6 h in the aqueous suspension under stirring. The ratio of monomer, dimer, trimer, and oligomer was 0:22:31:47 after the irradiation for 6 h. In contrast, the ratio of the monomer and the dimer in an aqueous solution of *p*-phenylenediacrylate (without the hydrotalcite) was 74:26, and the trimer and the oligomer were not obtained. The polymerization degree was up to 10. The oligomer was assigned to the *syn*-head-to-head structure as shown in Scheme 15. The oligomer of *p*-phenylenediacrylate was not obtained by the irradiation to the powder.

The stereoselective cycloaddition was achieved by the molecular packing in the interlayer space of clays. Aspect ratio [413] and layer charge density [414–417] affected the yield and the selectivity. The selective cycloadditions were also reported

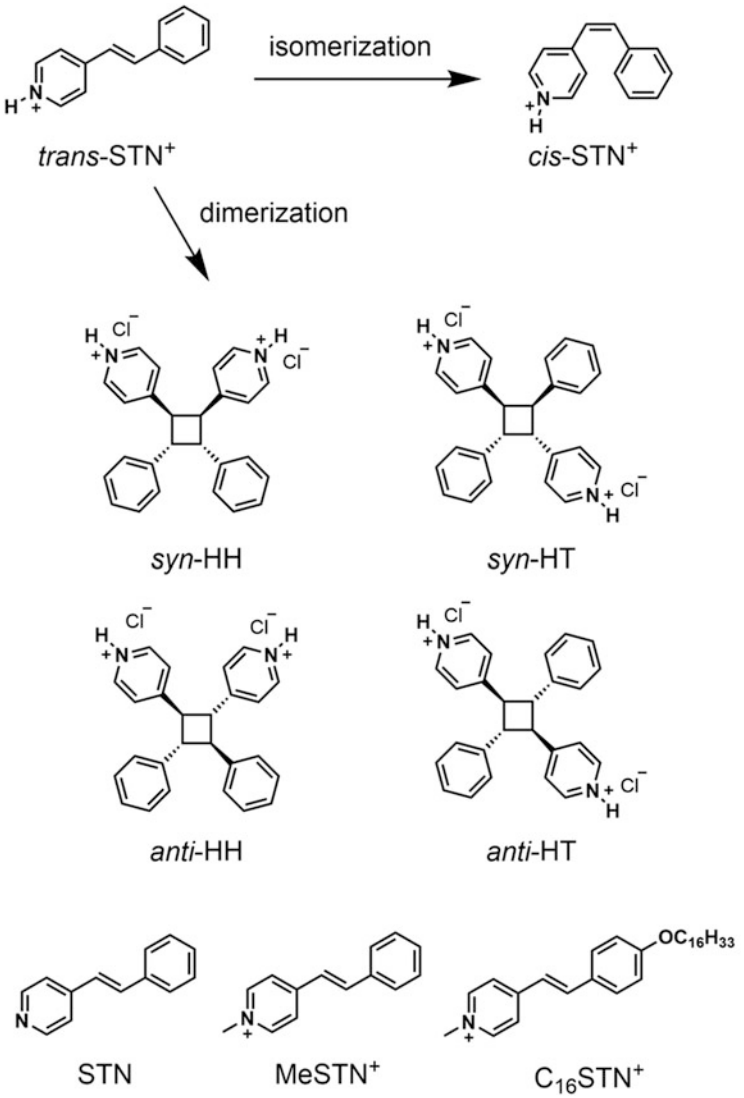

Scheme 14 Molecular structures of stilbene derivatives and photoreaction of *trans*-stilbene

in such nanospace materials [418] as zeolites [419, 420], mesoporous silicas [421], and a surfactant intercalated graphite oxide [422].

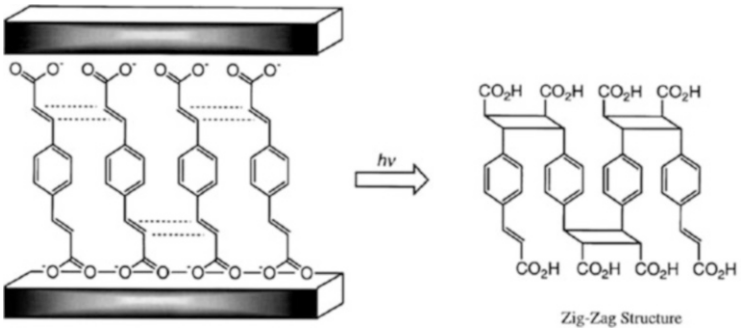

Scheme 15 Oligomerization of *p*-phenylenediacrylate in the interlayer space of the hydrotalcite (Reproduced from the reference [412] with permission)

5.3 *Uses of Photochemical Reactions as Trigger for Photoinduced Phenomena*

5.3.1 Photoinduced Change in the Basal Spacing

The change in the basal spacing by photoirradiation is the first example of photoinduced structural change in intercalation compounds [334]. Azobenzene (AZ) shows reversible photoisomerization between a rod-like-shaped *trans*-isomer and a bending structured *cis*-isomer (Scheme 8), and a molecular size of a long axis was switched between 1.21 nm for the *trans*-isomer and 0.74 nm for the *cis*-isomer. AZ was intercalated into n-dodecylammonium exchanged KF by mechanical mixing without a solvent [334]. The basal spacing of the organically modified KF increased from 1.8 to 3.0 nm by the intercalation of AZ. The basal spacing of the hybrid increased from 3.0 to 3.1 nm by UV irradiation, which is the first example of photoinduced change in the basal spacing.

It was reported that the basal spacing of magadiite intercalated with $AZC_2N^+C_2OH$ (Table 3) changed from 2.69 to 2.75 nm under UV irradiation and retuned to 2.69 nm by visible irradiation [165, 186], while those of KF intercalated $C_8AZC_{10}N^+$ and $C_{12}AZC_5N^+$ (Table 3) did not change by the isomerization of the cationic azobenzenes in the interlayer space [161]. Basal spacings of the montmorillonite with a cation exchange capacity of 143 meq/100 g intercalated aminoAZ and 4,4′-diaminoazobenzene were simulated [423]. The simulated basal spacings with the *trans*-isomers of aminoAZ and 4,4′-diaminoazobenzene were 2.0 and 2.1 nm, and those with the *cis*-isomers were 1.8 nm. The simulation did not match the experimental observations, suggesting that the photoswitching of the basal spacing was not explained simply by the isomerization of azobenzene.

To state the point, more recently, it was reported that the basal spacing of $AZC_2N^+C_2OH$-magadiite under humidity of 5% was negligibly small [346], while the change between 2.69 and 2.75 nm was observed when the reaction was conducted under ambient condition [165, 186]. It suggests that the basal spacing

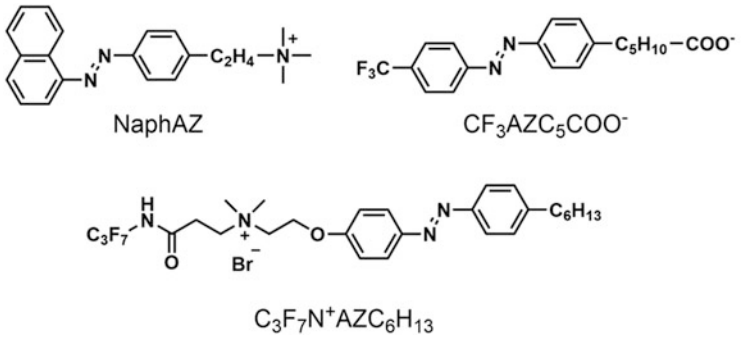

Scheme 16 Molecular structure of a naphthalene-substituted azobenzene and a trifluoromethyl-substituted anionic azobenzene

change was induced by the adsorption of vapors. The basal spacing of a naphthalene-substituted cationic azobenzene (NaphAZ in Scheme 16)-magadiite was observed during UV irradiation [346]. The basal spacing decreased by UV irradiation from 2.89 to 2.79 nm and did not return to the initial value, indicating that the molecular packing after the UV irradiation changed from the initial state.

The change of the basal spacing of clays was also induced by photoisomerization of a pyridine-substituted spiropyran (Py-SP in Scheme 12) [389]. Py-SP was intercalated into KF by two methods, (1) ion exchange with the interlayer sodium cation and (2) guest replacement using the ion exchange of the interlayer sodium cation with cetyltrimethylammonium bromide (CTAB) and subsequent exchange with Py-SP. The basal spacing of the hybrid prepared by the ion exchange was switched between 1.55 and 1.40 nm by 365 nm UV and 600 nm visible light irradiation, respectively. The basal spacing (1.55 nm) for the spiropyran form with a twisted molecular structure was larger than that for the merocyanine form with a planar molecular structure (1.40 nm). In contrast, the basal spacing (1.38 nm) of the hybrid prepared by the guest replacement did not change. The co-existing CTAB in KF expanded the inter-layer distance to accommodate Py-SP and Py-SP isomerized without changing the basal spacing.

The irradiation induced another change of a microscopic region. An azobenzene derivative with fluoroalkyl chain ($C_3F_7N^+AZC_6H_{13}$ in Scheme 16) was intercalated in potassium hexaniobate ($K_2Nb_6O_{17}$) [342, 424] to obtain a spiral tube structure [424]. The interlayer distance of the tube was changed by irradiation of 368 nm UV and 463 nm visible light irradiation with a simultaneous structure change of the tube [342]. The size changes of the tube from 244 to 93 nm and to 170 nm by UV and visible irradiation, respectively, were observed (Fig. 15). As shown in Fig. 16, a bottom edge of a hybrid film of $C_3F_7N^+AZC_6H_{13}$ and the niobate was slid out by UV irradiation (point A) up to 1.5 μm, and the edge returned to the initial position by the subsequent visible light irradiation (point C) [352, 425]. These reports suggest that the basal spacing change by photoisomerization of $C_3F_7N^+AZC_6H_{13}$ with a nanometer scale induced the structure change with a micrometer scale.

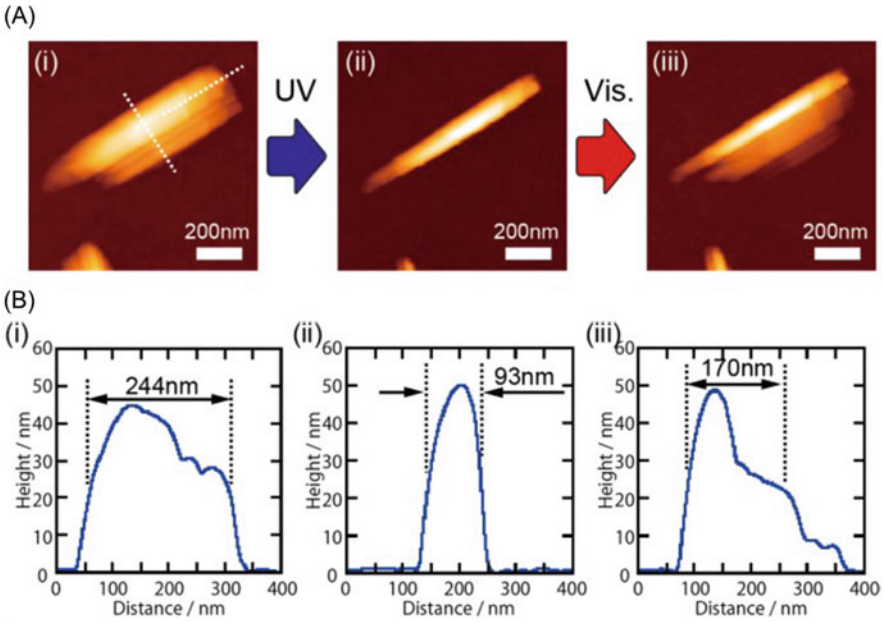

Fig. 15 Atomic force microscopic (AFM) images of morphological change of a hybrid of $C_3F_7N^+AZC_6H_{13}$ and the hexaniobate: (A) AFM top-view and (B) cross sections at the white dash lines of parallel of the short axis of the tube (Reproduced from the reference [342] with permission)

5.3.2 Photoswitching of Wettability

Photoswitching of surface properties of layered material films [426] by functionalization with photochromic compounds is expected owing to polarity change with photoisomerizations. Photoswitching of wettability of a layered double hydroxide film (ZnAl-NO_3-LDH film) was reported by functionalization with a trifluoromethyl-substituted anionic azobenzene ($CF_3AZC_5COO^-$ in Scheme 16) [427]. The film was synthesized by putting a porous anodic alumina/aluminum (PAO/Al) substrate into the solution containing zinc nitrate and ammonium nitrate [428] and the subsequent intercalation of $CF_3AZC_5COO^-$. The morphology of the film of the LDH crystal seemed to have a curved hexagonal sheet structure (Fig. 17a). A water contact angle of the film was 151 ± 1°, while the contact angle decreased to 73 ± 1° by 365 nm UV irradiation (Fig. 17b, c). The contact angle was returned to the initial value by subsequent visible light (420 nm) irradiation. The *cis*-isomer of azobenzene has larger polarity owing to the bending structure, indicating that the surface of the film with the *cis*-isomer had higher polarity than that with the *trans*-isomer. An advantage of this system is thought to be an easy preparation method of ion exchange method [35, 36, 283], which is expected to make a film with a large area compared to other films that showed photoswitching of wettability [429, 430].

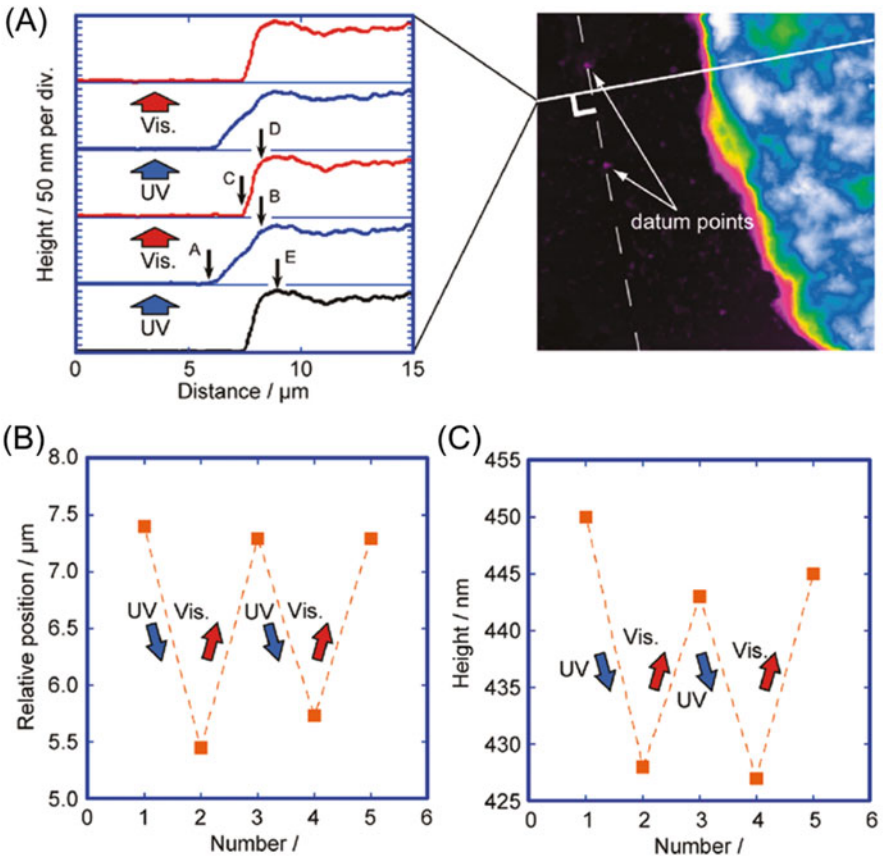

Fig. 16 3D morphology changes in the hybrid film. (**a**) Height profile of the hybrid film. (**b**) Relative distance from the reference point to the film edge vs the number of irradiation cycles. (**c**) Film thickness at a point E located a constant distance from the reference point vs the number of irradiation cycles (Reproduced from the reference [425] with permission)

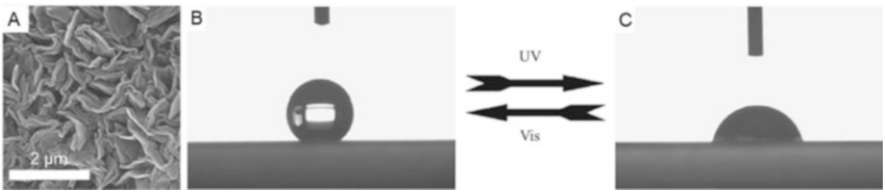

Fig. 17 SEM images of the top and cross section views of the hybrid of $CF_3AZC_5COO^-$ intercalated ZnAl-LDH (**a**) and shapes of a water droplet on the hybrid film surface (**b**) before the UV irradiation and (**c**) after the UV irradiation (Reproduced from the reference [427] with permission)

5.3.3 Photoswitching of Magnetism

Photoswitching of magnetism of layered double hydroxides (LDHs) was reported by intercalation of photochromic compounds of spiropyrans [431–435], azobenzenes [436, 437], and diarylethenes [438–440]. Two main contributions of intralayer superexchange interactions between metal cations and interlayer dipole interactions between the LDH layers were claimed to control the magnetism of the LDHs [441]. Because the photochromic compounds change shapes, sizes, and polarities by irradiation, the photochromic compounds affected the magnetism of the LDHs-dye hybrids.

Magnetism of layered $(C_3H_7)_4N[Fe^{II}Fe^{III}(C_2O_2S_2)_3]$ was explained by charge transfer at 120 and 6.5 K between Fe^{II} and Fe^{III} [432, 442, 443]. The phase transition at 120 K was attributed to the charge transfer between Fe^{II} (spin angular momentum $S = 1/2$) and Fe^{III} ($S = 2$) (the authors named high-temperature phase) to form the state with Fe^{III} ($S = 5/2$) and Fe^{II} ($S = 0$) (low-temperature phase). The layered $(C_3H_7)_4N[Fe^{II}Fe^{III}(C_2O_2S_2)_3]$ showed ferromagnetism below 6.5 K due to the charge transfer between the Fe^{III} ($S = 5/2$) and the Fe^{II} ($S = 0$). A hybrid of $[Fe^{II}Fe^{III}(C_2O_2S_2)_3]$ with MePy-SP (Scheme 17) [431, 433, 434] showed the charge transfer phase transition from the high-temperature phase to the low-temperature phase at 75 K and the ferromagnetic phase transition at 5 K [434]. Upon UV irradiation (365 nm), the intercalated MePy-SP isomerized to a merocyanine form (MePy-MC), and the isomerization induced the charge transfer between Fe^{II} and Fe^{III}. As a result, the charge transfer phase transition from the high-temperature phase to the low-temperature phase was not observed, and the ferromagnetic phase transition was observed at 22 K. Taking into account that an alkylammonium surfactant with a long alkyl chain stabilized the high-temperature phase and

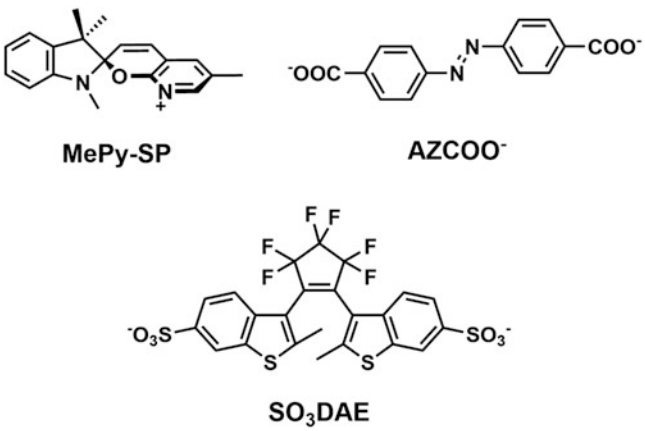

Scheme 17 Anionic photochromic compound intercalated into LDHs for photoswitching of magnetism

increased the ferromagnetic phase transition temperature T_C, [431] the longer molecular length of MePy-MC than that of MePy-SP increased T_C.

The magnetism of LDHs depended on the dipole interactions between the LDH layers which are smaller with longer interlayer distance [441]. A CoAl-LDH ($Co_{0.69}Al_{0.31}(OH)_2(CO_3)_{0.155}(H_2O)_{0.3}$) had spontaneous magnetization below the critical temperature T_M at 4.7 K [444]. T_M of a CoAl-LDH ($Co_{0.65}Al_{0.35}(OH)_2$) was switched by the *cis-trans* photoisomerization of the intercalated dicarboxylazobenzene (designated as $AZCOO^-$) [436]. T_M of the CoAl-LDH hybrid (4.5 K) increased to 5.2 K by 355 nm UV irradiation accompanied by the basal spacing change from 20.29 to 20.18 nm, suggesting that the change in the nanostructure was the reason of the increase of T_M. The basal spacing did not revert to the initial value by visible light irradiation in acetonitrile, while it reverted by exposure of water under the visible light irradiation. As discussed in Sect. 5.3.1, vapor played an important role in the change in the basal spacing [346]. It is thought that the adsorption of the water molecules triggered the backward reaction to the initial molecular packing.

Magnetism of alkylcarboxylate intercalated layered Co and Cu hydroxides ($Co_7(OH)_{11.6}$ and $Cu_2(OH)_2$) depended on the length and π-conjugate system of the alkylcarboxylate surfactants due to the interlayer ferromagnetic interaction [445]. The photocyclization of diarylethene, which accompanies the switching of the π-conjugate system, affected the magnetic interactions of two nitronyl nitroxide moieties substituted to the phenylthiophene moieties of the diarylethene [446, 447]. T_C of a hybrid of a layered $Co_4(OH)_7$ (designated as Co-LDH) intercalated an open-ring isomer of SO_3DAE in Scheme 17 was 9 K, while that after UV irradiation increased to 20 K [439]. Although the mechanism was not reported in detail [438, 440], the photoswitch of the π-conjugate system of the intercalated SO_3DAE seemed to affect the magnetism of Co-LDH [446, 447].

The photoswitching of the π-conjugate system by the photocyclization and the photoswitching of the basal spacing caused by photochromism affected to the magnetism of the LDHs. As discussed in Sects. 5.2.2 and 5.3.1, the design of the hybrids and the photoinduced adsorption of vapor are expected to make these phenomena effective, suggesting that the elucidation and improvement of the photoinduced phenomena of the hybrids induce the effective magnetism switching.

5.3.4 Photoinduced Adsorption

As discussed in Sect. 5.3.1, adsorption of vapor during the photochromic changes induced the change in the basal spacing [346]. Adsorption of phenol onto organically modified clay from an aqueous solution was also reported [101, 282, 448, 449]. Motivated by the phenomena, photoinduced adsorption of phenol was examined [166, 167, 344]. $AZC_2N^+C_2OH$ and $C_2AZC_2N^+$ (Table 3) intercalated KF were mixed with neat phenol. As shown in Fig. 18, gallery heights increased from 0.81 to 1.5 nm and 0.96 to 2.6 nm by mixing with phenol, respectively [344]. The gallery heights of the hybrids $AZC_2N^+C_2OH$-KF with phenol increased further from 1.5 to

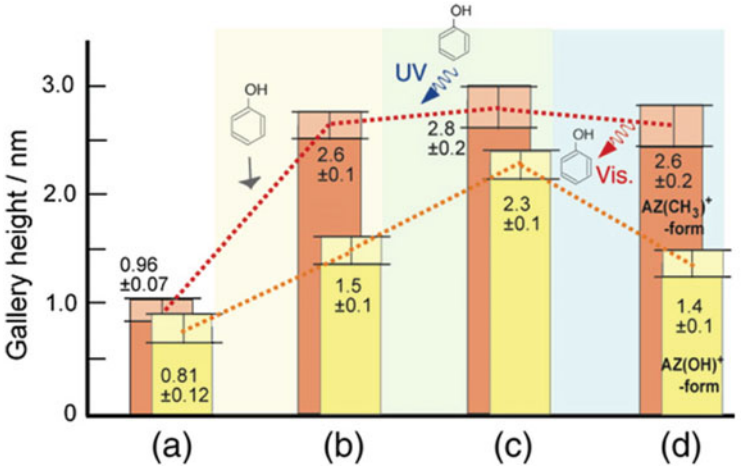

Fig. 18 The changes in the basal spacings of KF intercalated $AZC_2N^+C_2OH$ and $C_2AZC_2N^+$; (**a**) before the intercalation of phenol, (**b**) after phenol intercalation, (**c**) after UV irradiation, and (**d**) after subsequent visible light irradiation (Reproduced from the reference [344] with permission)

Table 4 Photoinduced expansion of basal spacings of azobenzene exchanged clays

Adsorbent	CEC/ meq/ 100 g	Adsorbed amount of $AZC_2N^+C_2OH$/ meq/100 g	Before intercalation of phenol	$d_{(001)}$/nm before UV irradiation	After UV irradiation	After visible light irradiation
KF	108	105	1.76	2.56	3.16	2.56
		91	1.63	2.56, 1.54	3.40, 2.56, 1.54	2.56, 1.54
		66	1.54	1.54	1.54	1.54
TSM	84	52	1.89	2.45	3.45, 2.45	2.45
SA	71	76	1.53	1.57	1.57	1.57

2.3 nm by UV irradiation. The large change of the gallery heights (0.8 nm) indicated that the phenol was intercalated into the hybrid by the UV irradiation. On the other hand, the gallery height of $C_2AZC_2N^+$-KF increased from 2.6 to 2.8 nm by the UV irradiation in the presence of phenol. Because the polarity of $C_2AZC_2N^+$ was thought to be smaller than that of $AZC_2N^+C_2OH$ from a comparison of dipole moments of *cis*-AZ (0.41 Debye) and 4-ethylazobenzene (0.34 Debye), the adsorbed amount of phenol in $C_2AZC_2N^+$-KF intercalated with phenol was thought to be smaller than that of $AZC_2N^+C_2OH$-KF. The basal spacing changes of $AZC_2N^+C_2OH$-KF with the adsorbed amount of 105, 91, and 66 meq/100 g were determined as summarized in Table 4 [167]. Observation of several basal spacing with 91 meq/100 g suggested the inhomogeneous adsorption of phenol. The changes in the basal spacings of $AZC_2N^+C_2OH$-smectites with varied CEC were also

examined to find $C_2AZC_2N^+$-clay (with CEC of 108 and 84 meq/100 g) increased by the UV irradiation, while that with 71 meq/100 g did not change. Changes of the basal spacings of KF, TSM, and SA intercalated $AZC_2N^+C_2OH$ in the presence of phenol by the UV irradiation are summarized in Table 4 [167]. The fraction of the *cis*-isomer of $AZC_2N^+C_2OH$ in TSM was estimated to be ca. 50%, and it was larger than that in KF (ca. 30%).

To enhance the structural change by the photoinduced adsorption, the following parameters were proposed: (1) fraction of *cis*-isomer at the photostationary state [167, 344], (2) amount [344], and (3) orientation [167] of azobenzene derivative (corresponding to the surface coverage).

The photoinduced adsorption of photochromic compounds was also reported recently [374, 382, 450, 451]. As discussed in Sect. 5.1.3, photochromism of spiropyran was affected by the presence of nanospace materials including mesoporous silicas and smectites. Color of 6-NO_2-MC (Scheme 12) photochemically formed from 6-NO_2-SP was blue in toluene under UV irradiation, while the color of it was red in the presence of HE [374]. Red-colored sediment was collected by storing the suspension in the dark so that the adsorbed amount of MC onto HE was followed, showing that the 6-NO_2-SP was adsorbed on HE with the first-order kinetics [374]. The adsorbed amount of 6-NO_2-MC was 2.8 mg/100 g. The photoinduced adsorption is thought as molecular migration between hydrophobic and hydrophilic phases by using the bistability of the photochromic compound.

Mesoporous silicas were used as adsorbent of photo 6-NO_2-MC, which is named as "photoinduced adsorption" [382, 450, 452]. Photoinduced migration of SA/MC between the mesoporous silicas and the organophilic clay [381, 382] was reported to lead the reversibility of the negative photochromisms. The organically modified clay was thought to host less polar 6-NO_2-SP, which formed by the negative photochromisms of 6-NO_2-MC accommodated in the mesoporous silica. The thermal coloration of 6-NO_2-SP to 6-NO_2-MC accelerated by using the mesoporous silicas with larger pore size [382] and that whose external surface was functionalized with phenyl groups [451], suggesting that the diffusion inside the pore is important and the intraparticle diffusion was more efficient than the interparticle diffusion.

6 Conclusions and Future Perspectives

Recent developments on the preparation and the photofunctions of dye-clay hybrids are reviewed. Photofunctions have been systematically controlled and discussed based on the variation of hosts, guests, and their compositions. These developments led to further understanding of the structure and composition-property relationships, which may provide advance knowledge to optimize materials' performances. Not only the nanostructure design by using host-guest interfaces has been revised, but the search for raw materials and their synthesis of new host materials have been also done. Successful morphosyntheses of known materials to obtain well-defined particles and single crystals with narrow particle size distribution expanded the

possibilities of the materials and made detailed characterization possible. Taking the advantages of the morphosyntheses, interfacial design and the developments of fabrication techniques, some dye-clay systems have been prepared as thin films. The application covers traditional pigments application to agriculture (on soil contamination), optical devices including light-emitting ones, sensors, photocatalysts, etc. Though the practical application is not seen, various unique photoinduced phenomena have been also ascribed.

Acknowledgments This work was supported by the Research Chair Grant 2017 (grant number FDA-CO-2560-5655) from the National Science and Technology Development Agency (NSTDA), Thailand.

References

1. Matsuura T, Anpo M (eds) (1989) Photochemistry on solid surfaces. Elsevier Science, Amsterdam
2. Anpo M (ed) (1996) Surface photochemistry. Wiley, Chichester
3. Klafter J, Drake J (eds) (1989) Molecular dynamics in restricted geometries. Wiley Interscience, New York
4. Ramamurthy V (ed) (1991) Photochemistry in organized and constrained media. VCH Publishers, New York
5. Ramamurthy V, Schanze KS (eds) (2000) Solid state and surface photochemistry. Marcel Dekker, New York
6. Fendler JH (ed) (1994) Membrane-mimetic approach to advanced materials. Springer-Verlag, Berlin
7. Yamaguchi T, Ogawa M (2019) Photochromic reactions in nanospace; host-guest interactions and opportunity. In: Douhal A, Anpo M (eds) Chemistry of silica and zeolite-based materials Synthesis, characterization and applications. Elsevier, Amsterdam, pp 163–177
8. Sohmiya M, Saito K, Ogawa M (2015) Host–guest chemistry of Mesoporous Silicas: precise Design of Location, density and orientation of molecular guests in Mesopores. Sci Technol Adv Mater 16:54201. https://doi.org/10.1088/1468-6996/16/5/054201
9. Ogawa M, Kuroda K (1995) Photofunctions of intercalation compounds. Chem Rev 95:399–438
10. Ogawa M, Saito K, Sohmiya M (2015) Possible roles of the spatial distribution of organic guest species in mesoporous silicas to control the properties of the hybrids. Eur J Inorg Chem:1126–1136. https://doi.org/10.1002/ejic.201402651
11. Ogawa M (2002) Photoprocesses in mesoporous silicas prepared by a supramolecular templating approach. J Photochem Photobiol C: Photochem Rev 3:129–146. https://doi.org/10.1016/S1389-5567(02)00023-0
12. Alberti G, Bein T (eds) (1996) Solid-state supramolecular chemistry: two- and three-dimensional inorganic networks. Pergamon, Oxford
13. Thomas JK (1987) Characterization of surfaces by excited states. J Phys Chem 91:267–276. https://doi.org/10.1021/j100286a008
14. Thomas JK (1993) Physical aspects of photochemistry and radiation chemistry of molecules adsorbed on silica, gamma-alumina, zeolites, and clays. Chem Rev 93:301–320. https://doi.org/10.1021/cr00017a014
15. Turro NJ, Grätzel M, Braun AM (1980) Photophysical and photochemical processes in micellar systems. Angew Chem Int Ed 19:675–696. https://doi.org/10.1002/anie.198006751

16. Thomas JK (1988) Photophysical and photochemical processes on clay surfaces. Acc Chem Res 21:275–280. https://doi.org/10.1021/ar00151a004
17. Fujimura T, Shimada T, Hamatani S, Onodera S, Sasai R, Inoue H, Takagi S (2013) High density intercalation of porphyrin into transparent clay membrane without aggregation. Langmuir 29:5060–5065. https://doi.org/10.1021/la4003737
18. Konno S, Fujimura T, Otani Y, Shimada T, Inoue H, Takagi S (2014) Microstructures of the porphyrin/viologen monolayer on the clay surface: segregation or integration? J Phys Chem C 118:20504–20510. https://doi.org/10.1021/jp5076274
19. Nakayama A, Mizuno J, Ohtani Y, Shimada T, Takagi S (2018) Elucidation of the adsorption distribution of cationic porphyrin on the inorganic surface by energy transfer as a molecular ruler. J Phys Chem C 122:4365–4371. https://doi.org/10.1021/acs.jpcc.7b12104
20. Sohmiya M, Nakamura T, Sugahara Y, Ogawa M (2018) Distribution control-oriented intercalation of a cationic metal complex into layered silicates modified with organosulfonic-acid moieties. Langmuir 34:4762–4773. https://doi.org/10.1021/acs.langmuir.8b00547
21. Eguchi M, Takagi S, Inoue H (2006) The orientation control of dicationic porphyrins on clay surfaces by solvent polarity. Chem Lett 35:14–15. https://doi.org/10.1246/cl.2006.14
22. Sasai R, Shichi T, Gekko K, Takagi K (2000) Continuously changing the conformational dependence of saponite hybrid materials on the intercalation degree: electric linear dichroism of stilbazolium derivatives intercalated in saponite clay. Bull Chem Soc Jpn 73:1925–1931. https://doi.org/10.1246/bcsj.73.1925
23. Neumann MG, Gessner F, Schmitt CC, Sartori R (2002) Influence of the layer charge and clay particle size on the interactions between the cationic dye methylene blue and clays in an aqueous suspension. J Colloid Interface Sci 255:254–259. https://doi.org/10.1006/jcis.2002.8654
24. Okada T, Ide Y, Ogawa M (2012) Organic-inorganic hybrids based on ultrathin oxide layers: designed nanostructures for molecular recognition. Chem Asian J 7:1980–1992. https://doi.org/10.1002/asia.201101015
25. Okada T, Seki Y, Ogawa M (2014) Designed nanostructures of clay for controlled adsorption of organic compounds. J Nanosci Nanotechnol 14:2121–2134. https://doi.org/10.1166/jnn.2014.8597
26. Ruiz-Hitzky E, Aranda P, Akkari M, Khaorapapong N, Ogawa M (2019) Photoactive nanoarchitectures based on clays incorporating TiO_2 and ZnO nanoparticles. Beilstein J Nanotechnol 10:1140–1156. https://doi.org/10.3762/bjnano.10.114
27. Deepracha S, Vibulyaseak K, Ogawa M (2019) Complexation of TiO_2 with clays and clay minerals for hierarchically designed functional hybrids. In: Advanced supramolecular nanoarchitectonics. Elsevier, Amsterdam, pp 125–150
28. Intasa-ard SG, Ogawa M (2018) Layered silicates as a possible drug carrier. In: Tamanoi F (ed) Mesoporous silica-based Nanomaterials and biomedical applications, part B. Elsevier, Amsterdam, pp 117–136
29. Ogawa M (1998) Organized molecular assemblies on the surfaces of inorganic solids-photofunctional inorganic-organic supramolecular systems. Annu Rep Prog Chem Sect C Phys Chem 94:209. https://doi.org/10.1039/pc094209
30. Lagaly G, Ogawa M, Dékány I (2006) Chapter 7.3 clay mineral organic interactions. Dev Clay Sci 1:309–377
31. Shichi T, Takagi K (2000) Clay minerals as photochemical reaction fields. J Photochem Photobiol C: Photochem Rev 1:113–130. https://doi.org/10.1016/S1389-5567(00)00008-3
32. Granquist WT, Pollack SS (1960) A study of the synthesis of hectorite. Pergamon Press, Oxford
33. Ogawa M, Wada T, Kuroda K (1995) Intercalation of pyrene into alkylammonium-exchanged swelling layered silicates: the effects of the arrangements of the interlayer alkylammonium ions on the states of adsorbates. Langmuir 11:4598–4600. https://doi.org/10.1021/la00011a068

34. Kloprogge JT, Komarneni S, Amonette JE (1999) Synthesis of smectite clay minerals: a critical review. Clay Clay Miner 47:529–554. https://doi.org/10.1346/CCMN.1999.0470501
35. Ogawa M, Handa T, Kuroda K, Kato C (1990) Formation of organoammonium-montmorillonites by solid-solid reaction. Chem Lett 19:71–74
36. Intasa-ard SG, Imwiset K, Bureekaew S, Ogawa M (2018) Mechanochemical methods for the preparation of intercalation compounds, from intercalation to the formation of layered double hydroxides. Dalton Trans 47:2896–2916. https://doi.org/10.1039/C7DT03736H
37. Nakamura T, Ogawa M (2013) Adsorption of cationic dyes within spherical particles of poly (*N*-isopropylacrylamide) hydrogel containing Smectite. Appl Clay Sci 83–84:469–473. https://doi.org/10.1016/j.clay.2013.05.005
38. Yariv S, Ghosh DK, Hepler LG (1991) Metachromasy in clay-mineral systems: adsorption of cationic dyes crystal violet and ethyl violet by kaolinite from aqueous and organic solutions. J Chem Soc Faraday Trans 87:1201–1207. https://doi.org/10.1039/FT9918701201
39. Yariv S, Nasser A, Bar-on P (1990) Metachromasy in clay minerals. Spectroscopic study of the adsorption of crystal violet by laponite. J Chem Soc Faraday Trans 86(1593). https://doi.org/10.1039/ft9908601593
40. Bergmann K, O'Konski CT (1963) A spectroscopic study of methylene blue monomer, dimer, and complexes with Montmorillonite. J Phys Chem 67:2169–2177. https://doi.org/10.1021/j100804a048
41. Yariv S, Lurie D (1971) Metachromasy in clay minerals. Part I. Sorption of methylene-blue by montmorillonite. Isr J Chem 9:537–552. https://doi.org/10.1002/ijch.197100070
42. Samuels M, Mor O, Rytwo G (2013) Metachromasy as an indicator of photostabilization of methylene blue adsorbed to clays and minerals. J Photochem Photobiol B Biol 121:23–26. https://doi.org/10.1016/j.jphotobiol.2013.02.004
43. Hang PT (1970) Methylene blue absorption by clay minerals. Determination of surface areas and cation exchange capacities (clay-organic studies XVIII). Clays Clay Miner 18:203–212. https://doi.org/10.1346/CCMN.1970.0180404
44. Brindley GW, Thompson TD (1970) Methylene blue absorption by montmorillonites. Determinations of surface areas and exchange capacities with different initial cation saturations (clay-organic studies XIX). Isr J Chem 8:409–415. https://doi.org/10.1002/ijch.197000047
45. Hepler LG, Yariv S, Dobrogowska C (1987) Calorimetric investigation of adsorption of an aqueous metachromic dye (crystal-violet) on montmorillonite. Thermochim Acta 121:373–379. https://doi.org/10.1016/0040-6031(87)80187-9
46. Schramm LL, Yariv S, Ghosh DK, Hepler LG (1997) Electrokinetic study of the adsorption of ethyl violet and crystal violet by montmorillonite clay particles. Can J Chem 75:1868–1877. https://doi.org/10.1139/v97-620
47. Lapides I, Yariv S, Golodnitsky D (2002) Simultaneous DTA-TG study of montmorillonite mechanochemically treated with crystal-violet. J Therm Anal Calorim 67:99–112. https://doi.org/10.1023/A:1013737914178
48. Grauer Z, Malter AB, Yariv S, Avnir D (1987) Sorption of rhodamine B by montmorillonite and laponite. Colloids Surf 25:41–65. https://doi.org/10.1016/0166-6622(87)80268-8
49. Grauer Z, Grauer GL, Avnir D, Yariv S (1987) Metachromasy in clay minerals. Sorption of pyronin Y by montmorillonite and laponite. J Chem Soc Faraday Trans 1 83:1685. https://doi.org/10.1039/f19878301685
50. Bose IS, Sunwar CB, Chakravarti SK (1987) Metachromasy of thiazine dyes when sorbed onto clay minerals (Montmorillonite). Indian J Chem 26:944–946
51. Sunwar CB, Bose H (1990) Effect of clay minerals on the visible spectra of thiazine dyes. J Colloid Interface Sci 136:54–60. https://doi.org/10.1016/0021-9797(90)90077-2
52. Breen C, Rock B (1994) The competitive adsorption of methylene blue on to montmorillonite from binary solution wih thioflavin T, proflavine and acridine yellow, steady-state and dynamic studies. Clay Miner 29:179–189. https://doi.org/10.1180/claymin.1994.029.2.04
53. Figueras F (1988) Pillared clays as catalysts. Catal Rev 30:457–499. https://doi.org/10.1080/01614948808080811

54. Gil A, Korili SA, Trujillano R, Vicente MA (eds) (2010) Pillared clays and related catalysts. Springer, New York
55. Ogawa M, Takahashi M, Kato C, Kuroda K (1994) Oriented microporous film of tetramethylammonium pillared saponite. J Mater Chem 4:519–523. https://doi.org/10.1039/jm9940400519
56. Ogawa M, Kuroda K (1997) Preparation of inorganic-organic nanocomposites through intercalation of organoammonium ions into layered silicates. Bull Chem Soc Jpn 70:2593–2618
57. Imwiset KJ, Hayakawa T, Fukushima Y, Yamada T, Ogawa M (2019) Novel flexible supramolecular assembly of dioleyldimethylammonium ion in a two-dimensional nanospace studied by neutron scattering. Langmuir 35:13977–13982. https://doi.org/10.1021/acs.langmuir.9b02504
58. Ogawa M (1997) Preparation of layered silica−dialkyldimethylammonium bromide nanocomposites. Langmuir 13:1853–1855. https://doi.org/10.1021/la9608775
59. Lagaly G (1986) Interaction of alkylamines with different types of layered compounds. Solid State Ionics 22:43–51. https://doi.org/10.1016/0167-2738(86)90057-3
60. Kanoh T, Shichi T, Takagi K (1999) Mono- and bilayer equilibria of stearate self-assembly formed in hydrotalcite interlayers by changing the intercalation temperature. Chem Lett 28:117–118. https://doi.org/10.1246/cl.1999.117
61. Burgentzlé D, Duchet J, Gérard JF, Jupin A, Fillon B (2004) Solvent-based nanocomposite coatings: I. Dispersion of organophilic montmorillonite in organic solvents. J Colloid Interface Sci 278:26–39. https://doi.org/10.1016/j.jcis.2004.05.015
62. Ogawa M (1996) Preparation of a cationic azobenzene derivative-montmorillonite intercalation compound and the photochemical behavior. Chem Mater 8:15–17. https://doi.org/10.1021/cm950602v
63. Valandro SR, Poli AL, Neumann MG, Schmitt CC (2015) Photophysics of auramine O adsorbed on solid clays. J Lumin 161:209–213. https://doi.org/10.1016/j.jlumin.2015.01.023
64. Takahashi N, Kuroda K (2011) Materials design of layered silicates through covalent modification of interlayer surfaces. J Mater Chem 21:14336–14353. https://doi.org/10.1039/c1jm10460h
65. Wijitwongwan RP, Intasa-ard SG, Ogawa M (2019) Preparation of layered double hydroxides toward precisely designed hierarchical organization. ChemEngineering 3:68. https://doi.org/10.3390/chemengineering3030068
66. Taviot-Guého C, Prévot V, Forano C, Renaudin G, Mousty C, Leroux F (2018) Tailoring hybrid layered double hydroxides for the development of innovative applications. Adv Funct Mater 28:1–33. https://doi.org/10.1002/adfm.201703868
67. Intasa-Ard S, Bureekaew S, Ogawa M (2019) Efficient production of MgAl layered double hydroxide nanoparticle. J Ceram Soc Jpn:11–17. https://doi.org/10.2109/jcersj2.18140
68. Park DH, Hwang SJ, Oh JM, Yang JH, Choy JH (2013) Polymer-inorganic supramolecular nanohybrids for red, white, green, and blue applications. Prog Polym Sci 38:1442–1486. https://doi.org/10.1016/j.progpolymsci.2013.05.007
69. Li W, Yan D, Gao R, Lu J, Wei M, Duan X (2013) Recent advances in stimuli-responsive photofunctional materials based on accommodation of chromophore into layered double hydroxide nanogallery. J Nanomater 2013. https://doi.org/10.1155/2013/586462
70. Akkari M, Aranda P, Ben Rhaiem H, Ben Haj Amara A, Ruiz-Hitzky E (2016) ZnO/clay Nanoarchitectures: synthesis, characterization and evaluation as photocatalysts. Appl Clay Sci 131:131–139. https://doi.org/10.1016/j.clay.2015.12.013
71. Aranda P, Kun R, Martín-Luengo MA, Letaïef S, Dékány I, Ruiz-Hitzky E (2008) Titania-sepiolite nanocomposites prepared by a surfactant templating colloidal route. Chem Mater 20:84–91. https://doi.org/10.1021/cm702251f
72. Hayakawa T, Minase M, Fujita K, Ogawa M (2016) Green synthesis of Organophilic clays; solid-state reaction of acidic clay with organoamine. Ind Eng Chem Res 55:6325–6330. https://doi.org/10.1021/acs.iecr.5b03344

73. Ide Y, Matsuoka M, Ogawa M (2012) Controlled photocatalytic oxidation of benzene in aqueous clay suspension. ChemCatChem 4:628–630. https://doi.org/10.1002/cctc.201200043
74. Hayakawa T, Oya M, Minase M, Fujita K, Teepakakorn AP, Ogawa M (2019) Preparation of sodium-type bentonite with useful swelling property by a mechanochemical reaction from a weathered bentonite. Appl Clay Sci 175:124–129. https://doi.org/10.1016/j.clay.2019.04.009
75. Ogawa M, Kanaoka N, Kuroda K (1998) Preparation of smectite/dodecyldimethylamine *N*-oxide intercalation compounds. Langmuir 14:6969–6973. https://doi.org/10.1021/la980173q
76. Minase M, Hayakawa T, Oya M, Fujita K, Ogawa M (2019) Improved rheological properties of organophilic-clay suspensions by a simple pretreatment with a wet type jet mill. Bull Chem Soc Jpn 92:1329–1334. https://doi.org/10.1246/bcsj.20190051
77. Tetsuka H, Ebina T, Tsunoda T, Nanjo H, Mizukami F (2007) Flexible organic electroluminescent devices based on transparent clay films. Nanotechnology 18:355701. https://doi.org/10.1088/0957-4484/18/35/355701
78. Deepracha S, Bureekaew S, Ogawa M (2019) Synergy effects of the complexation of a titania and a smectite on the film formation and its photocatalyst' performance. Appl Clay Sci 169:129–134. https://doi.org/10.1016/j.clay.2018.12.005
79. Isayama M, Sakata K, Kunitake T (1993) Preparation of a self-supporting, multilayered film of montmorillonite. Chem Lett 22:1283–1286. https://doi.org/10.1246/cl.1993.1283
80. Hotta Y, Taniguchi M, Inukai K, Yamagishi A (1997) Clay-modified electrodes prepared by the Langmuir-Blodgett method. Clay Miner 32:79–88. https://doi.org/10.1180/claymin.1997.032.1.09
81. Suzuki Y, Tenma Y, Nishioka Y, Kawamata J (2012) Efficient nonlinear optical properties of dyes confined in interlayer nanospaces of clay minerals. Chem Asian J 7:1170–1179. https://doi.org/10.1002/asia.201200049
82. Kleinfeld ER, Ferguson GS (1994) Stepwise formation of multilayered nanostructural films from macromolecular precursors. Science 265:370–373. https://doi.org/10.1126/science.265.5170.370
83. Kleinfeld ER, Ferguson GS (1996) Healing of defects in the stepwise formation of polymer/silicate multilayer films. Chem Mater 8:1575–1578. https://doi.org/10.1021/cm960073a
84. Lvov Y, Ariga K, Ichinose I, Kunitake T (1996) Formation of ultrathin multilayer and hydrated gel from montmorillonite and linear polycations. Langmuir 12:3038–3044. https://doi.org/10.1021/la951002d
85. Lotsch BV, Ozin GA (2008) Clay Bragg stack optical sensors. Adv Mater 20:4079–4084. https://doi.org/10.1002/adma.200800914
86. Ariga K, Ji Q, McShane MJ, Lvov YM, Vinu A, Hill JP (2012) Inorganic nanoarchitectonics for biological applications. Chem Mater 24:728–737. https://doi.org/10.1021/cm202281m
87. Nakamura T, Ogawa M (2012) Attachment of the sulfonic acid group in the interlayer space of a layered alkali silicate, octosilicate. Langmuir 28:7505–7511. https://doi.org/10.1021/la300390s
88. Leodopoulos C, Doulia D, Gimouhopoulos K (2014) Adsorption of cationic dyes onto Bentonite. Sep Purif Rev 44:74–107. https://doi.org/10.1080/15422119.2013.823622
89. Kukkadapu RK, Boyd SA (1995) Tetramethylphosphonium- and tetramethylammonium-smectites as adsorbents of aromatic and chlorinated hydrocarbons: effect of water on adsorption efficiency. Clay Clay Miner 43:318–323. https://doi.org/10.1346/CCMN.1995.0430306
90. Lawrence MAM, Kukkadapu RK, Boyd SA (1998) Adsorption of phenol and chlorinated phenols from aqueous solution by tetramethylammonium- and tetramethylphosphonium-exchanged montmorillonite. Appl Clay Sci 13:13–20. https://doi.org/10.1016/S0169-1317(98)00009-X
91. Deng Y, Dixon JB, White GN (2006) Bonding mechanisms and conformation of poly (ethylene oxide)-based surfactants in interlayer of smectite. Colloid Polym Sci 284:347–356. https://doi.org/10.1007/s00396-005-1388-0
92. Guégan R (2010) Intercalation of a nonionic surfactant ($C_{10}E_3$) bilayer into a Na-montmorillonite clay. Langmuir 26:19175–19180. https://doi.org/10.1021/la1039267

93. Guégan R, Veron E, Le Forestier L, Ogawa M, Cadars S (2017) Structure and dynamics of nonionic surfactant aggregates in layered materials. Langmuir 33:9759–9771. https://doi.org/10.1021/acs.langmuir.7b01831
94. Van Olphen H (1977) An introduction to clay colloid chemistry. Wiley-Interscience, New York
95. Auerbach SM, Carrado KA, Dutta PK (2004) Clay-organic interactions: organoclay complexes and polymer-clay nanocomposites. In: Auerbach SM, Carrado KA, Dutta PK (eds) Handbook of layered materials. Marcel Dekker, New York, pp 91–154
96. Galarneau A, Barodawalla A, Pinnavaia TJ (1995) Porous clay heterostructures formed by gallery-templated synthesis. Nature 374:529–531. https://doi.org/10.1038/374529a0
97. Michot LJ, Barrès O, Hegg EL, Pinnavaia TJ (1993) Cointercalation of Al_{13} polycations and nonionic surfactants in montmorillonite clay. Langmuir 9:1794–1800. https://doi.org/10.1021/la00031a030
98. Nakatsuji M, Ishii R, Wang ZM, Ooi K (2004) Preparation of porous clay minerals with organic-inorganic hybrid pillars using solvent-extraction route. J Colloid Interface Sci 272:158–166. https://doi.org/10.1016/j.jcis.2003.11.039
99. Malla PB, Ravindranathan P, Komarneni S, Roy R (1991) Intercalation of copper metal clusters in montmorillonite. Nature 353:412–414
100. Yamauchi Y, Itagaki T, Yokoshima T, Kuroda K (2012) Preparation of Ni nanoparticles between montmorillonite layers utilizing dimethylaminoborane as reducing agent. Dalton Trans 41:1210–1215. https://doi.org/10.1039/c1dt11395j
101. Seki Y, Ogawa M (2010) The removal of 2-phenylphenol from aqueous solution by adsorption onto organoclays. Bull Chem Soc Jpn 83:712–715. https://doi.org/10.1246/bcsj.20090191
102. Ogawa M, Takee R, Okabe Y, Seki Y (2017) Bio-Geo Hybrid Pigment; Clay-Anthocyanin Complex Which Changes Color Depending on the Atmosphere. Dye Pigment 139:561–565. https://doi.org/10.1016/j.dyepig.2016.12.054
103. Sanchez C, Julián B, Belleville P, Popall M (2005) Applications of hybrid organic-inorganic nanocomposites. J Mater Chem 15:3559–3592. https://doi.org/10.1039/b509097k
104. Parola S, Julián-López B, Carlos LD, Sanchez C (2016) Optical properties of hybrid organic-inorganic materials and their applications. Adv Funct Mater 26:6506–6544. https://doi.org/10.1002/adfm.201602730
105. Bujdák J (2017) Hybrids with functional dyes. In: Nakato T, Kawamata J, Takagi S (eds) Inorganic nanosheets and nanosheet-based materials. Springer, Tokyo, pp 419–465
106. Ngulube T, Gumbo JR, Masindi V, Maity A (2017) An update on synthetic dyes adsorption onto clay based minerals: a state-of-art review. J Environ Manag 191:35–57. https://doi.org/10.1016/j.jenvman.2016.12.031
107. Okada T, Konno T, Ogawa M (2008) Luminescence quenching of tris(2,2′-bipyridine)ruthenium(II) in the interlayer space of saponite by sulfur dioxide. Clay Sci 14:43–47. https://doi.org/10.11362/jcssjclayscience.14.1_43
108. Jaynes WF, Boyd SA (1991) Hydrophobicity of siloxane surfaces in smectites as revealed by aromatic hydrocarbon adsorption from water. Clay Clay Miner 39:428–436. https://doi.org/10.1346/CCMN.1991.0390412
109. Jaynes WF (1999) Sorption of benzene, toluene, Ethylbenzene, and xylene (BTEX) compounds by hectorite clays exchanged with aromatic organic cations. Clay Clay Miner 47:358–365. https://doi.org/10.1346/CCMN.1999.0470312
110. Kakegawa N, Ogawa M (2002) The intercalation of β-carotene into the organophilic interlayer space of dialkyldimethylammonium-montmorillonites. Appl Clay Sci 22:137–144. https://doi.org/10.1016/S0169-1317(02)00145-X
111. Kohno Y, Asai S, Shibata M, Fukuhara C, Maeda Y, Tomita Y, Kobayashi K (2014) Improved photostability of hydrophobic natural dye incorporated in organo-modified hydrotalcite. J Phys Chem Solids 75:945–950. https://doi.org/10.1016/j.jpcs.2014.04.010
112. Liu P, Zhang L (2007) Adsorption of dyes from aqueous solutions or suspensions with clay nano-adsorbents. Sep Purif Technol 58:32–39. https://doi.org/10.1016/j.seppur.2007.07.007

113. Elmoubarki R, Mahjoubi FZ, Tounsadi H, Moustadraf J, Abdennouri M, Zouhri A, El Albani A, Barka N (2015) Adsorption of textile dyes on raw and decanted moroccan clays: kinetics, equilibrium and thermodynamics. Water Resour Ind 9:16–29. https://doi.org/10.1016/j.wri.2014.11.001
114. Meral K, Ylmaz N, Kaya M, Tabak A, Onganer Y (2011) The molecular aggregation of pyronin Y in natural bentonite clay suspension. J Lumin 131:2121–2127. https://doi.org/10.1016/j.jlumin.2011.05.023
115. Bujdák J (2001) Methylene blue interactions with reduced-charge smectites. Clay Clay Miner 49:244–254. https://doi.org/10.1346/CCMN.2001.0490307
116. Teepakakorn AP, Yamaguchi T, Ogawa M (2019) The improved stability of molecular guests by the confinement into nanospaces. Chem Lett 48:398–409. https://doi.org/10.1246/cl.181026
117. Van Olphen H (1966) Maya blue: a clay-organic pigment? Science 154:645–646. https://doi.org/10.1126/science.154.3749.645
118. Teixeira-Neto ÂA, Izumi CMS, Temperini MLA, Ferreira AMDC, Constantino VRL (2012) Hybrid materials based on smectite clays and nutraceutical anthocyanins from the Açaí fruit. Eur J Inorg Chem:5411–5420. https://doi.org/10.1002/ejic.201200702
119. Chiari G, Giustetto R, Ricchiardi G (2003) Crystal structure refinements of palygorskite and Maya Blue from molecular modelling and powder synchrotron diffraction. Eur J Mineral 15:21–33. https://doi.org/10.1127/0935-1221/2003/0015-0021
120. Tilocca A, Fois E (2009) The color and stability of Maya Blue: TDDFT calculations. J Phys Chem C 113:8683–8687. https://doi.org/10.1021/jp810945a
121. Fuentes ME, Peña B, Contreras C, Montero AL, Chianelli R, Alvarado M, Olivas R, Rodríguez LM, Camacho H, Montero-Cabrera LA (2008) Quantum mechanical model for Maya Blue. Int J Quantum Chem 108:1664–1673. https://doi.org/10.1002/qua.21646
122. Leitão IMV, Seixas De Melo JS (2013) Maya Blue, an ancient guest-host pigment: synthesis and models. J Chem Educ 90:1493–1497. https://doi.org/10.1021/ed300425c
123. Sánchez-Ochoa F, Cocoletzi GH, Canto G (2017) Trapping and diffusion of organic dyes inside of palygorskite clay: the ancient Maya blue pigment. Microporous Mesoporous Mater 249:111–117. https://doi.org/10.1016/j.micromeso.2017.04.060
124. Bernardino ND, Constantino VRL, De Faria DLA (2018) Probing the indigo molecule in Maya Blue simulants with resonance Raman spectroscopy. J Phys Chem C 122:11505–11515. https://doi.org/10.1021/acs.jpcc.8b01406
125. Ribeiro HL, de Oliveira AV, Brito ESd, Ribeiro PRV, Souza Filho MM, Azeredo HMC (2018) Stabilizing effect of montmorillonite on Acerola juice anthocyanins. Food Chem 245:966–973. https://doi.org/10.1016/j.foodchem.2017.11.076
126. Marangoni R, Bouhent M, Taviot-Guého C, Wypych F, Leroux F (2009) Zn_2Al layered double hydroxides intercalated and adsorbed with anionic blue dyes: a physico-chemical characterization. J Colloid Interface Sci 333:120–127. https://doi.org/10.1016/j.jcis.2009.02.001
127. Raha S, Ivanov I, Quazi NH, Bhattacharya SN (2009) Photo-stability of rhodamine-B/montmorillonite nanopigments in polypropylene matrix. Appl Clay Sci 42:661–666. https://doi.org/10.1016/j.clay.2008.06.008
128. Smitha VS, Manjumol KA, Ghosh S, Brahmakumar M, Pavithran C, Perumal P, Warrier KG (2011) Rhodamine 6G intercalated montmorillonite nanopigments-polyethylene composites: facile synthesis and ultravioletstability study. J Am Ceram Soc 94:1731–1736. https://doi.org/10.1111/j.1551-2916.2010.04326.x
129. Yang L, Qian L, Feng Y, Tang P, Li D (2014) Acid blue 129 and salicylate cointercalated layered double hydroxides: assembly, characterization, and photostability. Ind Eng Chem Res 53:17961–17967. https://doi.org/10.1021/ie502893f
130. Guo S, Evans DG, Li D (2006) Preparation of C.I. Pigment 52:1 anion-pillared layered double hydroxide and the thermo- and photostability of the resulting intercalated material. J Phys Chem Solids 67:1002–1006. https://doi.org/10.1016/j.jpcs.2006.01.017

131. Liu P, Liu P, Zhao K, Li L (2015) Photostability enhancement of azoic dyes adsorbed and intercalated into Mg-Al-layered double hydroxide. Opt Laser Technol 74:23–28. https://doi.org/10.1016/j.optlastec.2015.05.008
132. Kohno Y, Totsuka K, Ikoma S, Yoda K, Shibata M, Matsushima R, Tomita Y, Maeda Y, Kobayashi K (2009) Photostability enhancement of anionic natural dye by intercalation into hydrotalcite. J Colloid Interface Sci 337:117–121. https://doi.org/10.1016/j.jcis.2009.04.065
133. Ogawa M, Sohmiya M, Watase Y (2011) Stabilization of photosensitizing dyes by complexation with clay. Chem Commun 47:8602–8604. https://doi.org/10.1039/c1cc12392k
134. Kohno Y, Hoshino R, Matsushima R, Tomita Y, Kobayashi K (2015) Stabilization of flavylium dyes by incorporation in the clay interlayer. J Jpn Soc Colour Mater 80:6–12. https://doi.org/10.4011/shikizai1937.80.6
135. Ambrogi V, Nocchetti M, Latterini L (2014) Promethazine-montmorillonite inclusion complex to enhance drug photostability. Langmuir 30:14612–14620. https://doi.org/10.1021/la5033898
136. Chakraborty C, Dana K, Malik S (2012) Lamination of cationic perylene in montmorillonite nano-gallery: induced J-aggregated nanostructure with enhanced PHOTOPHYSICAL AND THERMOGRAVIMETRIC aspect. J Phys Chem C 116:21116–21123. https://doi.org/10.1021/jp307293r
137. Fahn R, Fenderl K (1983) Reaction products of organic dye molecules with acid-treated montmorillonite. Clay Miner 18:447–458. https://doi.org/10.1180/claymin.1983.018.4.10
138. Chakraborty C, Dana K, Malik S (2011) Intercalation of perylenediimide dye into LDH clays: enhancement of photostability. J Phys Chem C 115:1996–2004. https://doi.org/10.1021/jp110486r
139. Kohno Y, Kinoshita R, Ikoma S, Yoda K, Shibata M, Matsushima R, Tomita Y, Maeda Y, Kobayashi K (2009) Stabilization of natural anthocyanin by intercalation into montmorillonite. Appl Clay Sci 42:519–523. https://doi.org/10.1016/j.clay.2008.06.012
140. Turro NJ, Ramamurthy V, Scaiano JC (2010) Modern molecular photochemistry of organic molecules. University Science Books, Carifornia
141. Soderquist CJ, Crosby DG, Moilanen KW, Seiber JN, Woodrow JE (1975) Occurrence of trifluralin and its photoproducts in air. J Agric Food Chem 23:304–309. https://doi.org/10.1021/jf60198a003
142. Margulies L, Margulies L, Stern T, Ruzo LO, Rubin B (1992) Photostabilization of trifluralin adsorbed on a clay matrix. J Agric Food Chem 40:152–155. https://doi.org/10.1021/jf00013a030
143. Teepakakorn AP, Bureekaew S, Ogawa M (2018) Adsorption induced dye stability of cationic dyes on clay nanosheet. Langmuir 34:14069–14075. https://doi.org/10.1021/acs.langmuir.8b02978
144. Sohmiya M, Omata S, Ogawa M (2012) Two dimensional size controlled confinement of poly (vinyl pyrrolidone) in the interlayer space of swelling clay mineral. Polym Chem 3:1069. https://doi.org/10.1039/c2py00465h
145. Sackett DD, Fox MA (1990) Adsorption of alkyl-substituted phenols onto montmorillonite: investigation of adsorbed intermediates via visible absorption spectroscopy and product analysis. Langmuir 6:1237–1245. https://doi.org/10.1021/la00097a008
146. Grigoryan L, Yakushi K, Liu CJ, Takano S, Wakata M, Yamauchi H (1993) Evolution of optical absorption and superconductivity in bi-2212 and 2223 oxides intercalated by metal-phthalocyanines. A systematical study as a function of intercalation level. Phys C Superconduct Appl 218:153–163. https://doi.org/10.1016/0921-4534(93)90278-X
147. Mao Y, Zhang G, Thomas JK (1993) Surface complexes as precursors of photoinduced radical cations of biphenyl and subsequent hydroxylation on laponite. Langmuir 9:1299–1305. https://doi.org/10.1021/la00029a024
148. Lee JH, Chang J, Cha JH, Jung DY, Kim SS, Kim JM (2010) Anthraquinone sulfonate modified, layered double hydroxide nanosheets for dye-sensitized solar cells. Chem A Eur J 16:8296–8299. https://doi.org/10.1002/chem.201000703

149. Kato HE, Zhang F, Yizhar O, Ramakrishnan C, Nishizawa T, Hirata K, Ito J, Aita Y, Tsukazaki T, Hayashi S, Hegemann P, Maturana AD, Ishitani R, Deisseroth K, Nureki O (2012) Crystal structure of the channelrhodopsin light-gated cation channel. Nature 482:369–374. https://doi.org/10.1038/nature10870
150. Kandori H, Ichioka T, Sasaki M (2002) Photoisomerization of the rhodopsin chromophore in clay interlayers at 77 K. Chem Phys Lett 354:251–255. https://doi.org/10.1016/S0009-2614(02)00096-9
151. Furutani Y, Ido K, Sasaki M, Ogawa M, Kandori H (2007) Clay mimics color tuning in visual pigments. Angew Chem Int Ed 46:8010–8012. https://doi.org/10.1002/anie.200702368
152. Margulies L, Rozen H (1986) Adsorption of methyl green on montmorillonite. J Mol Struct 141:219–226. https://doi.org/10.1016/0022-2860(86)80326-X
153. Kovar L, DellaGuardia R, Thomas JK (1984) Reaction of radical cations of tetramethylbenzidine with colloidal clays. J Phys Chem 88:3595–3599. https://doi.org/10.1021/j150660a043
154. Bujdák J, Iyi N (2006) Spectral and structural characteristics of oxazine 4/hexadecyltrimethylammonium montmorillonite films. Chem Mater 18:2618–2624. https://doi.org/10.1021/cm052715c
155. Bujdák J, Ratulovská J, Donauerová A, Bujdáková H (2016) Hybrid materials based on luminescent alkaloid berberine and saponite. J Nanosci Nanotechnol 16:7801–7804. https://doi.org/10.1166/jnn.2016.12550
156. Hirose M, Ito F, Shimada T, Takagi S, Sasai R, Okada T (2017) Photoluminescence by intercalation of a fluorescent β-diketone dye into a layered silicate. Langmuir 33:13515–13521. https://doi.org/10.1021/acs.langmuir.7b03460
157. Cohen R, Yariv S (1984) Metachromasy in clay minerals. sorption of acridine orange by montmorillonite. J Chem Soc Faraday Trans 1 80:1705. https://doi.org/10.1039/f19848001705
158. Taniguchi M, Yamagishi A, Iwamoto T (1990) Effects of alkyl chain length on the adsorption of an *N*-alkylated acridine orange cation by colloidally dispersed zirconium phosphate. J Phys Chem 94:2534–2537. https://doi.org/10.1021/j100369a057
159. Yamagishi A, Soma M (1981) Aliphatic tail effects on adsorption of acridine orange cation on a colloidal surface of montmorillonite. J Phys Chem 3398:3090–3092
160. Valenty SJ (1979) Monolayer films of surfactant derivatives of methylene blue. J Colloid Interface Sci 68:486–491. https://doi.org/10.1016/0021-9797(79)90306-0
161. Ogawa M, Ishikawa A (1998) Controlled microstructures of amphiphilic cationic azobenzene-montmorillonite intercalation compounds. J Mater Chem 8:463–467. https://doi.org/10.1039/a706507h
162. Ogawa M, Hama M, Kuroda K (1999) Photochromism of azobenzene in the hydrophobic interlayer spaces of dialkyldimethylammonium-fluor-tetrasilicic mica films. Clay Miner 34:213–220. https://doi.org/10.1180/000985599546127
163. Ogawa M, Goto R, Kanegawa N (2000) Intercalation of an amphiphilic azobenzene derivative into the interlayer space of clays. Clay Sci 11:231–241. https://doi.org/10.1017/CBO9781107415324.004
164. Ogawa M, Yamamoto M, Kuroda K (2001) Intercalation of an amphiphilic azobenzene derivative into the interlayer space of a layered silicate, magadiite. Clay Miner 36:263–266. https://doi.org/10.1180/000985501750177988
165. Ogawa M (2002) Photoisomerization of azobenzene in the interlayer space of magadiite. J Mater Chem 12:3304–3307. https://doi.org/10.1039/B204031J
166. Okada T, Watanabea Y, Ogawa M (2004) Photocontrol of the adsorption behavior of phenol for an azobenzene-montmorillonite intercalation compound. Chem Commun 1:320–321
167. Okada T, Watanabe Y, Ogawa M (2005) Photoregulation of the intercalation behavior of phenol for azobenzene-clay intercalation compounds. J Mater Chem 15:987. https://doi.org/10.1039/b412707b

168. Roulia M, Vassiliadis AA (2005) Interactions between C.I. basic blue 41 and aluminosilicate sorbents. J Colloid Interface Sci 291:37–44. https://doi.org/10.1016/j.jcis.2005.04.085
169. Giustetto R, Wahyudi O (2011) Sorption of red dyes on palygorskite: synthesis and stability of red/purple Mayan nanocomposites. Microporous Mesoporous Mater 142:221–235. https://doi.org/10.1016/j.micromeso.2010.12.004
170. Takagi K, Kurematsu T, Sawaki Y (1991) Intercalation and photochromism of spiropyrans on clay interlayers. J Chem Soc Perkin Trans 2:1517. https://doi.org/10.1039/p29910001517
171. Tomioka H, Itoh T (1991) Photochromism of spiropyrans in organized molecular assemblies. Formation of J- and H-aggregates of photomerocyanines in bilayers-clay matrices. J Chem Soc Chem Commun:532–533. https://doi.org/10.1039/C39910000532
172. Martínez VM, Arbeloa FL, Prieto JB, Arbeloa IL (2005) Characterization of rhodamine 6G aggregates intercalated in solid thin films of laponite clay. 2 fluorescence spectroscopy. J Phys Chem B 109:7443–7450. https://doi.org/10.1021/jp050440i
173. Martínez Martínez V, López Arbeloa F, Bañuelos Prieto J, Arbeloa López T, López Arbeloa I (2004) Characterization of rhodamine 6G aggregates intercalated in solid thin films of laponite clay. 1. absorption spectroscopy. J Phys Chem B 108:20030–20037. https://doi.org/10.1021/jp047552e
174. Tapia Estévez MJ, López Arbeloa F, López Arbeloa T, López Arbeloa I, Schoonheydt RA (1994) Spectroscopic study of the adsorption of rhodamine 6G on laponite B for low loadings. Clay Miner 29:105–113. https://doi.org/10.1180/claymin.1994.029.1.12
175. Estévez MJT, Arbeloa FL, Arbeloa TL, Arbeloa IL (1994) On the monomeric and dimeric states of rhodamine 6G adsorbed on laponite B surfaces. J Colloid Interface Sci 162:412–417. https://doi.org/10.1006/jcis.1994.1055
176. Grauer Z, Avnir D, Yariv S (1984) Adsorption characteristics of rhodamine 6G on montmorillonite and laponite, elucidated from electronic absorption and emission spectra. Can J Chem 62:1889–1894. https://doi.org/10.1139/v84-324
177. Baranyaiová T, Bujdák J (2018) Effects of dye surface concentration on the molecular aggregation of xanthene dye in colloidal dispersions of montmorillonite. Clay Clay Miner 66:114–126. https://doi.org/10.1346/CCMN.2018.064089
178. Fujii K, Iyi N, Sasai R, Hayashi S (2008) Preparation of a novel luminous heterogeneous system: rhodamine/coumarin/phyllosilicate hybrid and blue shift in fluorescence emission. Chem Mater 20:2994–3002. https://doi.org/10.1021/cm0716452
179. Huang M, He S, Liu W, Yao Y, Miao S (2015) Spectral inspections on molecular configurations of Nile blue a adsorbed on the elementary clay sheets. J Phys Chem B 119:13302–13308. https://doi.org/10.1021/acs.jpcb.5b05188
180. Banik S, Bhattacharjee J, Hussain SA, Bhattacharjee D (2015) Clay induced aggregation of a tetra-cationic metalloporphyrin in layer by layer self assembled film. J Phys Chem Solids 87:128–135. https://doi.org/10.1016/j.jpcs.2015.08.008
181. Park IY, Kuroda K, Kato C (1989) Preparation of a layered double hydroxide–porphyrin intercalation compound. Chem Lett 18:2057–2058. https://doi.org/10.1246/cl.1989.2057
182. Kameyama H, Suzuki H, Amano A (1988) Intercalation of co(II) meso-tetrakis(1-methyl-4-pyridyl)porphyrin into montmorillonite. Chem Lett 17:1117–1120. https://doi.org/10.1246/cl.1988.1117
183. Bujdák J (2006) Effect of the layer charge of clay minerals on optical properties of organic dyes. A review. Appl Clay Sci 34:58–73. https://doi.org/10.1016/j.clay.2006.02.011
184. Bujdák J (2018) The effects of layered nanoparticles and their properties on the molecular aggregation of organic dyes. J Photochem Photobiol C: Photochem Rev 35:108–133. https://doi.org/10.1016/j.jphotochemrev.2018.03.001
185. Kasha M, Rawls HR, El-Bayoumi MA (1965) The exciton model in molecular spectroscopy. Pure Appl Chem 11:371–392. https://doi.org/10.1351/pac196511030371
186. Ogawa M, Ishii T, Miyamoto N, Kuroda K (2001) Photocontrol of the basal spacing of azobenzene-magadiite intercalation compound. Adv Mater 13:1107–1109. https://doi.org/10.1002/1521-4095(200107)13:14<1107::AID-ADMA1107>3.0.CO;2-O

187. Kuykendall VG, Thomas JK (1991) Photophysical investigation of the degree of dispersion of aqueous colloidal clay. Langmuir 7:610–610. https://doi.org/10.1021/la00051a036
188. Quites FJ, Germino JC, Atvars TDZ (2014) Improvement in the emission properties of a luminescent anionic dye intercalated between the lamellae of zinc hydroxide-layered. Colloids Surf A Physicochem Eng Asp 459:194–201. https://doi.org/10.1016/j.colsurfa.2014.07.009
189. Hestand NJ, Spano FC (2018) Expanded theory of H- and J-molecular aggregates: the effects of vibronic coupling and intermolecular charge transfer. Chem Rev 118:7069–7163. https://doi.org/10.1021/acs.chemrev.7b00581
190. Schoonheydt RA, Cenens J, De Schrijver FC (1986) Spectroscopy of proflavine adsorbed on clays. J Chem Soc Faraday Trans 1 82:281. https://doi.org/10.1039/f19868200281
191. Hill EH, Zhang Y, Whitten DG (2015) Aggregation of cationic *p*-phenylene ethynylenes on laponite clay in aqueous dispersions and solid films. J Colloid Interface Sci 449:347–356. https://doi.org/10.1016/j.jcis.2014.12.006
192. Jelley EE (1936) Spectral absorption and fluorescence of dyes in the molecular state. Nature 138:1009–1010. https://doi.org/10.1038/1381009a0
193. Ogawa M, Kawai R, Kuroda K (1996) Adsorption and aggregation of a cationic cyanine dye on smectites. J Phys Chem 100:16218–16221. https://doi.org/10.1021/jp960261o
194. Bricks JL, Slominskii YL, Panas ID, Demchenko AP (2018) Fluorescent J-aggregates of cyanine dyes: basic research and applications review. Methods Appl Fluoresc 6. https://doi.org/10.1088/2050-6120/aa8d0d
195. Miyamoto N, Kawai R, Kuroda K, Ogawa M (2000) Adsorption and aggregation of a cationic cyanine dye on layered clay minerals. Appl Clay Sci 16:161–170. https://doi.org/10.1016/S0169-1317(99)00051-4
196. Valandro SR, Poli AL, Correia TFA, Lombardo PC, Schmitt CC (2017) Photophysical behavior of isocyanine/clay hybrids in the solid state. Langmuir 33:891–899. https://doi.org/10.1021/acs.langmuir.6b03898
197. Boháč P, Czímerová A, Bujdák J (2016) Enhanced luminescence of 3,3′-Diethyl-2,2'--thiacyanine cations adsorbed on saponite particles. Appl Clay Sci 127–128:64–69. https://doi.org/10.1016/j.clay.2016.04.008
198. Sato N, Fujimura T, Shimada T, Tani T, Takagi S (2015) J-aggregate formation behavior of a cationic cyanine dye on inorganic layered material. Tetrahedron Lett 56:2902–2905. https://doi.org/10.1016/j.tetlet.2015.04.084
199. Debnath P, Chakraborty S, Deb S, Nath J, Dey B, Bhattacharjee D, Soda H, Tominaga M, Suzuki Y, Kawamata J, Hussain SA (2017) Effect of nano clay laponite on stability of SHG active J-aggregate of a thiacyanine dye onto LB films. Appl Clay Sci 147:105–116. https://doi.org/10.1016/j.clay.2017.07.013
200. Mekhzoum MEM, Essassi EM, Qaiss A, Bouhfid R (2016) Fluorescent bio-nanocomposites based on chitosan reinforced hemicyanine dye-modified montmorillonite. RSC Adv 6:111472–111481. https://doi.org/10.1039/c6ra23320a
201. Miyamoto N, Kawai R, Kuroda K, Ogawa M (2001) Intercalation of a cationic cyanine dye into the layer silicate magadiite. Appl Clay Sci 19:39–46. https://doi.org/10.1016/S0169-1317(01)00054-0
202. Chakraborty S, Debnath P, Dey D, Bhattacharjee D, Hussain SA (2014) Formation of fluorescent H-aggregates of a cyanine dye in ultrathin film and its effect on energy transfer. J Photochem Photobiol A Chem 293:57–64. https://doi.org/10.1016/j.jphotochem.2014.07.018
203. Chakraborty S, Bhattacharjee D, Soda H, Tominaga M, Suzuki Y, Kawamata J, Hussain SA (2015) Temperature and concentration dependence of J-aggregate of a cyanine dye in a Laponite film fabricated by Langmuir-Blodgett technique. Appl Clay Sci 104:245–251. https://doi.org/10.1016/j.clay.2014.11.039
204. Matejdes M, Himeno D, Suzuki Y, Kawamata J (2017) Controlled formation of pseudoisocyanine J-aggregates in the interlayer space of synthetic saponite. Appl Clay Sci 140:119–123. https://doi.org/10.1016/j.clay.2017.02.007

205. Estévez MJT, Arbeloa FL, Arbeloa TL, Arbeloa IL (1993) Absorption and fluorescence properties of rhodamine 6G adsorbed on aqueous suspensions of Wyoming montmorillonite. Langmuir 9:3629–3634. https://doi.org/10.1021/la00036a045
206. Sasai R, Itoh H, Iyi N, Fujita T, Arbeloa FL, Martínez VM, Takagi K (2004) Luminescence properties of rhodamine 6G intercalated in surfactant/clay hybrid thin solid films. Langmuir 20:4715–4719. https://doi.org/10.1021/la049584z
207. Wu L, Lv G, Liu M, Li Z, Liao L, Pan C (2015) Adjusting the layer charges of host phyllosilicates to prevent luminescence quenching of fluorescence dyes. J Phys Chem C 119:22625–22631. https://doi.org/10.1021/acs.jpcc.5b07243
208. Kaya M, Meral K, Onganer Y (2015) Molecular aggregates of merocyanine 540 in aqueous suspensions containing natural and CTAB-modified bentonite. J Mol Struct 1083:101–105. https://doi.org/10.1016/j.molstruc.2014.11.046
209. Giannelis EP (1990) Highly organized molecular assemblies of porphyrin guest molecules in mica-type silicates: influence of guest–host interactions on molecular organization. Chem Mater 2:627–629. https://doi.org/10.1021/cm00012a002
210. Carrado KA, Winans RE (1990) Interactions of water-soluble porphyrins and metalloporphyrins with smectite clay surfaces. Chem Mater 2:328–335. https://doi.org/10.1021/cm00009a027
211. Bergaya F, Van Damme H (1982) Stability of metalloporphyrins adsorbed on clays: a comparative study. Geochim Cosmochim Acta 46:349–360. https://doi.org/10.1016/0016-7037(82)90226-5
212. Carrado KA, Thiyagarajan P, Winans RE, Botto RE (1991) Hydrothermal crystallization of porphyrin-containing layer silicates. Inorg Chem 30:794–799. https://doi.org/10.1021/ic00004a034
213. Grando SR, Santos FDS, Gallas MR, Costa TMH, Benvenutti EV, Rodembusch FS (2012) Photophysics of aminobenzazole dyes in silica-based hybrid materials. J Sol-Gel Sci Technol 63:235–241. https://doi.org/10.1007/s10971-012-2720-z
214. Kudo N, Tsukamoto T, Tokieda D, Shimada T, Takagi S (2018) Fluorescence enhancement behavior of hemicyanine derivatives on the clay nanosheets: aggregation induced emission (AIE) vs. surface-fixation induced emission (S-FIE). Chem Lett 47:636–639. https://doi.org/10.1246/cl.180043
215. Tokieda D, Tsukamoto T, Ishida Y, Ichihara H, Shimada T, Takagi S (2017) Unique fluorescence behavior of dyes on the clay minerals surface: surface fixation induced emission (S-FIE). J Photochem Photobiol A Chem 339:67–79. https://doi.org/10.1016/j.jphotochem.2017.01.013
216. Kawamata J, Suzuki Y, Tominaga M (2018) From adsorbed dyes to optical materials. In: Developments in clay science. Elsevier, Amsterdam, pp 361–375
217. Zhang X, Hong H, Li Z, Guan J, Schulz L (2009) Removal of azobenzene from water by kaolinite. J Hazard Mater 170:1064–1069. https://doi.org/10.1016/j.jhazmat.2009.05.073
218. van Damme H, Crespin M, Obrecht F, Cruz MI, Fripiat JJ (1978) Acid-base and complexation behavior of porphyrins on the intracrystal surface of swelling clays: meso-tetraphenylporphyrin and meso-tetra(4-pyridyl)porphyrin on montmorillonites. J Colloid Interface Sci 66:43–54. https://doi.org/10.1016/0021-9797(78)90182-0
219. Takagi S, Shimada T, Yui T, Inoue H (2001) High density adsorption of porphyrins onto clay layer without aggregation: characterization of smectite-cationic porphyrin complex. Chem Lett 30:128–129. https://doi.org/10.1246/cl.2001.128
220. Takagi S, Shimada T, Eguchi M, Yui T, Yoshida H, Tryk DA, Inoue H (2002) High-density adsorption of cationic porphyrins on clay layer surfaces without aggregation: the size-matching effect. Langmuir 18:2265–2272. https://doi.org/10.1021/la011524v
221. Ishida Y, Masui D, Shimada T, Tachibana H, Inoue H, Takagi S (2012) The mechanism of the porphyrin spectral shift on inorganic nanosheets: the molecular flattening induced by the strong host–guest interaction due to the "size-matching rule". J Phys Chem C 116:7879–7885. https://doi.org/10.1021/jp300842f

222. Ogawa M, Handa T, Kuroda K, Kato C, Tani T (1992) Photochemical hole burning of 1,4-dihydroxyanthraquinone intercalated in a pillered layered clay mineral. J Phys Chem 96:8116–8119
223. Ferreira AUC, Poli AL, Gessner F, Neumann MG, Schmitt Cavalheiro CC (2013) Interaction of auramine O with montmorillonite clays. J Lumin 136:63–67. https://doi.org/10.1016/j.jlumin.2012.11.022
224. Tsukamoto T, Shimada T, Takagi S (2013) Unique photochemical properties of *p*-substituted cationic triphenylbenzene derivatives on a clay layer surface. J Phys Chem C 117:2774–2779. https://doi.org/10.1021/jp3092144
225. Tsukamoto T, Shimada T, Takagi S (2013) Photochemical properties of mono-, tri-, and penta-cationic antimony(V) metalloporphyrin derivatives on a clay layer surface. J Phys Chem A 117:7823–7832. https://doi.org/10.1021/jp405767s
226. Tsukamoto T, Shimada T, Takagi S (2015) Structure resembling effect of clay surface on photochemical properties of meso-phenyl or pyridyl-substituted monocationic antimony (V) porphyrin derivatives. RSC Adv 5:8479–8485. https://doi.org/10.1039/C4RA15650A
227. Villemure G, Detellier C, Szabo AG (1986) Fluorescence of clay-intercalated methylviologen. J Am Chem Soc 108:4658–4659. https://doi.org/10.1021/ja00275a071
228. Miyata H, Sugahara Y, Kuroda K, Kato C (1987) Synthesis of montmorillonite-viologen intercalation compounds and their photochromic behaviour. J Chem Soc Faraday Trans 1 83:1851–1858. https://doi.org/10.1039/F19878301851
229. Raupach M, Emerson WW, Slade PG (1979) The arrangement of paraquat bound by vermiculite and montmorillonite. J Colloid Interface Sci 69:398–408. https://doi.org/10.1016/0021-9797(79)90129-2
230. Hayes MHB, Pick ME, Toms BA (1978) The influence of organocation structure on the adsorption of mono- and of bipyridinium cations by expanding lattice clay minerals. J Colloid Interface Sci 65:254–265. https://doi.org/10.1016/0021-9797(78)90156-X
231. Villemure G, Detellier C, Szabo AG (1991) Fluorescence of methylviologen intercalated into montmorillonite and hectorite aqueous suspensions. Langmuir 7:1215–1221. https://doi.org/10.1021/la00054a032
232. Okada T, Ogawa M (2003) 1,1′-dimethyl-4,4′-bipyridinium-smectites as a novel adsorbent of phenols from water through charge-transfer interactions. Chem Commun:1378–1379. https://doi.org/10.1039/b302144k
233. Kakegawa N, Kondo T, Ogawa M (2003) Variation of electron-donating ability of smectites as probed by photoreduction of methyl viologen. Langmuir 19:3578–3582. https://doi.org/10.1021/la020763v
234. Miyata H, Sugahara Y, Kuroda K, Kato C (1988) Synthesis of a viologen-tetratitanate intercalation compound and its photochemical behaviour. J Chem Soc Faraday Trans 84:2677–2682. https://doi.org/10.1039/F19888402677
235. Nakato T, Kuroda K, Kato C (1989) Photoreduction of methylviologen in the interlayer of $K_4Nb_6O_{17}$. J Chem Soc Chem Commun 1144. https://doi.org/10.1039/c39890001144
236. Nakato T, Kuroda K, Kato C (1992) Syntheses of intercalation compounds of layered niobates with methylviologen and their photochemical behavior. Chem Mater 4:128–132. https://doi.org/10.1021/cm00019a027
237. Nakato T, Ito K, Kuroda K, Kato C (1993) Photochemical behavior of perovskite-related layered niobates $HA_2Nb_3O_{10}$ (a = Ca, Sr) intercalated with methylviologen. Microporous Mater 1:283–286. https://doi.org/10.1016/0927-6513(93)80071-2
238. Nakato T, Miyata H, Kuroda K, Kato C (1988) Synthesis of methylviologen-$HTiNbO_5$ intercalation compound and its photochemical behavior. React Solids 6:231–238. https://doi.org/10.1016/0168-7336(88)80063-9
239. Vermeulen LA, Snover JL, Sapochak LS, Thompson ME (1993) Efficient photoinduced charge separation in layered zirconium viologen phosphonate compounds. J Am Chem Soc 115:11767–11774. https://doi.org/10.1021/ja00078a015

240. Vermeulen LA, Thompson ME (1992) Stable photoinduced charge separation in layered viologen compounds. Nature 358:656–658. https://doi.org/10.1038/358656a0
241. Liu X, Iu KK, Thomas JK (1992) Studies of surface properties of clay Laponite using pyrene as a photophysical probe molecule. 2. Photoinduced electron transfer. Langmuir 8:539–545. https://doi.org/10.1021/la00038a038
242. Viaene K, Caigui J, Schoonheydt RA, De Schryver FC (1987) Study of the adsorption on clay particles by means of a fluorescent probe. Langmuir 3:107–111. https://doi.org/10.1021/la00073a019
243. Viaene K, Schoonheydt RA, Crutzen M, Kunyima B, De Schryver FC (1988) Study of the adsorption on clay particles by means of fluorescent probes. Langmuir 4:749–752. https://doi.org/10.1021/la00081a044
244. Labbé P, Reverdy G (1988) Adsorption characteristics of polycyclic aromatic compounds on clay: pyrene as a photophysical probe on Laponite. Langmuir 4:419–425. https://doi.org/10.1021/la00080a028
245. Kunyima B, Viaene K, Khalil MMH, Schoonheydt RA, Crutzen M, De Schryver FC (1990) Study of the adsorption and polymerization of functionalized organic ammonium derivatives on a clay surface. Langmuir 6:482–486. https://doi.org/10.1021/la00092a031
246. Liu X, Thomas JK (1991) Study of surface properties of clay Laponite using pyrene as a photophysical probe molecule. Langmuir 7:2808–2816. https://doi.org/10.1021/la00059a065
247. Ikeda M, Yoshii T, Matsui T, Tanida T, Komatsu H, Hamachi I (2011) Montmorillonite−supramolecular hydrogel hybrid for fluorocolorimetric sensing of polyamines. J Am Chem Soc 133:1670–1673. https://doi.org/10.1021/ja109692z
248. Kavanagh RJ, Iu KK, Thomas JK (1992) Spectroscopic determination of refractive index and dielectric constant at interfaces, using photophysical probe molecules. Langmuir 8:3008–3013. https://doi.org/10.1021/la00048a026
249. Nakamura T, Thomas JK (1986) The interaction of alkylammonium salts with synthetic clays. A fluorescence and laser excitation study. J Phys Chem 90:641–644. https://doi.org/10.1021/j100276a032
250. Nakamura T, Thomas JK (1987) Formation of surfactant double layers on Laponite clay colloids. Langmuir 3:234–239. https://doi.org/10.1021/la00074a016
251. Dellaguardia RA, Thomas JK (1983) Photoprocesses on colloidal clay systems. 2. Quenching studies and the effect of surfactants on the luminescent properties of pyrene and pyrene derivatives adsorbed on clay colloids. J Phys Chem 87:3550–3557
252. DellaGuardia RA, Thomas JK (1984) Photoprocesses on colloidal clay systems. 3. Interaction of dodecanol and its micelles with colloidal montmorillonite. J Phys Chem 88:964–970. https://doi.org/10.1021/j150649a024
253. Wang T, Hu X, Zheng S, Liu X, Wang C, Tong Z (2012) Adsorption of fluorophores and *N*-isopropylacrylamide on Laponite. Appl Clay Sci 58:102–107. https://doi.org/10.1016/j.clay.2012.01.021
254. Kawamata J, Suzuki Y, Tenma Y (2010) Fabrication of clay mineral-dye composites as nonlinear optical materials. Philos Mag 90:2519–2527. https://doi.org/10.1080/14786430903581304
255. Tominaga M, Oniki Y, Mochida S, Kasatani K, Tani S, Suzuki Y, Kawamata J (2016) Clay-organic hybrid films exhibiting reversible fluorescent color switching induced by swelling and drying of a clay mineral. J Phys Chem C 120:23813–23822. https://doi.org/10.1021/acs.jpcc.6b07537
256. Barloy L, Battioni P, Mansuy D (1990) Manganese porphyrins supported on montmorillonite as hydrocarbon mono-oxygenation catalysts: particular efficacy for linear alkane hydroxylation. J Chem Soc Chem Commun:1365–1367. https://doi.org/10.1039/C39900001365
257. Gaillon L, Bedioui F, Devynck J, Battioni P (1993) Electrochemical characterization of manganese Porphyrins fixed onto silica and layered Dihydroxide matrices. J Electroanal Chem 347:435–442. https://doi.org/10.1016/0022-0728(93)80108-T

258. Liu J, Zhang G (2014) Recent advances in synthesis and applications of clay-based photocatalysts: a review. Phys Chem Chem Phys 16:8178–8192. https://doi.org/10.1039/c3cp54146k
259. Kameyama H, Narumi F, Hattori T, Kameyama H (2006) Oxidation of cyclohexene with molecular oxygen catalyzed by cobalt porphyrin complexes immobilized on montmorillonite. J Mol Catal A Chem 258:172–177. https://doi.org/10.1016/j.molcata.2006.05.022
260. Tsukamoto T, Shimada T, Takagi S (2018) Artificial photosynthesis model: photochemical reaction system with efficient light-harvesting function on inorganic nanosheets. ACS Omega 3:18563–18571. https://doi.org/10.1021/acsomega.8b02594
261. Remello SN, Kuttassery F, Mathew S, Thomas A, Yamamoto D, Nabetani Y, Sano K, Tachibana H, Inoue H (2018) Two-electron oxidation of water to form hydrogen peroxide catalysed by silicon-porphyrins. Sustain Energy Fuels 2:1966–1973. https://doi.org/10.1039/c8se00102b
262. Tatsumi D, Tsukamoto T, Honna R, Hoshino S, Shimada T, Takagi S (2017) Highly selective photochemical epoxidation of cyclohexene sensitized by Ru(II) porphyrinclay hybrid catalyst. Chem Lett 46:1311–1314. https://doi.org/10.1246/cl.170521
263. Jain A, Achari A, Eswaramoorthy M, George SJ (2016) Light induced: in situ post-modification of clay-chromophore hybrids for multiple white light emissions. J Mater Chem C 4:2748–2751. https://doi.org/10.1039/c5tc03319e
264. Ishida Y, Shimada T, Masui D, Tachibana H, Inoue H, Takagi S (2011) Efficient excited energy transfer reaction in clay/porphyrin complex toward an artificial light-harvesting system. J Am Chem Soc 133:14280–14286. https://doi.org/10.1021/ja204425u
265. Takagi S, Eguchi M, Shimada T, Hamatani S, Inoue H (2007) Energy transfer reaction of cationic porphyrin complexes on the clay surface: effect of sample preparation method. Res Chem Intermed 33:177–189. https://doi.org/10.1163/156856707779160889
266. Takagi S, Shimada T, Ishida Y, Fujimura T, Masui D, Tachibana H, Eguchi M, Inoue H (2013) Size-matching effect on inorganic nanosheets: control of distance, alignment, and orientation of molecular adsorption as a bottom-up methodology for nanomaterials. Langmuir 29:2108–2119. https://doi.org/10.1021/la3034808
267. Rao KV, Datta KKR, Eswaramoorthy M, George SJ (2013) Highly pure solid-state white-light emission from solution-processable soft-hybrids. Adv Mater 25:1713–1718. https://doi.org/10.1002/adma.201204407
268. Sato K, Matsubara K, Hagiwara S, Saito K, Yagi M, Takagi S, Yui T (2015) Remarkable stimulation of emission quenching on a clay surface. Langmuir 31:27–31. https://doi.org/10.1021/la504597t
269. Takagi S, Eguchi M, Tryk DA, Inoue H (2006) Porphyrin photochemistry in inorganic/organic hybrid materials: clays, layered semiconductors, nanotubes, and mesoporous materials. J Photochem Photobiol C: Photochem Rev 7:104–126. https://doi.org/10.1016/j.jphotochemrev.2006.04.002
270. Nakato T, Iwata Y, Kuroda K, Kaneko M, Kato C (1993) Intercalation of a free-base porphyrin into layered tetratitanic acid. J Chem Soc Dalt Trans:1405–1409. https://doi.org/10.1039/DT9930001405
271. Sasai R, Kato Y, Soontornchaiyakul W, Usami H, Masumori A, Norimatsu W, Fujimura T, Takagi S (2017) Photoinduced electron transfer in layer-by-layer thin solid films containing cobalt oxide nanosheets, porphyrin, and methyl viologen. Phys Chem Chem Phys 19:5611–5616. https://doi.org/10.1039/c6cp07250j
272. Gu Z, Gao M, Lu L, Liu Y, Yang S (2015) Montmorillonite functionalized with zwitterionic surfactant as a highly efficient adsorbent for herbicides. Ind Eng Chem Res 54:4947–4955. https://doi.org/10.1021/acs.iecr.5b00438
273. Si Y, Zhou J, Chen H, Zhou D (2004) Photostabilization of the herbicide bensulfuron-methyl by using organoclays. Chemosphere 54:943–950. https://doi.org/10.1016/j.chemosphere.2003.09.033

274. El-Nahhal Y, Nir S, Margulies L, Rubin B (1999) Reduction of photodegradation and volatilization of herbicides in Organo-clay formulations. Appl Clay Sci 14:105–119. https://doi.org/10.1016/S0169-1317(98)00053-2
275. Margulies L, Rozen H, Cohen E (1985) Energy transfer at the surface of clays and protection of pesticides from photodegradation. Nature 315:658–659. https://doi.org/10.1038/315658a0
276. Undabeytia T, Nir S, Tel-Or E, Rubin B (2000) Photostabilization of the herbicide norflurazon by using organoclays. J Agric Food Chem 48:4774–4779. https://doi.org/10.1021/jf9912405
277. Goto T, Ogawa M (2015) Visible-light-responsive photocatalytic flow reactor composed of Titania film photosensitized by metal complex-clay hybrid. ACS Appl Mater Interfaces 7:12631–12634. https://doi.org/10.1021/acsami.5b03128
278. Goto T, Ogawa M (2016) Efficient photocatalytic oxidation of benzene to phenol by metal complex-clay/TiO_2 hybrid photocatalyst. RSC Adv 6:23794–23797. https://doi.org/10.1039/c5ra25430b
279. Kakegawa N, Ogawa M (2004) Effective luminescence quenching of Tris (2,2-bipyridine) ruthenium (II) by methylviologen on clay by the aid of poly (vinylpyrrolidone). Langmuir 20:7004–7009
280. Lu L, Jones RM, McBranch D, Whitten D (2002) Surface-enhanced superquenching of cyanine dyes as J-aggregates on Laponite clay nanoparticles. Langmuir 18:7706–7713. https://doi.org/10.1021/la0259306
281. Kanegawa N, Ogawa M (2003) The synthesis of dihexadecylviologen- intercalation compounds and the photochemical reactions. Clay Sci 12:153–157
282. Okada T, Ogawa M (2002) Adsorption of phenols onto 1,1′-dimethyl-4,4′-bipyridinium-smectites. Chem Lett 31:812–813
283. Yui T, Tsuchino T, Itoh T, Ogawa M, Fukushima Y, Takagi K (2005) Photoinduced one-electron reduction of MV^{2+} in titania nanosheets using porphyrin in mesoporous silica thin films. Langmuir 21:2644–2646. https://doi.org/10.1021/la047385+
284. Yui T, Kobayashi Y, Yamada Y, Yano K, Fukushima Y, Torimoto T, Takagi K (2011) Photoinduced electron transfer between the anionic porphyrins and viologens in titania nanosheets and monodisperse mesoporous silica hybrid films. ACS Appl Mater Interfaces 3:931–935. https://doi.org/10.1021/am101281n
285. Okada T, Matsutomo T, Ogawa M (2010) Nanospace engineering of methylviologen modified hectorite-like layered silicates with varied layer charge density for the adsorbents design. J Phys Chem C 114:539–545. https://doi.org/10.1021/jp9089886
286. Ogawa M, Matsutomo T, Okada T (2008) Preparation of hectorite-like swelling silicate with controlled layer charge density. J Ceram Soc Jpn 116:1309–1313. https://doi.org/10.2109/jcersj2.116.1309
287. Takagi S, Tryk DA, Inoue H (2002) Photochemical energy transfer of cationic porphyrin complexes on clay surface. J Phys Chem B 106:5455–5460. https://doi.org/10.1021/jp0200977
288. Fujimura T, Ramasamy E, Ishida Y, Shimada T, Takagi S, Ramamurthy V (2016) Sequential energy and electron transfer in a three-component system aligned on a clay nanosheet. Phys Chem Chem Phys 18:5404–5411. https://doi.org/10.1039/c5cp06984j
289. Miyamoto N, Kuroda K, Ogawa M (2004) Exfoliation and film preparation of a layered titanate, $Na_2Ti_3O_7$, and intercalation of pseudoisocyanine dye. J Mater Chem 14:165. https://doi.org/10.1039/b308800f
290. Eguchi M, Tachibana H, Takagi S, Tryk DA, Inoue H (2007) Dichroic measurements on dicationic and tetracationic porphyrins on clay surfaces with visible-light-attenuated total reflectance. Bull Chem Soc Jpn 80:1350–1356. https://doi.org/10.1246/bcsj.80.1350
291. Takenawa R, Komori Y, Hayashi S, Kawamata J, Kuroda K (2001) Intercalation of nitroanilines into kaolinite and second harmonic generation. Chem Mater 13:3741–3746. https://doi.org/10.1021/cm010095j

292. Yan D, Lu J, Wei M, Evans DG, Duan X (2011) Recent advances in photofunctional guest/layered double hydroxide host composite systems and their applications: experimental and theoretical perspectives. J Mater Chem 21:13128–13139. https://doi.org/10.1039/c1jm11594d
293. Yan D, Lu J, Wei M, Qin S, Chen L, Zhang S, Evans DG, Duan X (2011) Heterogeneous transparent ultrathin films with tunable-color luminescence based on the assembly of photoactive organic molecules and layered double hydroxides. Adv Funct Mater 21:2497–2505. https://doi.org/10.1002/adfm.201002446
294. López Arbeloa F, Martínez Martínez V (2006) Orientation of adsorbed dyes in the interlayer space of clays. 2 fluorescence polarization of rhodamine 6G in Laponite films. Chem Mater 18:1407–1416. https://doi.org/10.1021/cm051518a
295. López Arbeloa F, Martínez Martínez V, Arbeloa T, López Arbeloa I (2007) Photoresponse and anisotropy of rhodamine dye intercalated in ordered clay layered films. J Photochem Photobiol C: Photochem Rev 8:85–108. https://doi.org/10.1016/j.jphotochemrev.2007.03.003
296. Yan D, Lu J, Wei M, Evans DG, Duan X (2009) Sulforhodamine B intercalated layered double hydroxide thin film with polarized photoluminescence. J Phys Chem B 113:1381–1388. https://doi.org/10.1021/jp8084217
297. Wang Z, Teng X, Lu C (2013) Universal chemiluminescence flow-through device based on directed self-assembly of solid-state organic chromophores on layered double hydroxide matrix. Anal Chem 85:2436–2442. https://doi.org/10.1021/ac303487b
298. Shi W, Lin Y, Kong X, Zhang S, Jia Y, Wei M, Evans DG, Duan X (2011) Fabrication of pyrenetetrasulfonate/layered double hydroxide ultrathin films and their application in fluorescence chemosensors. J Mater Chem 21:6088–6094. https://doi.org/10.1039/c1jm00073j
299. Yan D, Lu J, Ma J, Wei M, Li S, Evans DG, Duan X (2011) Near-infrared absorption and polarized luminescent ultrathin films based on sulfonated cyanines and layered double hydroxide. J Phys Chem C 115:7939–7946. https://doi.org/10.1021/jp2002029
300. Zhao Y, Lin H, Chen M, Yan D (2014) Niflumic anion intercalated layered double hydroxides with Mechano-induced and solvent-responsive luminescence. Ind Eng Chem Res 53:3140–3147. https://doi.org/10.1021/ie404054v
301. Yan D, Lu J, Chen L, Qin S, Ma J, Wei M, Evans DG, Duan X (2010) A strategy to the ordered assembly of functional small cations with layered double hydroxides for luminescent ultra-thin films. Chem Commun 46:5912–5914. https://doi.org/10.1039/c0cc00522c
302. Li S, Lu J, Ma H, Xu J, Yan D, Wei M, Evans DG, Duan X (2011) Ordered blue luminescent ultrathin films by the effective coassembly of tris(8-hydroxyquinolate-5-sulfonate)aluminum and polyanions with layered double hydroxides. Langmuir 27:11501–11507. https://doi.org/10.1021/la202139f
303. Yan D, Lu J, Ma J, Wei M, Wang X, Evans DG, Duan X (2010) Anionic poly(*p*-phenylenevinylene)/layered double hydroxide ordered ultrathin films with multiple quantum well structure: a combined experimental and theoretical study. Langmuir 26:7007–7014. https://doi.org/10.1021/la904228b
304. Yan D, Lu J, Ma J, Wei M, Evans DG, Duan X (2011) Fabrication of an anionic polythiophene/layered double hydroxide ultrathin film showing red luminescence and reversible pH photoresponse. AICHE J 57:1926–1935. https://doi.org/10.1002/aic.12400
305. Valeur B, Berberan-Santos MN (2012) Molecular fluorescence. Wiley-VCH Verlag GmbH & Co. KGaA, Weinheim
306. Yan D, Zhao Y, Wei M, Liang R, Lu J, Evans DG, Duan X (2013) Regular assembly of 9-fluorenone-2,7-dicarboxylate within layered double hydroxide and its solid-state photoluminescence: a combined experiment and computational study. RSC Adv 3:4303. https://doi.org/10.1039/c3ra23064c
307. Jain A, Achari A, Mothi N, Eswaramoorthy M, George SJ (2015) Shining light on clay-Chromophore hybrids: layered templates for accelerated ring closure photo-oxidation. Chem Sci 6:6334–6340. https://doi.org/10.1039/c5sc02215k

308. Hartley GS (1938) 113. The *cis*-form of azobenzene and the velocity of the thermal *cis→trans*-conversion of azobenzene and some derivatives. J Chem Soc:633–642. https://doi.org/10.1039/JR9380000633
309. Ciccone S, Halpern J (1959) Catalysis of the *cis - trans* isomerization of azobenzene by acids and cupric salts. Can J Chem 37:1903–1910. https://doi.org/10.1139/v59-278
310. Siampiringue N, Guyot G, Monti S, Bortolus P (1987) The *cis → trans* photoisomerization of azobenzene: an experimental re-examination. J Photochem 37:185–188. https://doi.org/10.1016/0047-2670(87)85039-6
311. Bortolus P, Monti S (1979) Cis-trans photoisomerization of azobenzene.solvent and triplet donors effects. J Phys Chem 83:648–652. https://doi.org/10.1021/j100469a002
312. Saremi F, Tieke B (1998) Photoinduced switching in self-assembled multilayers of an azobenzene bolaamphiphile and polyelectrolytes. Adv Mater 10:389–391. https://doi.org/10.1002/(SICI)1521-4095(199803)10:5<389::AID-ADMA388>3.0.CO;2-9
313. Kojima M, Takagi T, Goshima T (2000) Photoisomerization of Azobenzene in zeolite cavities. Mol Cryst Liq Cryst Sci Technol Sect A 344:179–184. https://doi.org/10.1080/10587250008023833
314. Fischer E, Frankel M, Wolovsky R (1955) Wavelength dependence of photoisomerization equilibria in azocompounds. J Chem Phys 23:1367–1367. https://doi.org/10.1063/1.1742302
315. Bandara HMD, Burdette SC (2012) Photoisomerization in different classes of azobenzene. Chem Soc Rev 41:1809–1825. https://doi.org/10.1039/c1cs15179g
316. Ueda M, Kim HB, Ikeda T, Ichimura K (1992) Photoisomerization of an azobenzene in sol-gel glass films. Chem Mater 4:1229–1233. https://doi.org/10.1021/cm00024a022
317. Suzuki I, Ishizaki T, Hoshi T, Anzai J (2002) Fully reversible isomerization of azobenzene chromophores in polyelectrolyte layered assemblies. Macromolecules 35:577–580. https://doi.org/10.1021/ma010388y
318. Beattie MS, Jackson C, Jaycox GD (1998) Azobenzene modified poly(aryl ether ketone amide)s. 2. Photo- and thermo-responsive behaviour in dilute solution. Polymer 39:2597–2605. https://doi.org/10.1016/S0032-3861(97)00559-4
319. Gegiou D, Muszkat KA, Fischer E (1968) Temperature dependence of Photoisomerization. V the effect of substituents on the photoisomerization of stilbenes and azobenzenes. J Am Chem Soc 90:3907–3918. https://doi.org/10.1021/ja01017a002
320. Yabe A, Kawabata Y, Niino H, Tanaka M, Ouchi A, Takahashi H, Tamura S, Tagaki W, Nakahara H, Fukuda K (1988) *cis–trans* isomerization of the azobenzenes included as guests in Langmuir–Blodgett films of amphiphilic β-cyclodextrin. Chem Lett 17:1–4. https://doi.org/10.1246/cl.1988.1
321. Nishiyama K, Fujihira M (1988) *cis–trans* reversible photoisomerization of an amphiphilic azobenzene derivative in its pure LB film prepared as polyion complexes with polyallylamine. Chem Lett 17:1257–1260. https://doi.org/10.1246/cl.1988.1257
322. Matsumoto M, Tachibana H, Sato F, Terrettaz S (1997) Photoinduced self-organization in Langmuir-Blodgett films. J Phys Chem B 101:702–704. https://doi.org/10.1021/jp9629093
323. Matsumoto M, Miyazaki D, Tanaka M, Azumi R, Manda E, Kondo Y, Yoshino N, Tachibana H (1998) Reversible light-induced morphological change in Langmuir-Blodgett films. J Am Chem Soc 120:1479–1484. https://doi.org/10.1021/ja970577p
324. Tachibana H, Goto A, Nakamura T, Matsumoto M, Manda E, Niino H, Yabe A, Kawabata Y (1989) Photoresponsive conductivity in Langmuir-Blodgett films. Thin Solid Films 179:207–213. https://doi.org/10.1016/0040-6090(89)90184-3
325. Tachibana H, Nakamura T, Matsumoto M, Komizu H, Manda E, Niino H, Yabe A, Kawabata Y (1989) Photochemical switching in conductive Langmuir-Blodgett films. J Am Chem Soc 111:3080–3081. https://doi.org/10.1021/ja00190a061
326. Nishiyama K, Kurihara MA, Fujihira M (1989) Photochromism of an amphiphilic azobenzene derivative in its Langmuir-Blodgett films prepared as polyion complexes with ionic polymers. Thin Solid Films 179:477–483. https://doi.org/10.1016/0040-6090(89)90224-1

327. Seki T, Tamaki T, Ichimura K, Aoki K (1989) Photochemical alignment regulation of a nematic liquid crystal by Langmuir-Blodgett layers of azobenzene polymers as "command surfaces". Macromolecules 22:3505–3506
328. Tachibana H, Azumi R, Nakamura T, Matsumoto M, Kawabata Y (1992) New types of photochemical switching phenomena in Langmuir-Blodgett films. Chem Lett:173–176. https://doi.org/10.1246/cl.1992.173
329. Tachibana H, Manda E, Azumi R, Nakamura T, Matsumoto M, Kawabata Y (1992) Multiple photochemical switching device based on Langmuir-Blodgett films. Appl Phys Lett 61:2420–2421. https://doi.org/10.1063/1.108184
330. Tachibana H, Manda E, Matsumoto M (1995) Conductivity switching of Langmuir-Blodgett films using photoisomerization of phenylazonaphthalene. Mol Cryst Liq Cryst Sci Technol Sect A Mol Cryst Liq Cryst 267:341–346. https://doi.org/10.1080/10587259508034014
331. Tachibana H, Azumi R, Tanaka M, Matsumoto M, Sako SI, Sakai H, Abe M, Kondo Y, Yoshino N (1996) Structures and photoisomerization of the polyion complex Langmuir-Blodgett films of an amphiphile bearing two azobenzene units. Thin Solid Films 284–285:73–75. https://doi.org/10.1016/S0040-6090(95)08274-3
332. Maack J, Ahuja RC, Möbius D, Tachibana H, Matsumoto M (1994) Molecular cis-trans switching in amphiphilic monolayers containing azobenzene moieties. Thin Solid Films 242:122–126. https://doi.org/10.1016/0040-6090(94)90514-2
333. Shimura N, Ogawa M (2004) Preparation of aluminum-containing self-standing mesoporous silica films. Bull Chem Soc Jpn 77:1599–1606. https://doi.org/10.1246/bcsj.77.1599
334. Ogawa M, Fujii K, Kuroda K, Kato C (1991) Preparation of montmorillonite-*p*-aminoazobenzene intercalation compounds and their photochemical behavior. Mater Res Soc Symp Proc 233:89–94
335. Adams JM, Reid PI (1977) Azobenzene intercalates of montmorillonite. Clay Clay Miner 25:228–230
336. Ogawa M, Okutomo S, Kuroda K (1998) Control of interlayer microstructures of a layered silicate by surface modification with organochlorosilanes. J Am Chem Soc 120:7361–7362. https://doi.org/10.1021/ja981055s
337. Bujdák J, Iyi N, Fujita T (2003) Isomerization of cationic azobenzene derivatives in dispersions and films of layered silicates. J Colloid Interface Sci 262:282–289. https://doi.org/10.1016/S0021-9797(03)00235-2
338. Koteja A, Matusik J (2016) Preparation and characterization of azobenzene-smectite photoactive mineral nanomaterials. Geol Geophys Environ 41:99. https://doi.org/10.7494/geol.2015.41.1.99
339. Kosuge K, Yamazaki A, Tsunashima A, Otsuka R (1992) Hydrothermal synthesis of magadiite and kenyaite. J Ceram Soc Jpn 100:326–331. https://doi.org/10.2109/jcersj.100.326
340. Okutomo S, Kuroda K, Ogawa M (1999) Preparation and characterization of silylated-magadiites. Appl Clay Sci 15:253–264. https://doi.org/10.1016/S0169-1317(99)00010-1
341. Iyi N, Kurashima K, Fujita T (2002) Orientation of an organic anion and second-staging structure in layered double-hydroxide intercalates. Chem Mater 14:583–589. https://doi.org/10.1021/cm0105211
342. Nabetani Y, Takamura H, Uchikoshi A, Hassan SZ, Shimada T, Takagi S, Tachibana H, Masui D, Tong Z, Inoue H (2016) Photo-induced morphological winding and unwinding motion of nanoscrolls composed of niobate nanosheets with a polyfluoroalkyl azobenzene derivative. Nanoscale 8:12289–12293. https://doi.org/10.1039/C6NR02177H
343. Tong Z, Sasamoto S, Shimada T, Takagi S, Tachibana H, Zhang X, Tryk DA, Inoue H (2008) Preparation and photochemical behavior of polyfluorinated cationic azobenzene-titanoniobate intercalation compounds. J Mater Chem 18:4641. https://doi.org/10.1039/b805879b
344. Okada T, Sakai H, Ogawa M (2008) The effect of the molecular structure of a cationic azo dye on the photoinduced intercalation of phenol in a montmorillonite. Appl Clay Sci 40:187–192. https://doi.org/10.1016/j.clay.2007.09.001

345. Ogawa M, Kimura H, Kuroda K, Kato C (1996) Intercalation and the photochromism of azo dye in the hydrophobic interlayer spaces of organoammonium-fluor-tetrasilisic micas. Clay Sci 65:57–65. https://doi.org/10.11362/jcssjclayscience1960.10.57
346. Okada T, Nozaki N, Seo J, Kwon JE, Park SY, Hashizume H, Sasaki T, Ogawa M (2017) Photoinduced structural changes of cationic azo dyes confined in a two dimensional nanospace by two different mechanisms. RSC Adv 7:8077–8081. https://doi.org/10.1039/C6RA27749G
347. Ohtani O, Itoh T, Monna Y, Sasai R, Shichi T, Yui T, Takagi K (2005) Design of photofunctional laminated organized thin films: photochromism of ammoniumazobenzene arenecarboxylates cast on silica glass. Bull Chem Soc Jpn 78:698–702. https://doi.org/10.1246/bcsj.78.698
348. Umemoto T, Ohtani Y, Tsukamoto T, Shimada T, Takagi S (2014) Pinning effect for photoisomerization of a dicationic azobenzene derivative by anionic sites of the clay surface. Chem Commun 50:314–316. https://doi.org/10.1039/c3cc47353h
349. Fujita T, Iyi N, Klapyta Z (1998) Preparation of azobenzene-mica complex and its photoresponse to ultraviolet irradiation. Mater Res Bull 33:1693–1701
350. Ueda M, Kim HB, Ichimura K (1994) Photochemical and thermal isomerization of azobenzene derivatives in sol-gel bulk materials. Chem Mater 6:1771–1775. https://doi.org/10.1021/cm00046a033
351. Eisenbach CD (1978) Effect of polymer matrix on the *cis-trans* isomerization of azobenzene residues in bulk polymers. Macromol Chem Phys 179:2489–2506. https://doi.org/10.1002/macp.1978.021791014
352. Nabetani Y, Takamura H, Hayasaka Y, Sasamoto S, Tanamura Y, Shimada T, Masui D, Takagi S, Tachibana H, Tong Z, Inoue H (2013) An artificial muscle model unit based on inorganic nanosheet sliding by photochemical reaction. Nanoscale 5:3182–3193. https://doi.org/10.1039/c3nr34308a
353. Koteja A, Szczerba M, Matusik J (2017) Smectites intercalated with azobenzene and aminoazobenzene: structure changes at nanoscale induced by UV light. J Phys Chem Solids 111:294–303. https://doi.org/10.1016/j.jpcs.2017.08.015
354. Irie M, Fukaminato T, Matsuda K, Kobatake S (2014) Photochromism of diarylethene molecules and crystals: memories, switches, and actuators. Chem Rev 114:12174–12277
355. Taniguchi H, Shinpo A, Okazaki T, Matsui F, Irie M (1992) Photodegradation mechanism of photochromic diarylethene derivatives. Nippon Kagaku Kaishi 112:1138–1140. https://doi.org/10.1246/nikkashi.1992.1138
356. Irie M, Lifka T, Uchida K, Kobatake S, Shindo Y (1999) Fatigue resistant properties of photochromic dithienylethenes: by-product formation. Chem Commun:747–748
357. Higashiguchi K, Matsuda K, Kobatake S, Yamada T, Kawai T, Irie M (2000) Fatigue mechanism of photochromic 1,2-bis(2,5-dimethyl-3-thienyl)perfluorocyclopentene. Bull Chem Soc Jpn 73:2389–2394. https://doi.org/10.1246/bcsj.73.2389
358. Yokoyama S, Hirose T, Matsuda K (2015) Photoinduced four-state three-step ordering transformation of photochromic terthiophene at a liquid/solid interface based on two principles: photochromism and polymorphism. Langmuir 31:6404–6414. https://doi.org/10.1021/acs.langmuir.5b01404
359. Frath D, Sakano T, Imaizumi Y, Yokoyama S, Hirose T, Matsuda K (2015) Diarylethene self-assembled monolayers: cocrystallization and mixing-induced cooperativity highlighted by scanning tunneling microscopy at the liquid/solid interface. Chem A Eur J 21:11350–11358. https://doi.org/10.1002/chem.201500804
360. Fukumoto S, Nakashima T, Kawai T (2011) Photon-quantitative reaction of a dithiazolylarylene in solution. Angew Chem Int Ed 50:1565–1568. https://doi.org/10.1002/anie.201006844
361. Iijima S, Nakashima T, Kawai T (2016) Stereoselective photoreaction in P-stereogenic dithiazolylbenzo[*b*]phosphole chalcogenides. New J Chem 40:10048–10055. https://doi.org/10.1039/c6nj02446g

362. Yokoyama Y, Shiozawa T, Tani Y, Ubukata T (2009) A unified strategy for exceptionally high diastereoselectivity in the photochemical ring closure of chiral diarylethenes. Angew Chem Int Ed 48:4521–4523. https://doi.org/10.1002/anie.200901156
363. Yokoyama Y, Hasegawa T, Ubukata T (2011) Highly diastereoselective photochromic ring closure of bisbenzothienylethenes possessing dual fluorinated stereocontrollers. Dyes Pigments 89:223–229. https://doi.org/10.1016/j.dyepig.2010.03.008
364. Okada H, Nakajima N, Tanaka T, Iwamoto M (2005) Improvement in photocyclization efficiency of diaryl ethenes by adjusting the pore size of mesoporous silica. Angew Chem Int Ed 44:7233–7236. https://doi.org/10.1002/anie.200501992
365. Fukagawa M, Kawamura I, Ubukata T, Yokoyama Y (2013) Enantioselective photochromism of diarylethenes in human serum albumin. Chem A Eur J 19:9434–9437. https://doi.org/10.1002/chem.201301459
366. Sasai R, Ogiso H, Shindachi I, Shichi T, Takagi K (2000) Photochromism in oriented thin films prepared by the hybridization of diarylethenes in clay interlayers. Tetrahedron 56:6979–6984. https://doi.org/10.1016/S0040-4020(00)00519-6
367. Sasai R, Itoh H, Shindachi I, Shichi T, Takagi K (2001) Photochromism of clay - diarylethene hybrid materials in optically transparent gelatin films. Chem Mater 13:2012–2016. https://doi.org/10.1021/cm000822v
368. Shindachi I, Hanaki H, Sasai R, Shichi T, Yui T, Takagi K (2004) The effect of layered sodium–magadiite on the photochromic reversibility of diarylethene immobilized on its surfaces. Chem Lett 33:1116–1117. https://doi.org/10.1246/cl.2004.1116
369. Shindachi I, Hanaki H, Sasai R, Shichi T, Yui T, Takagi K (2007) Preparation and photochromism of diarylethene covalently bonded onto layered sodium-magadiite surfaces. Res Chem Intermed 33:143–153. https://doi.org/10.1163/156856707779160870
370. Klajn R (2014) Spiropyran-based dynamic materials. Chem Soc Rev 43:148–184. https://doi.org/10.1039/C3CS60181A
371. Wojtyk JTC, Wasey A, Kazmaier PM, Hoz S, Buncel E (2000) Thermal reversion mechanism of *N*-functionalized merocyanines to spiropyrans: a solvatochromic, solvatokinetic, and semiempirical study. J Phys Chem A 104:9046–9055. https://doi.org/10.1021/jp001533x
372. Shimizu I, Kokado H, Inoue E (1969) Photoreversible photographic systems. V. Reverse photochromism of (photospiran/acid) system in acetone. Bull Chem Soc Jpn 42:1726–1729. https://doi.org/10.1246/bcsj.42.1726
373. Raymo FM, Giordani S (2001) Signal processing at the molecular level. J Am Chem Soc 123:4651–4652. https://doi.org/10.1021/ja005699n
374. Yamaguchi T, Ogawa M (2018) Photochromism of a spiropyran in the presence of a synthetic hectorite. Chem Lett 47:189–191. https://doi.org/10.1246/cl.170982
375. Mitchell RH, Ward TR, Chen Y, Wang Y, Weerawarna SA, Dibble PW, Marsella MJ, Almutairi A, Wang Z (2003) Synthesis and photochromic properties of molecules containing [*e*] -annelated dihydropyrenes. two and three way π-switches based on the valence isomerization. J Am Chem Soc 125:2974–2988
376. Honda K, Komizu H, Kawasaki M (1982) Reverse photocharomism of stenhouse salts. J Chem Soc Chem Commun:253. https://doi.org/10.1039/c39820000253
377. Lerch MM, Szymański W, Feringa BL (2018) The (photo)chemistry of stenhouse photoswitches: guiding principles and system design. Chem Soc Rev 47:1910–1937. https://doi.org/10.1039/c7cs00772h
378. Hatano S, Horino T, Tokita A, Oshima T, Abe J (2013) Unusual negative photochromism via a short-lived imidazolyl radical of 1,1'-binaphthyl-bridged imidazole dimer. J Am Chem Soc 135:3164–3172. https://doi.org/10.1021/ja311344u
379. Yamaguchi T, Kobayashi Y, Abe J (2015) Fast negative photochromism of 1,1′-binaphthyl-bridged phenoxyl−imidazolyl radical complex. J Am Chem Soc 138:906–913. https://doi.org/10.1021/jacs.5b10924

380. Yamaguchi T, Ogawa M (2018) Hydrophilic internal pore and hydrophobic particle surface of organically modified mesoporous silica particle to host photochromic molecules. Chem Lett 48:170–172
381. Yamaguchi T, Maity A, Polshettiwar V, Ogawa M (2018) Negative photochromism based on molecular diffusion between hydrophilic and hydrophobic particles in the solid-state. Inorg Chem 57:3671–3674
382. Yamaguchi T, Leelaphattharaphan NN, Shin H, Ogawa M (2019) Acceleration of photochromism and negative photochromism by the interactions with mesoporous silicas. Photochem Photobiol Sci 18:1742–1749. https://doi.org/10.1039/C9PP00081J
383. Schomburg C, Wark M, Rohlfing Y, Schulz-Ekloff G, Wöhrle D (2001) Photochromism of spiropyran in molecular sieve voids: effects of host–guest interaction on isomer status, switching stability and reversibility. J Mater Chem 11:2014–2021. https://doi.org/10.1039/b101516h
384. Casades I, Constantine S, Cardin D, García H, Gilbert A, Márquez F (2000) Ship-in-a-bottle synthesis and photochromism of spiropyrans encapsulated within zeolite Y supercages. Tetrahedron 56:6951–6956. https://doi.org/10.1016/S0040-4020(00)00515-9
385. Kahle I, Spange S (2010) Internal and external acidity of faujasites as measured by a solvatochromic spiropyran. J Phys Chem C 114:15448–15453. https://doi.org/10.1021/jp1048106
386. Tagaya H, Kuwahara T, Sato S, Kadokawa J, Karasu M, Chiba K (1993) Photoisomerization of indolinespirobenzopyran in layered double hydroxides. J Mater Chem 3:317. https://doi.org/10.1039/jm9930300317
387. Tagaya H, Sato S, Kuwahara T, Kadokawa J, Masa K, Chibaa K (1994) Photoisomerization of Indolinespirobenzopyran in anionic clay matrices of layered double hydroxides. J Mater Chem 4:1907. https://doi.org/10.1039/jm9940401907
388. Aiken S, Edgar RJL, Gabbutt CD, Heron BM, Hobson PA (2018) Negatively photochromic organic compounds: exploring the dark side. Dyes Pigments 149:92–121. https://doi.org/10.1016/j.dyepig.2017.09.057
389. Kinashi K, Kita H, Misaki M, Koshiba Y, Ishida K, Ueda Y, Ishihara M (2009) Fabrication and optical properties of photochromic compound/clay hybrid films. Thin Solid Films 518:651–655. https://doi.org/10.1016/j.tsf.2009.07.042
390. Saso N, Yamamoto T, Umemura Y, Einaga Y (2008) Normal photochromism of spiropyran in montmorillonite interlayer. Colloids Surf A Physicochem Eng Asp 317:309–315. https://doi.org/10.1016/j.colsurfa.2007.10.036
391. Seki T, Ichimura K (1990) Thermal isomerization behaviors of a spiropyran in bilayers immobilized with a linear polymer and a smectitic clay. Macromolecules:31–35
392. Takagi K, Kurematsu T, Sawaki Y (1995) Photochromic behaviour of surfactant spiro[2*H*-1-benzopyran-2,2′-[2,3]-dihydroindole]s (spiropyrans) adsorbed into clay interlayers. J Chem Soc Perkin Trans 2:1667–1671. https://doi.org/10.1039/P29950001667
393. Mal NK, Fujiwara M, Tanaka Y (2003) Photocontrolled reversible release of guest molecules from coumarin-modified mesoporous silica. Nature 421:350–353. https://doi.org/10.1038/nature01337.1
394. Bach T (1998) Stereoselective intermolecular [2+2]-photocycloaddition reactions and their application in synthesis. Synthesis:683–703
395. González-López M, Shaw JT (2009) Cyclic anhydrides in formal cycloadditions and multicomponent reactions. Chem Rev 109:164–189. https://doi.org/10.1021/cr8002714
396. Laszlo P, Lucchetti J (1984) Catalysis of the diels-alder reaction in the presence of clays. Tetrahedron Lett 25:1567–1570. https://doi.org/10.1016/S0040-4039(01)90012-7
397. Laszlo P, Lucchetti J (1984) Acceleration of the diels-alder reaction by clays suspended in organic solvents. Tetrahedron Lett 25:2147–2150. https://doi.org/10.1016/S0040-4039(01)81184-9
398. Valentine D, Turro NJ, Hammond GS (1964) Thermal and photosensitized dimerizations of cyclohexadiene. J Am Chem Soc 86:5202–5208. https://doi.org/10.1021/ja01077a033

399. Schuster DI, Lem G, Kaprinidis NA (1993) New insights into an old mechanism: [2 + 2] photocycloaddition of enones to alkenes. Chem Rev 93:3–22. https://doi.org/10.1021/cr00017a001
400. Usami H, Takagi K, Sawaki Y (1992) Regioselective photocyclodimerization of cyclohexenones intercalated on clay layers. Chem Lett 21:1405–1408. https://doi.org/10.1246/cl.1992.1405
401. Madhavan D, Pitchumani K (2002) Photodimerisation of enones in a clay microenvironment. Photochem Photobiol Sci 1:991–995. https://doi.org/10.1039/b208030c
402. Takagi K, Usami H, Fukaya H, Sawaki Y (1989) Spatially controlled photocycloaddition of a clay-intercalated stilbazolium cation. J Chem Soc Chem Commun:1174. https://doi.org/10.1039/c39890001174
403. Usami H, Takagi K, Sawaki Y (1990) Controlled photocycloaddition of stilbazolium ions intercalated in saponite clay layers. J Chem Soc Perkin Trans 2:1723. https://doi.org/10.1039/p29900001723
404. Usami H, Takagi K, Sawaki Y (1992) Clay-inclusion photocyclodimerization: intercalation and migration of stilbazolium ions. J Chem Soc Faraday Trans 88:77–81. https://doi.org/10.1039/FT9928800077
405. Nakahira T, Hama M, Fukuchi O, Okamura T, Iwabuchi S, Shimazu S, Uematsu T, Kikuchi H (1995) Control of photochemistry of stilbazolium ion by adsorption to poly(potassium vinylsulfate) and to hectorite clay. Macromol Rapid Commun 16:717–723. https://doi.org/10.1002/marc.1995.030161003
406. Shichi T, Takagi K, Sawaki Y (1996) Organized photocycloaddition of 4-benzoylbenzoate with unsaturated carboxylates in hydrotalcite clay interlayers. Chem Lett 25:781–782. https://doi.org/10.1246/cl.1996.781
407. Takagi K, Nakamura T, Katsu H, Itoh M, Sawaki Y, Imae T (1996) Photochemical cyclodimerization of cinnmamic acids included in surfactant amine oxides. Mol Cryst Liq Cryst Sci Technol Sect A Mol Cryst Liq Cryst 276–277:135–138. https://doi.org/10.1080/10587259608046014
408. Elsherbiny AS, Salem MA, Ismail AA (2012) Influence of the alkyl chain length of cyanine dyes on their adsorption by Na^+-montmorillonite from aqueous solutions. Chem Eng J 200–202:283–290. https://doi.org/10.1016/j.cej.2012.06.050
409. Yui T, Takagi K, Inoue H (2018) Microscopic environment and molecular orientation of guest molecules within polyfluorinated surfactant and clay hybrids: photochemical studies of stilbazolium derivatives. J Photochem Photobiol A Chem 363:61–67. https://doi.org/10.1016/j.jphotochem.2018.05.022
410. Zhong J, Cui X, Guan W, Lu C (2018) Direct observation of adsorption kinetics on clays by cation-π interaction-triggered aggregation luminescence. J Mater Chem C 6:13218–13224. https://doi.org/10.1039/c8tc04837a
411. Sasai R, Shin'ya N, Shichi T, Takagi K, Gekko K (2002) Molecular alignment and photodimerization of 4'-Chloro-4-stilbenecarboxylic acid in hydrotalcite clays: bilayer formation in the interlayers. Langmuir 15:413–418. https://doi.org/10.1021/la980699a
412. Shichi T, Yamashita S, Takagi K (1998) Photopolymerization of 4-vinylbenzoate and *m*- and *p*-phenylenediacrylates in hydrotalcite interlayers. Supramol Sci 5:303–308. https://doi.org/10.1016/S0968-5677(98)00023-6
413. Kalo H, Möller MW, Kunz DA, Breu J (2012) How to maximize the aspect ratio of clay nanoplatelets. Nanoscale 4:5633–5639. https://doi.org/10.1039/c2nr31322g
414. Hofmann U, Klemen R (1950) Verlust der Austauschfähigkeit von Lithiumionen an Bentonit durch Erhitzung. Zeitschrift für Anorg Chemie 262:95–99. https://doi.org/10.1002/zaac.19502620114
415. Zemanová M, Link G, Takayama S, Nüesch R, Janek M (2006) Modification of layer charge in smectites by microwaves. Appl Clay Sci 32:271–282. https://doi.org/10.1016/j.clay.2006.01.002

416. Skoubris EN, Chryssikos GD, Christidis GE, Gionis V (2013) Structural characterization of reduced-charge montmorillonites. Evidence based on FTIR spectroscopy, thermal behavior, and layer-charge systematics. Clays Clay Miner 61:83–97. https://doi.org/10.1346/CCMN.2013.0610207
417. Takahashi K, Ishii R, Suzuki A, Nakamura T, Yoshida M, Ebina T (2017) Preparation of Lignin–Montmorillonite nanocomposite films and its characterization for electronic devices. Clay Sci 21:1–6. https://doi.org/10.11362/jcssjclayscience.21.1_1
418. Ramamurthy V, Sivaguru J (2016) Supramolecular photochemistry as a potential synthetic tool: photocycloaddition. Chem Rev 116:9914–9993. https://doi.org/10.1021/acs.chemrev.6b00040
419. Ramamurthy V, Corbin DR, Kumar CV, Turro NJ (1990) Modification of photochemical reactivity by zeolites: cation controlled photodimerisation of acenaphthylene within faujasites. Tetrahedron Lett 31:47–50. https://doi.org/10.1016/S0040-4039(00)94330-2
420. Lalitha A, Pitchumani K, Srinivasan C (2000) Photodimerization of *trans*-2-styrylpyridine in zeolite cages. J Photochem Photobiol A Chem 134:193–197. https://doi.org/10.1016/S1010-6030(00)00271-9
421. Kim SW, Son SU, Lee SI, Hyeon T, Chung YK (2000) Cobalt on mesoporous silica: the first heterogeneous pauson-khand catalyst. J Am Chem Soc 122:1550–1551. https://doi.org/10.1021/ja9939237
422. Matsuo Y, Fukunaga T, Fukutsuka T, Sugie Y (2002) Photochemical dimerization of acenaphthylene in hydrophobized graphite oxide. Mol Cryst Liq Cryst Sci Technol Sect A Mol Cryst Liq Cryst 386:45–50. https://doi.org/10.1080/10587250290113178
423. Heinz H, Vaia RA, Koerner H, Farmer BL (2008) Photoisomerization of azobenzene grafted to layered silicates: simulation and experimental challenges. Chem Mater 20:6444–6456. https://doi.org/10.1021/cm801287d
424. Tong Z, Takagi S, Shimada T, Tachibana H, Inoue H (2006) Photoresponsive multilayer spiral nanotubes: intercalation of polyfluorinated cationic azobenzene surfactant into potassium niobate. J Am Chem Soc 128:684–685. https://doi.org/10.1021/ja0564564
425. Nabetani Y, Takamura H, Hayasaka Y, Shimada T, Takagi S, Tachibana H, Masui D, Tong Z, Inoue H (2011) A Photoactivated artificial muscle model unit: reversible, photoinduced sliding of nanosheets. J Am Chem Soc 133:17130–17133. https://doi.org/10.1021/ja207278t
426. Guo W, Yu C, Li S, Yang J, Liu Z, Zhao C, Huang H, Zhang M, Han X, Niu Y, Qiu J (2017) High-stacking-density, superior-roughness LDH bridged with vertically aligned graphene for high-performance asymmetric supercapacitors. Small 13:1–9. https://doi.org/10.1002/smll.201701288
427. Chen T, Xu S, Zhang F, Evans DG, Duan X (2009) Formation of photo- and thermo-stable layered double hydroxide films with photo-responsive wettability by intercalation of functionalized azobenzenes. Chem Eng Sci 64:4350–4357. https://doi.org/10.1016/j.ces.2009.07.005
428. Zhang F, Zhao L, Chen H, Xu S, Evans DG, Duan X (2008) Corrosion resistance of superhydrophobic layered double hydroxide films on aluminum. Angew Chem Int Ed 47:2466–2469. https://doi.org/10.1002/anie.200704694
429. Uchida K, Izumi N, Sukata S, Kojima Y, Nakamura S, Irie M (2006) Photoinduced reversible formation of microfibrils on a photochromic diarylethene microcrystalline surface. Angew Chem Int Ed 45:6470–6473. https://doi.org/10.1002/anie.200602126
430. Wang S, Song Y, Jiang L (2007) Photoresponsive surfaces with controllable wettability. J Photochem Photobiol C: Photochem Rev 8:18–29. https://doi.org/10.1016/j.jphotochemrev.2007.03.001
431. Kashima I, Okubo M, Qno Y, Itoi M, Kida N, Hikita M, Enomoto M, Kojima N (2005) Ferromagnetism and its photo-induced effect in 2D Iron mixed-valence complex coupled with photochromic spiropyran. Synth Met 155:703–706. https://doi.org/10.1016/j.synthmet.2005.09.033

432. Enomoto M, Kojima N (2005) Charge transfer phase transition and ferromagnetism in a novel iron mixed-valence complex (n-C_3H_7)4N[$Fe^{II}Fe^{III}$(tto)$_3$] (tto=C_2OS_3). Synth Met 152:457–460. https://doi.org/10.1016/j.synthmet.2005.07.177
433. Kida N, Hikita M, Kashima I, Enomoto M, Itoi M, Kojima N (2009) Mössbauer spectroscopic study of photo-sensitive organic-inorganic hybrid system, (SP)[Fe(II)Fe(III)(dto)$_3$](dto = $C_2O_2S_2$, SP = spiropyran). Polyhedron 28:1694–1697. https://doi.org/10.1016/j.poly.2008.10.060
434. Kida N, Hikita M, Kashima I, Okubo M, Itoi M, Enomoto M, Kato K, Takata M, Kojima N (2009) Control of charge transfer phase transition and ferromagnetism by photoisomerization of spiropyran for an organic-inorganic hybrid system, (SP)[FeIIFeIII(dto)$_3$] (SP = spiropyran, dto = $C_2O_2S_2$). J Am Chem Soc 131:212–220. https://doi.org/10.1021/ja806879a
435. Tanaka N, Okazawa A, Sugahara A, Kojima N (2015) Development of a photoresponsive organic-inorganic hybrid magnet: layered cobalt hydroxides intercalated with spiropyran anions. Bull Chem Soc Jpn 88:1150–1155. https://doi.org/10.1246/bcsj.20150129
436. Abellán G, Coronado E, Martí-Gastaldo C, Ribera A, Jordá JL, García H (2014) Photo-switching in a hybrid material made of magnetic layered double hydroxides intercalated with azobenzene molecules. Adv Mater 26:4156–4162. https://doi.org/10.1002/adma.201400713
437. Abellán G, Jordá JL, Atienzar P, Varela M, Jaafar M, Gómez-Herrero J, Zamora F, Ribera A, García H, Coronado E (2015) Stimuli-responsive hybrid materials: breathing in magnetic layered double hydroxides induced by a thermoresponsive molecule. Chem Sci 6:1949–1958. https://doi.org/10.1039/C4SC03460K
438. Okubo M, Enomoto M, Kojima N (2005) Study on photomagnetism of 2-D magnetic compounds coupled with photochromic diarylethene cations. Synth Met 152:461–464. https://doi.org/10.1016/j.synthmet.2005.07.181
439. Shimizu H, Okubo M, Nakamoto A, Enomoto M, Kojima N (2006) Enhancement of the curie temperature by isomerization of diarylethene (DAE) for an organic-inorganic hybrid system: $Co_4(OH)_7(DAE)_{0.5}\cdot 3H_2O$. Inorg Chem 45:10240–10247. https://doi.org/10.1021/ic061498u
440. Kojima N, Okubo M, Shimizu H, Enomoto M (2007) Control of magnetism by isomerization of intercalated molecules in organic-inorganic hybrid systems. Coord Chem Rev 251:2665–2673. https://doi.org/10.1016/j.ccr.2007.08.025
441. Abellán G, Coronado E, Martí-Gastaldo C, Waerenborgh J, Ribera A (2013) Interplay between chemical composition and Cation ordering in the magnetism of Ni/Fe layered double hydroxides. Inorg Chem 52:10147–10157. https://doi.org/10.1021/ic401576q
442. Kojima N, Aoki W, Itoi M, Ono Y, Seto M, Kobayashi Y, Maeda Y (2001) Charge transfer phase transition and ferromagnetism in a mixed-valence iron complex, (n-C_3H_7)4N[$Fe^{II}Fe^{III}$(dto)$_3$] (dto = $C_2O_2S_2$). Solid State Commun 120:165–170. https://doi.org/10.1016/S0038-1098(01)00366-0
443. Ono Y, Okubo M, Kojima N (2003) Crystal structure and ferromagnetism of (n-C_3H_7)4N[$Co^{II}Fe^{III}$(dto)$_3$] (dto = $C_2O_2S_2$). Solid State Commun 126:291–296. https://doi.org/10.1016/S0038-1098(02)00825-6
444. Carrasco JA, Abellán G, Coronado E (2018) Influence of morphology in the magnetic properties of layered double hydroxides. J Mater Chem C 6:1187–1198. https://doi.org/10.1039/c7tc05569b
445. Hornick C, Rabu P, Drillon M (2000) Hybrid organic-inorganic multilayer materials: influence of π electrons as magnetic media in a series of bridged-layer compounds $M_2(OH)_{4-x}A_{x/2}$ (M = cu(II) or co(II), a = dicarboxylate anion). Polyhedron 19:259–266. https://doi.org/10.1016/S0277-5387(99)00355-1
446. Matsuda K, Irie M (2000) Photoswitching of intramolecular magnetic interaction: a diarylethene photochromic spin coupler. Chem Lett 29:16–17. https://doi.org/10.1246/cl.2000.16

447. Bousquet D, Peltier C, Masselin C, Jacquemin D, Adamo C, Ciofini I (2012) A DFT study of magnetic interactions in photoswitchable systems. Chem Phys Lett 542:13–18. https://doi.org/10.1016/j.cplett.2012.05.040
448. Okada T, Morita T, Ogawa M (2005) Tris(2,2′-bipyridine)ruthenium(II)-clays as adsorbents for phenol and chlorinated phenols from aqueous solution. Appl Clay Sci 29:45–53. https://doi.org/10.1016/j.clay.2004.09.004
449. Seki Y, Ide Y, Okada T, Ogawa M (2015) Concentration of 2-phenylphenol by organoclays from aqueous sucrose solution. Appl Clay Sci 109–110:64–67. https://doi.org/10.1016/j.clay.2014.12.021
450. Yamaguchi T, Maity A, Polshettiwar V, Ogawa M (2017) Photochromism of a spiropyran in the presence of a dendritic fibrous nanosilica; simultaneous photochemical reaction and adsorption. J Phys Chem A 121:8080–8085. https://doi.org/10.1021/acs.jpca.7b08466
451. Yamaguchi T, Ogawa M (2018) Hydrophilic internal pore and hydrophobic particle surface of organically modified mesoporous silica particle to host photochromic molecules. Chem Lett 48:170–172. https://doi.org/10.1246/cl.180908
452. Okabe Y, Ogawa M (2015) Photoinduced adsorption of spiropyran into mesoporous silicas as photomerocyanine. RSC Adv 5:101789–101793. https://doi.org/10.1039/C5RA18252B